



3 1176 00168 6949

NASA CR-165,710

NASA Contractor Report 165710

NASA-CR-165710
19810015491

COMPARISON OF SELECTED LIFT AND SIDESLIP
CHARACTERISTICS OF THE AYRES THRUSH S2R-800,
WINGLETS OFF AND WINGLETS ON, TO FULL-SCALE
WIND-TUNNEL DATA

J. Roskam and M. Williams

THE UNIVERSITY OF KANSAS CENTER FOR RESEARCH, INC.
Lawrence, Kansas 66045

NASA Grant NSG-1574
April 1981

MAY 5 1981

NASA
National Aeronautics and
Space Administration

Langley Research Center
Hampton, Virginia 23665

Langley Research Center
Hampton, Virginia
Hampton, Virginia

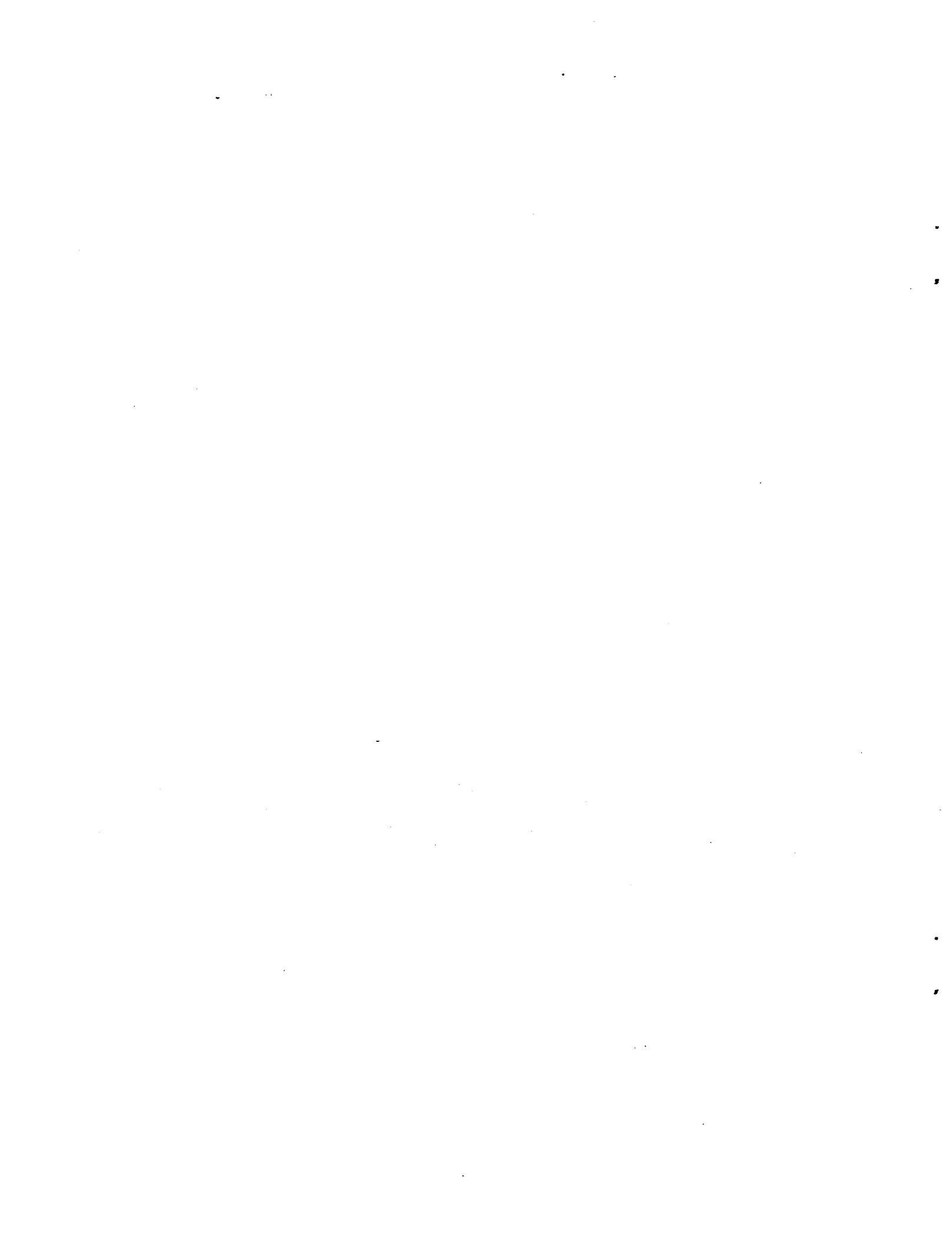


TABLE OF CONTENTS

	<u>Page</u>
<u>LIST OF TABLES</u>	iv
<u>LIST OF FIGURES</u>	vi
<u>LIST OF SYMBOLS</u>	ix
CHAPTER 1 <u>INTRODUCTION</u>	1.1
CHAPTER 2 <u>THE AYRES THRUSH S2R-800 AIRPLANE</u>	2.1
2.1 <u>Geometric Parameters of Fuselage, Wing, Winglet, and Tails</u>	2.8
2.2 <u>Flight Condition Used in the Analysis.</u>	2.12
CHAPTER 3 <u>PRESENTATION OF RESULTS</u>	3.1
3.1 <u>Lift Curve</u>	3.1
3.2 <u>Sideslip Derivatives</u>	3.1
CHAPTER 4 <u>PREDICTION OF PROPELLOR-OFF, HORIZONTAL TAIL-OFF LIFT CHARACTERISTICS USING AN ANALYTICAL METHOD</u>	4.1
4.1 <u>Zero Lift Angle of Attack.</u>	4.1
4.1.1 Wing Contribution.	4.1
4.1.2 α_0 of the Ayres Thrush	4.2
4.2 <u>Lift-Curve Slope, $C_{L\alpha}$</u>	4.2
4.2.1 Wing Contribution to $C_{L\alpha}$	4.3
4.2.2 Fuselage Contribution to $C_{L\alpha}$	4.4
4.2.3 $C_{L\alpha}$ of the Complete Airplane Horizontal Tail Off.	4.4
4.3 <u>Lift-Curve in the Non-Linear Region.</u>	4.5
4.3.1 $C_{L_{max}}$ of the Wing, Wing-Fuselage	4.5
4.3.2 The Wing and Wing-Fuselage Angle of Attack at $C_{L_{max}}$	4.7
4.3.3 Upper Limit of Linearity of the Lift Curve	4.8

TABLE OF CONTENTS (continued)

	<u>Page</u>
4.4 <u>Summary</u>	4.8
CHAPTER 5 PREDICTION OF PROPELLER-OFF LATERAL-DIRECTIONAL STATIC STABILITY USING AN ANALYTICAL METHOD	5.1
5.1 <u>Side Force Derivative, $C_{y\beta}$</u>	5.1
5.1.1 Wing Contribution.	5.1
5.1.2 Fuselage Contribution to $C_{y\beta}$	5.2
5.1.3 Vertical Tail Contribution to $C_{y\beta}$	5.3
5.1.4 Winglet Contribution to $C_{y\beta}$	5.5
5.1.5 $C_{y\beta}$ of the Complete Airplane, Winglets On and Winglets Off	5.6
5.2 <u>Yawing Moment Derivative, $C_{n\beta}$</u>	5.7
5.2.1 Wing Contribution to $C_{n\beta}$	5.7
5.2.2 Fuselage Contribution to $C_{n\beta}$	5.8
5.2.3 Vertical Tail Contribution to $C_{n\beta}$	5.9
5.2.4 Winglet Contribution to $C_{n\beta}$	5.9
5.2.5 Weathercock Stability of the Complete Airplane, Winglets On and Winglets Off	5.10
5.3 <u>Rolling Moment Derivative, $C_{l\beta}$</u>	5.11
5.3.1 Wing Contribution to $C_{l\beta}$	5.11
5.3.2 Effect of Fuselage on Wing Contribution to $C_{l\beta}$	5.12
5.3.3 Vertical Tail Contribution to $C_{l\beta}$	5.12
5.3.4 Winglet Contribution to $C_{l\beta}$	5.13
5.3.5 $C_{l\beta}$ of the Complete Airplane, Winglets On and Winglets Off.	5.14

TABLE OF CONTENTS (continued)

	<u>Page</u>
CHAPTER 6 <u>PREDICTION OF LIFT AND SIDESLIP STABILITY</u> <u>CHARACTERISTICS USING A COMPUTER METHOD.</u>	6.1
6.1 <u>Description of QVLM.</u>	6.1
6.2 <u>QVLM Predicted $C_{L\alpha}$ and α_0</u>	6.2
6.3 <u>QVLM Predicted C_y, C_n and C_β</u>	6.2
CHAPTER 7 <u>CONCLUSIONS AND RECOMMENDATIONS.</u>	7.1
<u>REFERENCES</u>	R.1

LIST OF TABLES

<u>Table</u>	<u>Title</u>	<u>Page</u>
2.1	Specifications of the Ayres Thrush S2 R-800.	2.2
2.2	Airfoil Coordinates for Winglets.	2.5
4.4.1	Lift Characteristics of the Ayres Thrush, Tail and Propeller Off.	4.9
4.1.1.1	Wing Contribution to α_0	4.10
4.2.1.1	Wing Contribution to C_{L_α}	4.11
4.2.2.1	Fuselage Contribution to C_{L_α}	4.12
4.2.3.1	Linear C_{L_α} of the Ayres Thrush.	4.13
4.3.1.1	Maximum Wing Lift Coefficient	4.13
4.3.1.2	Summary Calculation for Wing-Fuselage $C_{L_{max}}$	4.14
4.3.2.1	Summary Calculation for α_{C_L}	4.15
4.3.3.1	Summary for α^+ Calculations ^{max}	4.16
5.1.2.1	Fuselage Contribution to C_{y_β}	5.15
5.1.3.1	Vertical Tail Contribution to C_{y_β}	5.16
5.1.4.1	Winglet Contribution to C_{y_β}	5.19
5.1.5.1	C_{y_β} of the Complete Airplane.	5.21
5.2.1.1	Wing Contribution to C_{n_β}	5.22
5.2.2.1	Fuselage Contribution to C_{n_β}	5.23
5.2.3.1	Vertical Tail Contribution to C_{n_β}	5.24
5.2.4.1	Winglet Contribution to C_{n_β}	5.25
5.2.5.1	C_{n_β} of the Complete Airplane: Winglets On and Winglets Off.	5.26
5.3.1.1	Wing Contribution to C_{ℓ_β}	5.27
5.3.2.1	Effect of Fuselage on Wing Contribution to C_{ℓ_β}	5.28

LIST OF TABLES (continued)

<u>Table</u>	<u>Title</u>	<u>Page</u>
5.3.3.1	Vertical Tail Contribution to $C_{l\beta}$	5.29
5.3.4.1	Winglet Contribution to $C_{l\beta}$	5.30
5.3.5.1	$C_{l\beta}$ of the Complete Airplane: Winglets On and Winglets Off.	5.31

LIST OF FIGURES

<u>Figure</u>	<u>Title</u>	<u>Page</u>
2.1	Three-View of Ayres Thrush S2R-800.	2.6
2.2	Three-View sketch of Ayres Thrush S2R-800 showing winglet installation.	2.7
2.1.1	Geometric parameters of the fuselage.	2.9
2.1.2	Definition sketch of wing dimensions.	2.10
2.1.3	Definition sketch of horizontal tail.	2.11
2.1.4	Definition sketch of vertical tail.	2.11
3.1.1	Lift curve of Ayres Thrush S2R-800.	3.3
3.2.1	Comparison of predicted $C_{y\beta}$, winglets off, to full scale wind tunnel data for the Ayres Thrush S2R-800.	3.4
3.2.2	Comparison of predicted $C_{n\beta}$, winglets off, to full scale wind tunnel data for the Ayres Thrush S2R-800.	3.5
3.2.3	Comparison of predicted $C_{l\beta}$, winglets off, to full scale wind tunnel data for the Ayres Thrush S2R-800.	3.6
3.2.4	Effect of winglet cant angle on airplane $C_{y\beta}$ based on DATCOM methods	3.7
3.2.5	Effect of winglet cant angle on airplane $C_{n\beta}$ based on DATCOM methods	3.8
3.2.6	Effect of winglet cant angle on airplane $C_{l\beta}$ based on DATCOM methods	3.9
3.2.7	Effect of winglet cant angle on $C_{y\beta}$ based on QVLM computations for the S2R-800	3.10
3.2.8	Effect of winglet cant angle on $C_{n\beta}$ based on QVLM computations for the S2R-800	3.11

LIST OF FIGURES (continued)

<u>Figure</u>	<u>Title</u>	<u>Page</u>
3.2.9	Effect of winglet cant angle on C_L based on QVLM computations for the S2R-800.	3.12
4.1.1.1	Change in wing zero lift angle of attack due to wing twist	4.17
4.2.1.1	Lift ratios $K_w(f)$ and $K_f(w)$	4.18
4.3.1.1	Coefficients for additional and basic lift distribution.	4.19
4.3.1.2	Correction factors for C_L $_{max}$	4.20
4.3.2.1	Angle of attack increment for subsonic maximum lift.	4.21
4.3.2.2	Angle of attack for maximum lift.	4.22
4.4.1	S2R-800 lift curve based on DATCOM methods. . . .	4.23
5.1.2.1	Wing-body interference factor for sideslip derivative $C_{y\beta}$	5.32
5.1.3.1	Charts for estimating $(C_{y\beta})_{v(wfh)}$	5.33
5.1.4.1	Charts for estimating winglet contribution to $C_{y\beta}$	5.35
5.1.5.1	Predicted $C_{y\beta}$, winglets off, for the Ayres Thrust S2R-800.	5.36
5.1.5.2	Effect of winglet cant angle on airplane $C_{y\beta}$ based on DATCOM methods	5.37
5.2.1.1	Wing alone lift curve for the S2R-800	5.38
5.2.2.1	Empirical factor K_N related to the derivative C_n for the fuselage plus wing-fuselage interference.	5.39
5.2.5.1	Comparison of predicted C_n , winglets off, β to full scale wind tunnel data for the Ayres Thrush S2R-800.	5.40

LIST OF FIGURES (continued)

<u>Figure</u>	<u>Title</u>	<u>Page</u>
5.2.5.2	Effect of winglet cant angle on airplane $C_{n\beta}$ based on DATCOM methods	5.41
5.3.1.1	Effect of wing dihedral on wing $C_{\ell\beta}$	5.42
5.3.1.2	Aspect ratio contribution to $C_{\ell\beta}$	5.42
5.3.5.1	Comparison of predicted $C_{\ell\beta}$, winglets off, to full scale wind tunnel data for the Ayres Thrush S2R-800.	5.43
5.3.5.2	Effect of winglet cant angle on airplane $C_{\ell\beta}$ based on DATCOM methods	5.44
6.2.1	Lift curve of S2R-800 based on QVLM computations.	6.3
6.3.1	Effect of cant angle on $C_{y\beta}$ based on QVLM computations for the S2R-800.	6.4
6.3.2	Effect of winglet cant angle on $C_{n\beta}$ based on QVLM computations for the S2R-800	6.5
6.3.3	Effect of winglet cant angle on $C_{\ell\beta}$ based on QVLM computations for the S2R-800	6.6

LIST OF SYMBOLS

<u>Symbol</u>	<u>Definition</u>	<u>Dimension</u>
A	Aspect ratio	
$A_{v_{\text{eff}}}$	Effective vertical tail aspect ratio	
$\frac{A_v(f)}{A_v}$	Ratio of vertical tail aspect ratio in presence of fuselage to isolated vertical tail aspect ratio	
$\frac{A_v(fh)}{A_v(f)}$	Ratio of vertical tail aspect ratio in presence of fuselage and horizontal tail to aspect ratio of tail in presence of fuselage alone	
$b, \left(\frac{b}{2}\right)_e$	Span, exposed wing half span	m (ft)
\bar{c}	Mean aerodynamic chord	m (ft)
$c_r, (c_r)_e$	Root chord, exposed wing root chord	m (ft)
c_t	Tip chord	m (ft)
$(c_v)_h$	Vertical tail chord at horizontal tail quarter chord	m (ft)
c_l	Wing section lift coefficient	
c_{l_a}	Wing section lift coefficient due to wing angle of attack	
c_{l_b}	Wing section lift coefficient due to wing twist	
c_{l_i}	Wing section design lift coefficient	
$c_{l_{\max}}$	Wing section maximum lift coefficient	
c_{l_a}	Wing section lift curve slope	$\deg^{-1}, \text{rad}^{-1}$
$(c_{l_v})_a$	Vertical tail section lift curve slope	$\deg^{-1}, \text{rad}^{-1}$

LIST OF SYMBOLS (continued)

<u>Symbol</u>	<u>Definition</u>	<u>Dimension</u>
$C_{\lambda \beta}$	Rolling moment due to sideslip	$\text{deg}^{-1}, \text{rad}^{-1}$
$(C_{\lambda \beta})_{f(w)}$	Fuselage rolling moment due to sideslip in the presence of the wing	
$(C_{\lambda \beta})_{v(wfh)}$	Vertical tail rolling moment due to sideslip in the presence of the wing, fuselage, and horizontal tail	$\text{deg}^{-1}, \text{rad}^{-1}$
$(C_{\lambda \beta})_w$	Wing rolling moment due to sideslip	$\text{deg}^{-1}, \text{rad}^{-1}$
$(C_{\lambda \beta})_{WLT}$	Winglet rolling moment due to sideslip	$\text{deg}^{-1}, \text{rad}^{-1}$
$\frac{C_{\lambda \beta}}{C_{L_w}}$	Low-speed variation of $C_{\lambda \beta}$ as a function of wing lift	$\text{deg}^{-1}, \text{rad}^{-1}$
$\frac{C_{\lambda \beta}}{\Gamma_w}$	Effect of geometric dihedral on $C_{\lambda \beta}$	$\text{deg}^{-2}, \text{rad}^{-2}$
C_L	Lift coefficient	
$C_{L_{\max}}$	Maximum lift coefficient	
$(C_{L_{\max}})_w$	Wing maximum lift coefficient	
$(C_{L_{\max}})_{wf}$	Wing maximum lift coefficient in the presence of the fuselage	
$C_{L_{\alpha}}$	Lift curve slope	$\text{deg}^{-1}, \text{rad}^{-1}$
$(C_{L_{\alpha}})_{f(w)}$	Lift curve slope of the fuselage in the presence of the wing	
$(C_{L_{\alpha}})_{v(fh)}$	Vertical tail lift curve slope in the presence of the fuselage and horizontal tail	$\text{deg}^{-1}, \text{rad}^{-1}$

LIST OF SYMBOLS (continued)

<u>Symbol</u>	<u>Definition</u>	<u>Dimension</u>
$(C_L)_w(e)$	Exposed wing lift curve slope	$\text{deg}^{-1}, \text{rad}^{-1}$
$(C_L)_w(f)$	Wing lift curve slope in the presence of the fuselage	$\text{deg}^{-1}, \text{rad}^{-1}$
$(C_L')_v$	Effective lift curve slope of the vertical tail	$\text{deg}^{-1}, \text{rad}^{-1}$
C_{n_β}	Yawing moment due to sideslip	$\text{deg}^{-1}, \text{rad}^{-1}$
$(C_{n_\beta})_{f(w)}$	Fuselage yawing moment due to sideslip in the presence of the wing	$\text{deg}^{-1}, \text{rad}^{-1}$
$(C_{n_\beta})_{v(wfh)}$	Vertical tail yawing moment due to sideslip in the presence of the wing, fuselage, and horizontal tail	$\text{deg}^{-1}, \text{rad}^{-1}$
$(C_{n_\beta})_w$	Wing yawing moment due to sideslip	$\text{deg}^{-1}, \text{rad}^{-1}$
$(C_{n_\beta})_{WLT}$	Winglet yawing moment due to sideslip	$\text{deg}^{-1}, \text{rad}^{-1}$
C_{y_β}	Side force due to sideslip	$\text{deg}^{-1}, \text{rad}^{-1}$
$(C_{y_\beta})_B$	Body side force due to sideslip	$\text{deg}^{-1}, \text{rad}^{-1}$
$(C_{y_\beta})_f$	Fuselage side force due to sideslip including wing-fuselage interference contribution	$\text{deg}^{-1}, \text{rad}^{-1}$
$(C_{y_\beta})_{v(wfh)}$	Vertical tail side force due to sideslip in the presence of the wing, fuselage, and horizontal tail	$\text{deg}^{-1}, \text{rad}^{-1}$
$(C_{y_\beta})_{w\Gamma}$	Wing side force due to sideslip contribution due to wing dihedral	$\text{deg}^{-1}, \text{rad}^{-1}$
$(C_{y_\beta})_{WLT}$	Winglet side force due to sideslip	$\text{deg}^{-1}, \text{rad}^{-1}$
$(d_f)_h$	Diameter of the fuselage at the horizontal tail	m (ft)

LIST OF SYMBOLS (continued)

<u>Symbol</u>	<u>Definition</u>	<u>Dimension</u>
$(d_f)_v$	Diameter of the fuselage at the vertical tail	m (ft)
$(d_f)_w$	Diameter of the fuselage at the wing	m (ft)
$(d_f)_{WLT}$	Diameter of the fuselage at the winglet	m (ft)
h	Fuselage height	m (ft)
h_1	Fuselage height at one-quarter of the fuselage length from the nose	m (ft)
h_2	Fuselage height at three-quarters of the fuselage length from the nose	m (ft)
i_{WLT}	Incidence angle of winglet	deg, rad
K_h	Relative tail size factor	
K_i	Wing-body interference factor	
K_N	Empirical factor for fuselage C_{n_β} in the presence of the wing	
K'_1	Relative body size factor	
k_v	$(C_{\ell_\alpha})_v / 2\pi$	
ℓ_f	Length of fuselage	m (ft)
ℓ_v	Distance from the center of gravity to the quarter-chord of the mean aerodynamic chord of the vertical tail	
M	Mach number	
N_{Re}	Reynolds number	
prop	Propeller	
\bar{q}	Dynamic pressure	N/m^2 (lb/ft^2)

LIST OF SYMBOLS (continued)

<u>Symbol</u>	<u>Definition</u>	<u>Dimension</u>
$\frac{\bar{q}_v}{\bar{q}_\infty}$	Dynamic pressure ratio at the vertical tail	
S	Area	m^2 (ft^2)
$(S_f)_s$	Fuselage side area	m^2 (ft^2)
t/c	Airfoil thickness ratio	
\bar{V}	Fuselage volume	m^3 (ft^3)
WLT	Winglets	
w _{max}	Maximum fuselage width	m (ft)
$x_{ac_h}(c_r)_e$	Distance from leading edge of the vertical tail to the a.c. of the horizontal tail, in plane of the horizontal tail	m (ft)
$x_{c.g.}$	Distance from the center of gravity to the leading edge of the wing mean aerodynamic chord	m (ft)
$x_{c_r_h}(c_r_v)$	Distance from root chord of vertical tail to root chord of horizontal tail	m (ft)
x_m	Distance from the airplane nose to the center of gravity	m (ft)
$z_{c_r_h}(c_r_v)$	Distance from the root chord of the vertical tail to the root chord of the horizontal tail	m (ft)
z_v	Distance from the center of gravity to the vertical tail chord, perpendicular to the X-body axis	m (ft)
z'_w	Vertical distance from the X-axis of the equivalent circular fuselage to the quarter chord of the root chord of the exposed wing	m (ft)

LIST OF SYMBOLS (continued)

Greek Symbols:

<u>Symbol</u>	<u>Definition</u>	<u>Dimension</u>
α	Angle of attack relative to the Z-body axis	deg, rad
α_i	Angle of attack for the wing section design lift coefficient	deg, rad
α^+	Angle of attack at which the lift-curve slope is no longer linear	deg, rad
α_1^+	Section angle of attack at which the lift curve is no longer linear	deg, rad
α_0	Zero lift angle of attack	deg, rad
$(\alpha_0)_{\theta=0}$	Zero lift angle of attack for an untwisted wing	deg, rad
$(\alpha_{C_L})_{w_{max}}$	Wing angle of attack at the maximum lift coefficient	deg, rad
$(\alpha_{C_L})_{wf_{max}}$	Wing-fuselage angle of attack at the maximum lift coefficient	deg, rad
$\Delta\alpha_{C_L}$	Increment in angle of attack for wing maximum lift	deg, rad
β	Sideslip angle	deg, rad
Γ	Dihedral angle	deg, rad
$\frac{\Delta q}{q_\infty}$	Dynamic pressure increase behind the propeller as a ratio of the free stream dynamic pressure	
$\frac{\partial \sigma}{\partial \beta}$	Variation of sidewash with sideslip	
η	Non-dimensional spanwise station, $y/(b/2)$	
θ	Wing twist	deg, rad
Λ	Sweep angle	deg, rad

LIST OF SYMBOLS (continued)

<u>Symbol</u>	<u>Definition</u>	<u>Dimension</u>
$(\Lambda_{c/2})_v$	Sweep angle of vertical tail half chord	deg, rad
λ	Taper ratio	deg, rad
ϕ_{TE}	Section trailing-edge angle	deg, rad

Subscripts:

c/2	Half-chord line
c/4	Quarter-chord line
c.g.	Center of gravity
e	Exposed panel
f	Fuselage
fh	Fuselage-horizontal tail combination
h	Horizontal tail
l_e	Leading edge
max	Maximum
prop off	Propellers removed
r	Root
t	Tip
v	Vertical tail
w	Wing
wf	Wing-fuselage combination
wfh	Wing-fuselage-horizontal tail combination
WLT	Winglets

CHAPTER 1

INTRODUCTION

This report describes work carried out by the Flight Research Laboratory of the University of Kansas (KU-FRL) and sponsored by Grant NSG 1574 from the National Aeronautics and Space Administration (NASA), Langley Research Center. The purpose of this project was to correlate theoretically predicted aerodynamic characteristics of the Ayres Thrush S2R-800 airplane with full scale wind tunnel data. The theoretical prediction schemes have been documented in this report to provide an analytical method for calculating selected longitudinal and lateral-directional characteristics of the Ayres Thrush, winglets on and winglets off.

It has been previously found that winglets have favorable effects on wing tip vortex entrainment and wake interaction characteristics of chemical sprays dispensed from the airplane. These effects are especially important for an agricultural type airplane such as the S2R-800; therefore, this report investigates the winglet effect on the S2R-800 lateral-directional stability.

The two methods used in this report for theoretical predictions were a Quasi-Vortex Lattice Method (QVLM, Reference 3), which is a computer method, and DATCOM analytical methods (Reference 1). The results of these calculations are compared to full scale wind tunnel data where possible, and recommendations and conclusions given concerning these comparisons. All calculations have been done in the stability axes system.

CHAPTER 2

THE AYRES THRUSH S2R-800 AIRPLANE

The Ayres Thrush S2R-800 is designed especially for agricultural flying. Typical applications for the S2R-800 include seeding, fertilization, insect control, and defoliation. The S2R-800 is a monoplane featuring a full cantilever low wing and, with the exception of fabric empennage surfaces, is of all-metal construction. The major physical characteristics are listed in Table 2.1, and a three-view drawing is shown in Figure 2.1

The winglets used on the S2R-800 consist of a modified GA(W)-2 airfoil. Table 2.2 lists the airfoil coordinates of the winglets. Figure 2.2 shows a three-view sketch of the aircraft with winglet installation.

Table 2.1: Specifications of the Ayres Thrush S2R-800

Wing:

Airfoil	NACA 4412
Section Characteristics	
α_1 , deg	0.4933
C_{ℓ_1}	0.5067
C_{ℓ_α} , per deg	0.105
α_1^+ , deg	7.5
Area, m^2 (ft^2)	30.34 (326.6)
Exposed area, m^2 (ft^2)	27.45 (295.5)
Span, m (ft)	13.27 (43.5)*
Exposed Span, m (ft)	12.00 (39.4)
Aspect ratio	5.81
Exposed aspect ratio	5.25
Thickness ratio	0.12
Dihedral, deg	3.5
Taper ratio	1.0
Root chord, m (ft)	2.29 (7.5)
Mean aerodynamic chord, m (ft)	2.29 (7.5)
Incidence angle at root, deg	0
Incidence angle at tip, deg	-1.5
Sweep angle of quarter chord line, deg	0

Horizontal tail:

Airfoil	NACA 0003
Area (including elevator and tabs), m^2 (ft^2)	5.25 (56.47)

*See Section 2.1, page 2.8 and Figure 2.10.

Table 2.1: (continued)

Span, m (ft)	4.71 (15.45)
Aspect ratio	4.23
Thickness ratio	0.03
Dihedral, deg	0
Taper ratio	0.66
Root chord, m (ft)	1.34 (4.4)
Mean aerodynamic chord, m (ft)	1.13 (3.71)
Incidence angle at root and tip, deg	0
Quarter chord sweep angle, deg	8.5

Vertical Tail:

Airfoil	NACA 0003
Area (including rudder), m^2 (ft^2)	2.12 (22.77)
Span, m (ft)	1.51 (4.96)
Aspect ratio	1.08
Taper ratio	0.5
Root chord, m (ft)	1.87 (6.14)
Mean aerodynamic chord, m (ft)	1.3 (4.26)
Quarter chord sweep angle, deg	14.0

Winglet:

Airfoil	Modified GA(W)-2
Area, m^2 (ft^2) (per winglet)	1.80 (19.34)
Span, m (ft)	1.52 (4.98)
Aspect ratio	1.28
Taper ratio	0.56

Table 2.1: (concluded)

Root chord, m (ft)	1.52 (4.98)
Mean aerodynamic chord, m (ft)	1.22 (3.99)
Leading edge sweep angle, deg	12.5

Weights:

Typical operating weight, N (lb)	34,696 (7800)
Empty weight, N (lb)	18,238 (4100)

Powerplant:

Number of engines	1
Manufacturer	Wright
Model	R-1300-1B Cyclone
Takeoff power, kw (hp)	1072.4 (800)
Takeoff rpm	2600

Propeller:

Manufacturer	Hamilton Standard
Model	3 D40/EAC
Number of blades	3
Diameter, m (ft)	2.74 (9)

Table 2.2: Airfoil Coordinates for Winglets

x/c	z/c for -	
	Upper surface	Lower surface
0	0	0
.0020	.0077	-.0032
.0050	.0119	-.0041
.0125	.0179	-.0060
.0250	.0249	-.0077
.0375	.0296	-.0090
.0500	.0333	-.0100
.0750	.0389	-.0118
.1000	.0433	-.0132
.1250	.0469	-.0144
.1500	.0499	-.0154
.1750	.0525	-.0161
.2000	.0547	-.0167
.2500	.0581	-.0175
.3000	.0605	-.0176
.3500	.0621	-.0174
.4000	.0628	-.0168
.4500	.0627	-.0158
.5000	.0618	-.0144
.5500	.0599	-.0122
.5750	.0587	-.0106
.6000	.0572	-.0090
.6250	.0554	-.0071
.6500	.0533	-.0052
.6750	.0508	-.0033
.7000	.0481	-.0015
.7250	.0451	.0004
.7500	.0419	.0020
.7750	.0384	.0036
.8000	.0349	.0049
.8250	.0311	.0060
.8500	.0270	.0065
.8750	.0228	.0064
.9000	.0184	.0059
.9250	.0138	.0045
.9500	.0089	.0021
.9750	.0038	-.0013
1.0000	-.0020	-.0067

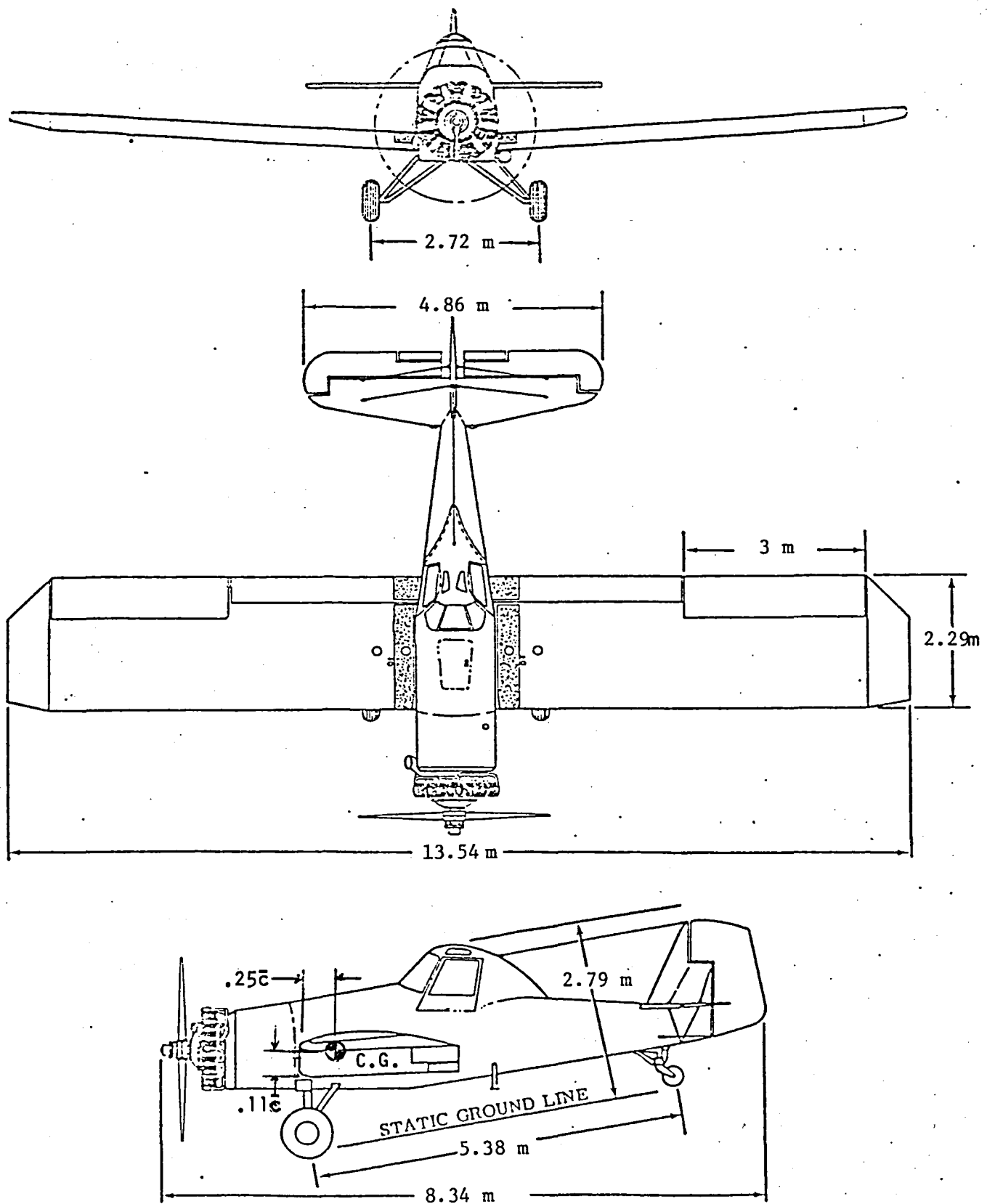


Figure 2.1: Three-view of Ayres Thrush S2R-800

2.7

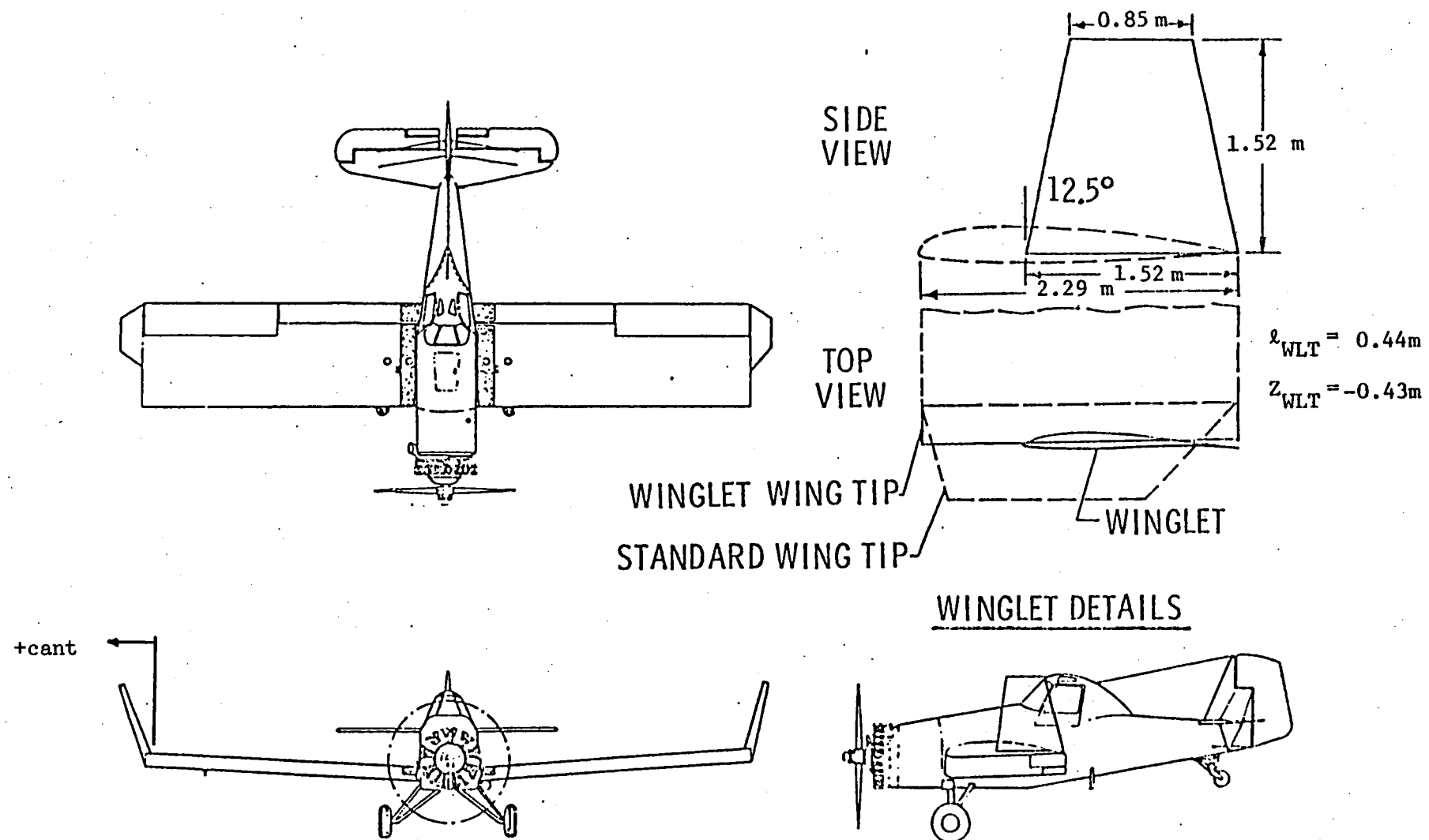
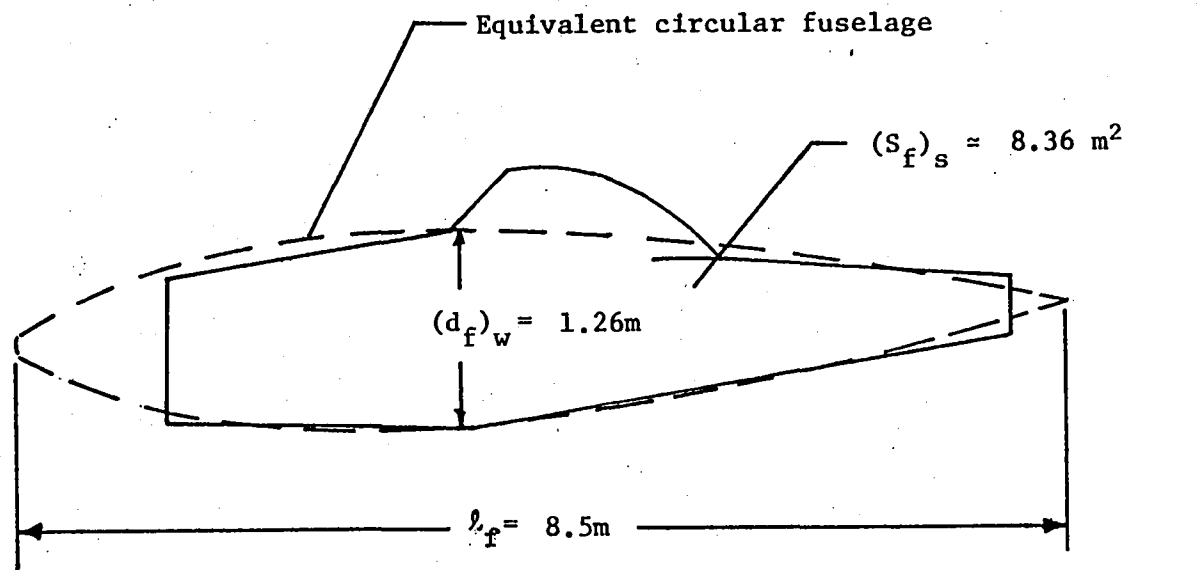


Figure 2.2: Three-view sketch of Ayres Thrush S2R-800 showing winglet installation (Reference 5)

2.1 Geometric Parameters of Fuselage, Wing, Winglet, and Tails

Many of the geometric parameters used in the subsequent analysis were taken from manufacturer's specifications or actual blueprints. Pertinent dimensions for the fuselage, wing, winglet, horizontal tail, and vertical tail are shown in Figures 2.1.1, 2.1.2, 2.1.3, and 2.1.4, respectively. It should be noticed that the wing span as defined in Figure 2.1.2 is different from the wing span definition in Figure 2.1. This is done for convenience in the analysis so that the wing may be considered to be an untapered wing, i.e., the tapered wing tips have been replaced with an untapered tip of equivalent area. This has little, if any, significant effects on the accuracy of the analysis as evidenced by Figures 3.1.1 - 3.2.3. Care must be taken not to generalize this conclusion to other airplane configurations.



$$\begin{aligned}(d_f)_{WLT} &= 1.62\text{ m} \\ (d_f)_v &= 0.61\text{ m} \\ \bar{V} &= 7.72\text{ m}^3 \\ w &= 1.26\text{ m} \\ z_w &= 0.43\text{ m} \\ h &= 1.26\text{ m}\end{aligned}$$

Figure 2.1.1 Geometric parameters of the fuselage

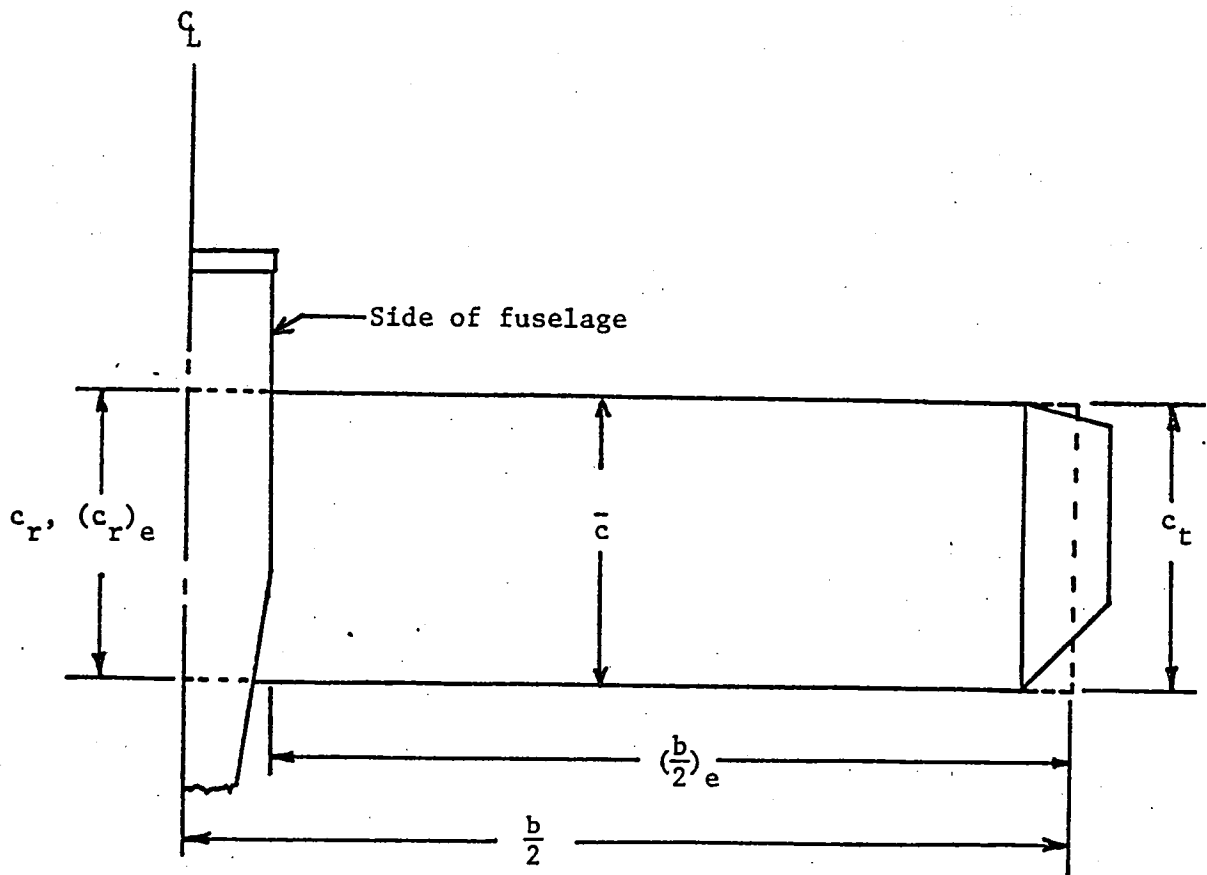


Figure 2.1.2: Definition sketch of wing dimensions

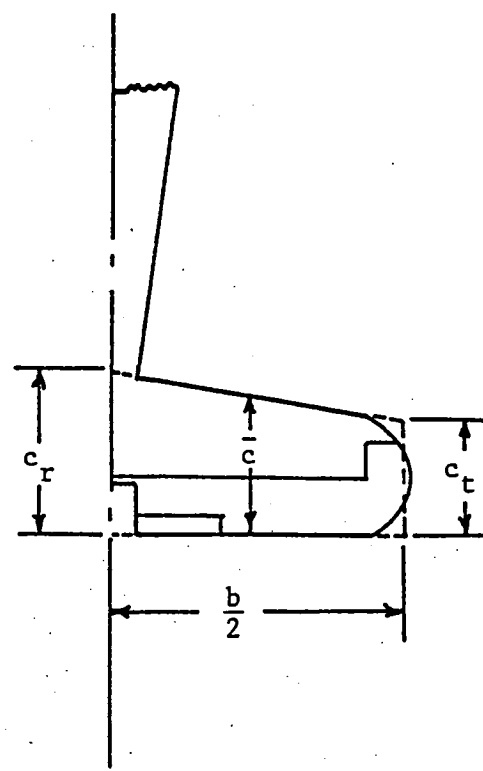


Figure 2.1.3: Definition sketch of horizontal tail

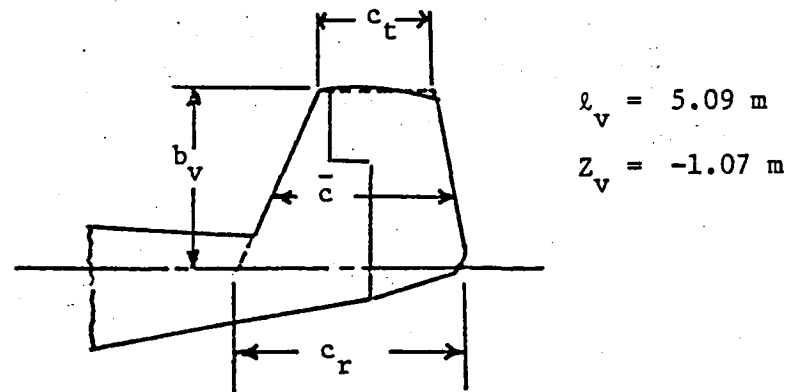


Figure 2.1.4: Definition sketch of vertical tail

2.2 Flight Condition Used in the Analysis

The center of gravity of the airplane was fixed at 25 percent of the wing mean aerodynamic chord in the longitudinal direction and at 11 percent of the wing mac above the wing root. See Figure 2.1.

Since the S2R-800 is a low subsonic regime vehicle, the flow has been assumed to be incompressible; therefore, the results of the analysis are valid for both the climb and cruise speeds of the Ayres Thrush.

CHAPTER 3

PRESENTATION OF RESULTS

In this chapter the results of the analysis are presented and discussed. Full scale wind-tunnel data ($\bar{q} = 718.2 \text{ N/m}^2$, Reference 4) are compared to theoretical results where applicable. These results apply to both cruise and climb speeds of the Ayres Thrush S2R-800.

3.1 Lift Curve

The analytical method used in predicting the lift curve of the S2R-800 is presented in Chapter 4. The Quasi-Vortex-Lattice Method (QVLM) prediction of the lift curve is discussed in Section 6.2. The results of both methods are compared to each other and to full-scale wind-tunnel data in Figure 3.1.1.

Figure 3.1.1 shows that both predictions agree very well with wind tunnel data. The QVLM prediction underestimates the lift curve slope because QVLM assumes that the wing dominates the lift behavior of the total airplane and therefore doesn't take into account fuselage and/or empennage lift effects.

3.2 Sideslip Derivatives

In Figures 3.2.1 through 3.2.3, the calculated sideslip derivatives for the winglet off configuration are compared to full scale wind tunnel data. The calculations compare favorably with the tunnel data. In Figure 3.2.2 the predicted $C_{n\beta}$ increases with increasing angle of attack, while the tunnel data shows $C_{n\beta}$ decreasing with increasing angle of attack. This is to be expected, since the

analytical method taken from Reference 1 does not account for fuselage and wing-fuselage interference effects on $C_{n\beta}$. However, the nominal predicted value of $C_{n\beta}$ agrees well with the average tunnel $C_{n\beta}$.

Comparing Figures 3.2.4 - 3.2.6 to 3.2.7 - 3.2.9, it can be seen that winglet effect on the sideslip derivatives has not been properly accounted for in the analytical method of Reference 1. This is especially evident in the sideslip derivative $C_{\lambda\beta}$, where the computer results (Reference 3) indicate that winglets have a very strong influence on $C_{\lambda\beta}$, while the analytical results (Reference 1) show only a weak influence.

Figures 3.2.7 - 3.2.9 show that winglet cant angle has a significant influence on the sideslip derivatives. No wind tunnel data for the airplane-winglet configuration were available.

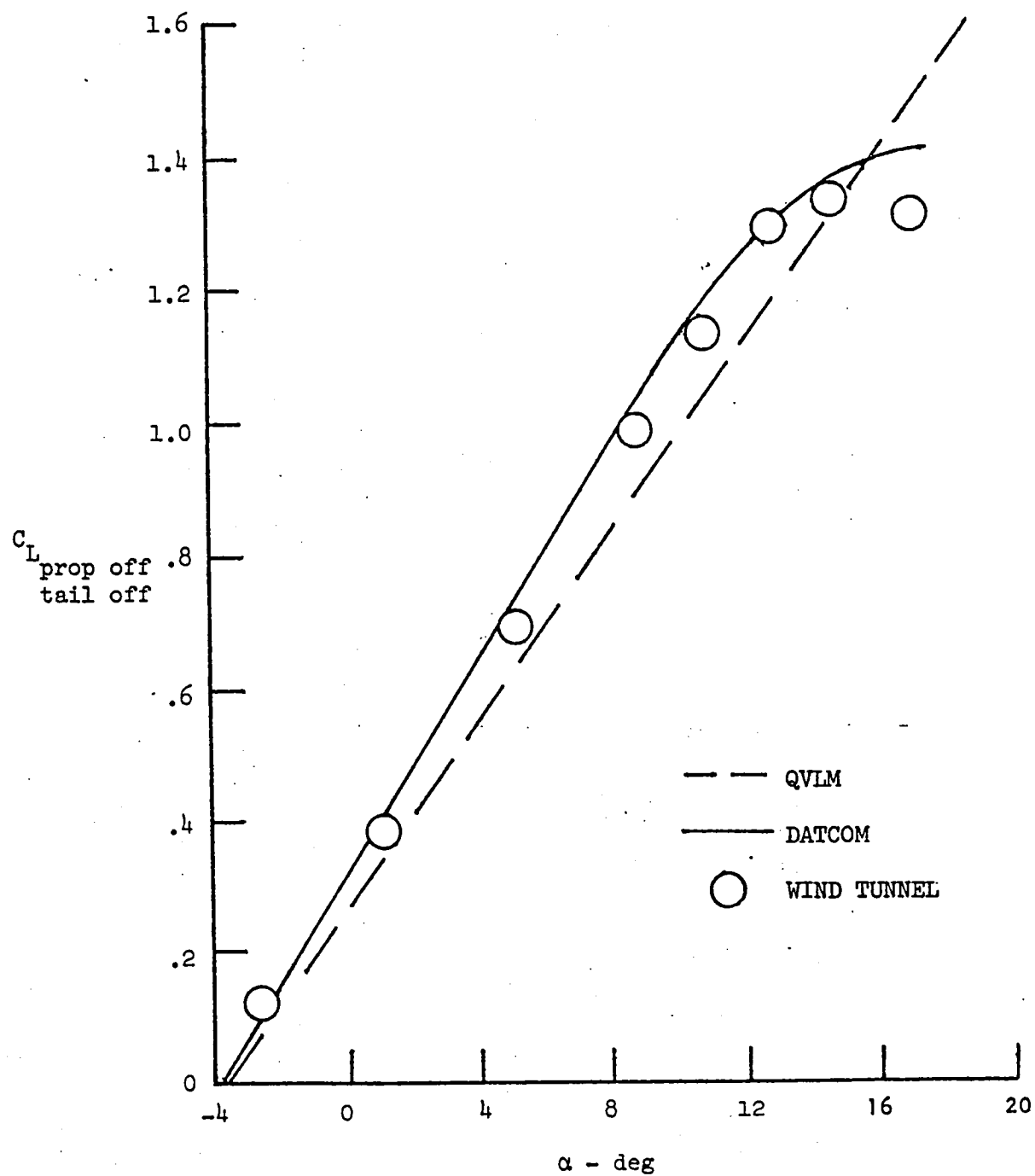


Figure 3.1.1: Lift curve of Ayres Thrush S2R-800.

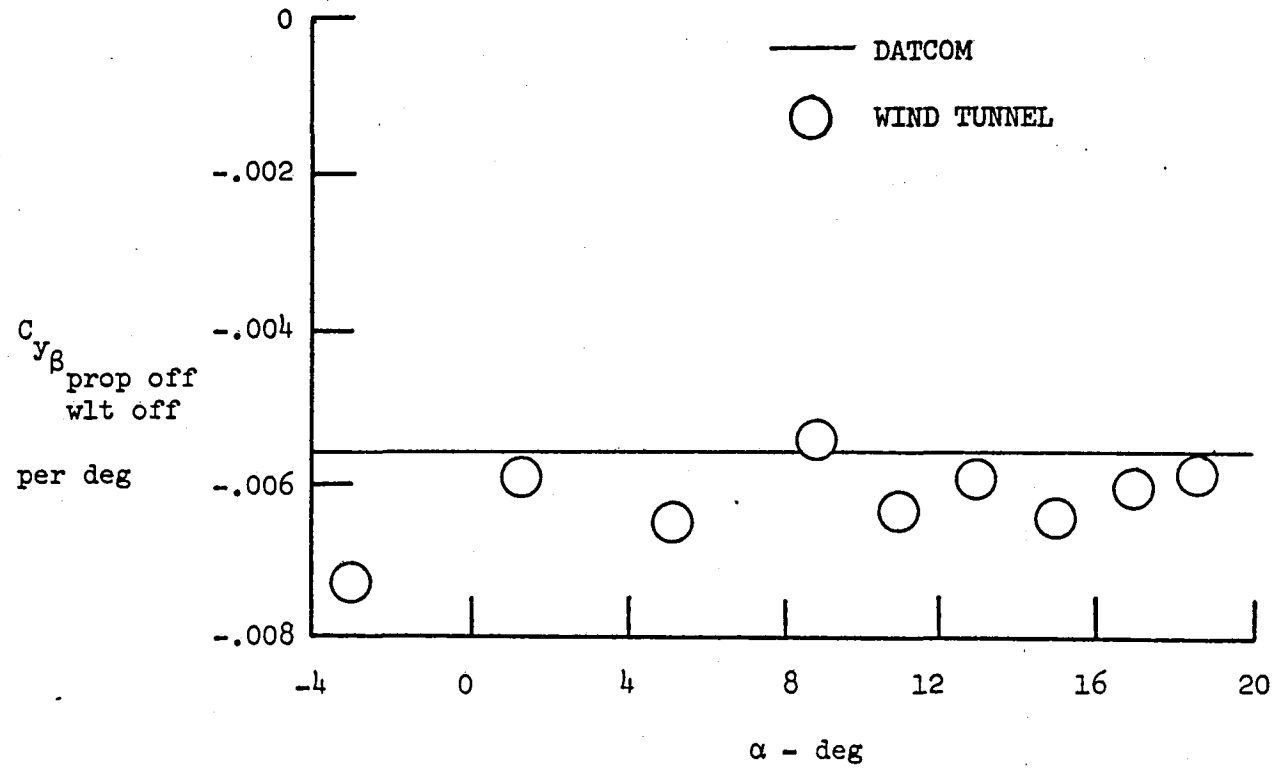


Figure 3.2.1: Comparison of predicted $C_{y\beta}$, winglets off,
 to full-scale wind tunnel data for the
 Ayres Thrush S2R-800.

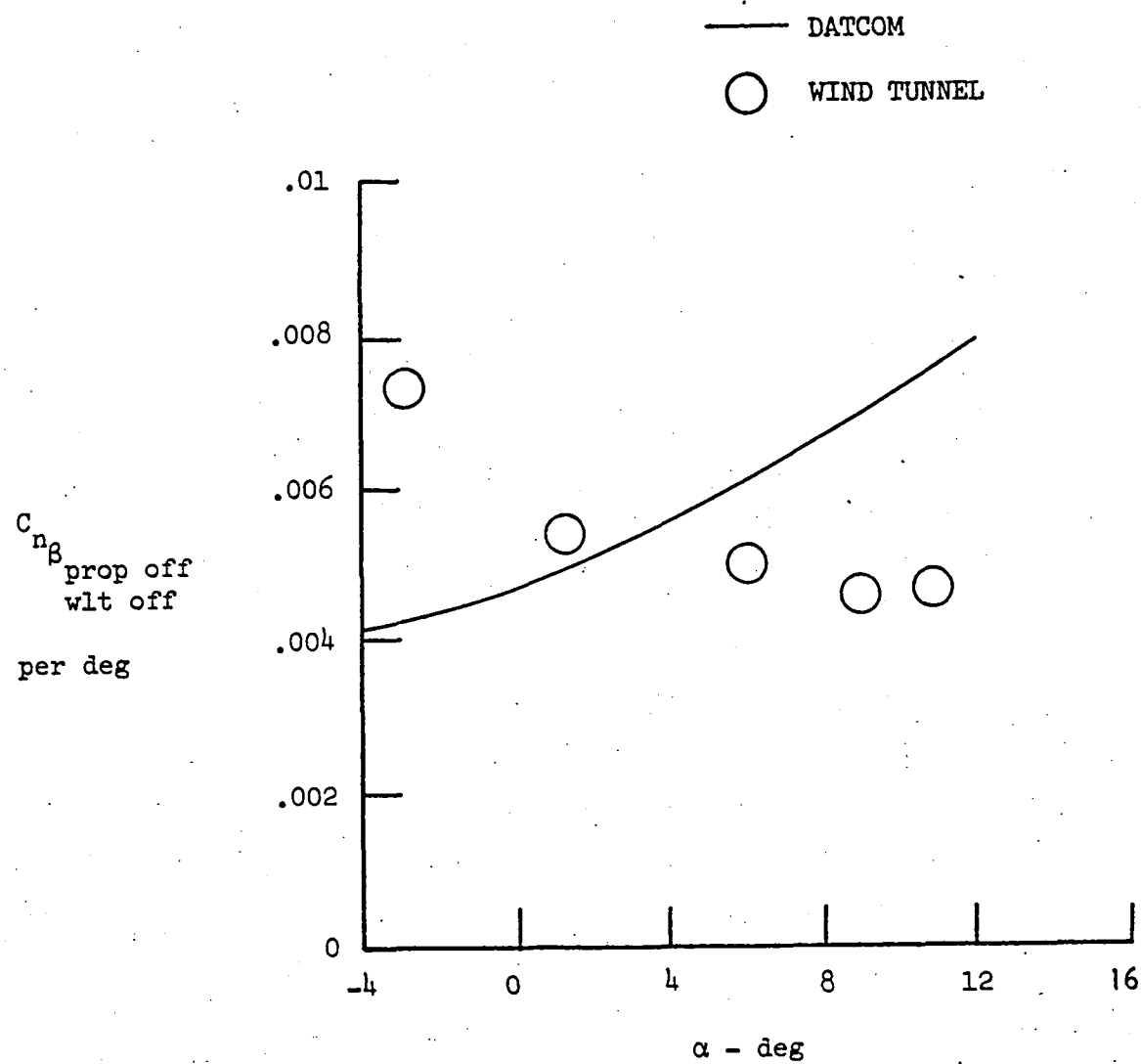


Figure 3.2.2: Comparison of predicted $C_{n\beta}$,
 winglets off, to full scale wind
 tunnel data for the Ayres Thrush
 S2R-800.

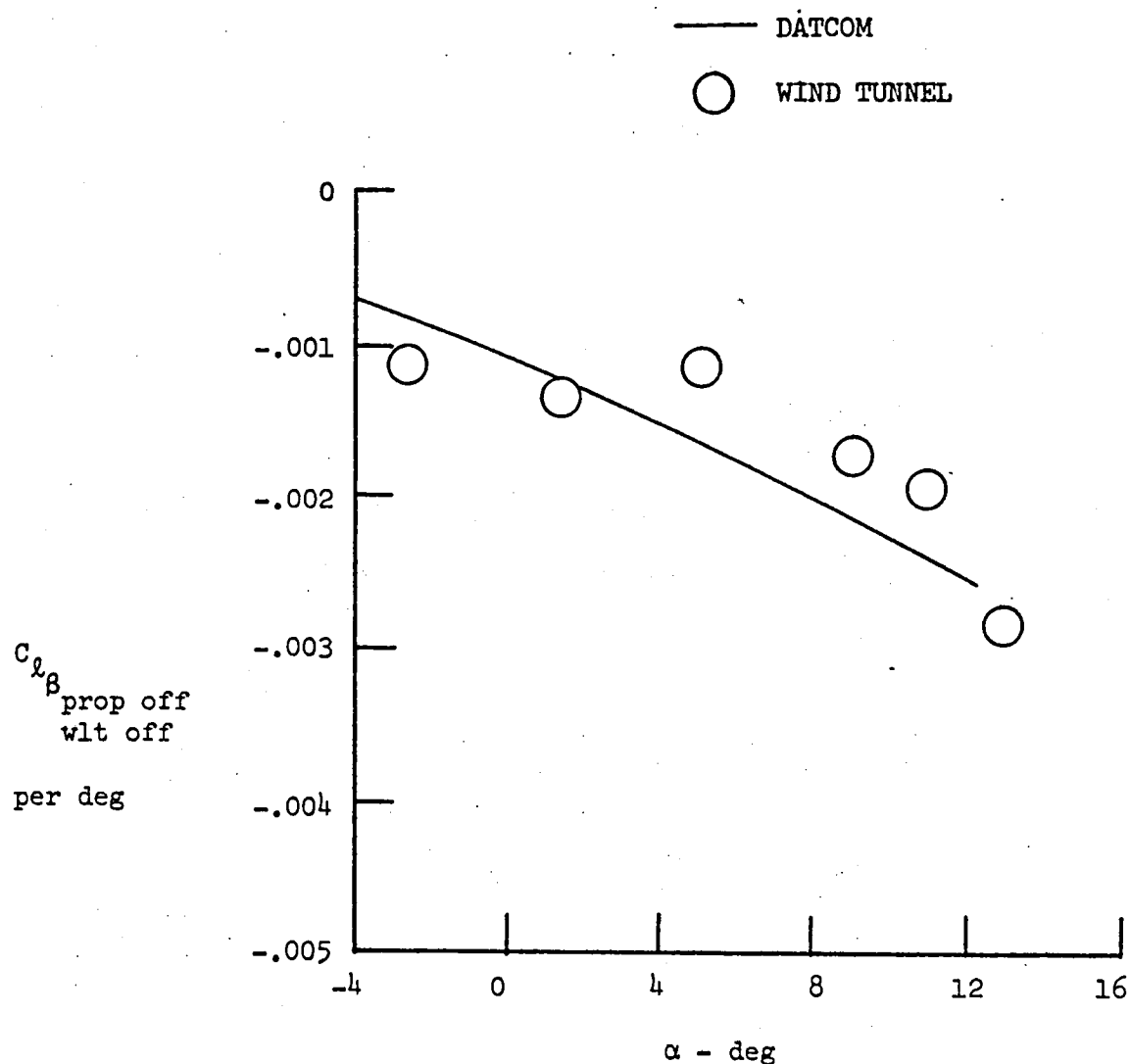


Figure 3.2.3: Comparison of predicted $C_{l\beta}$,

winglets off, to full scale wing
tunnel data for the Ayres Thrush
S2R-800.

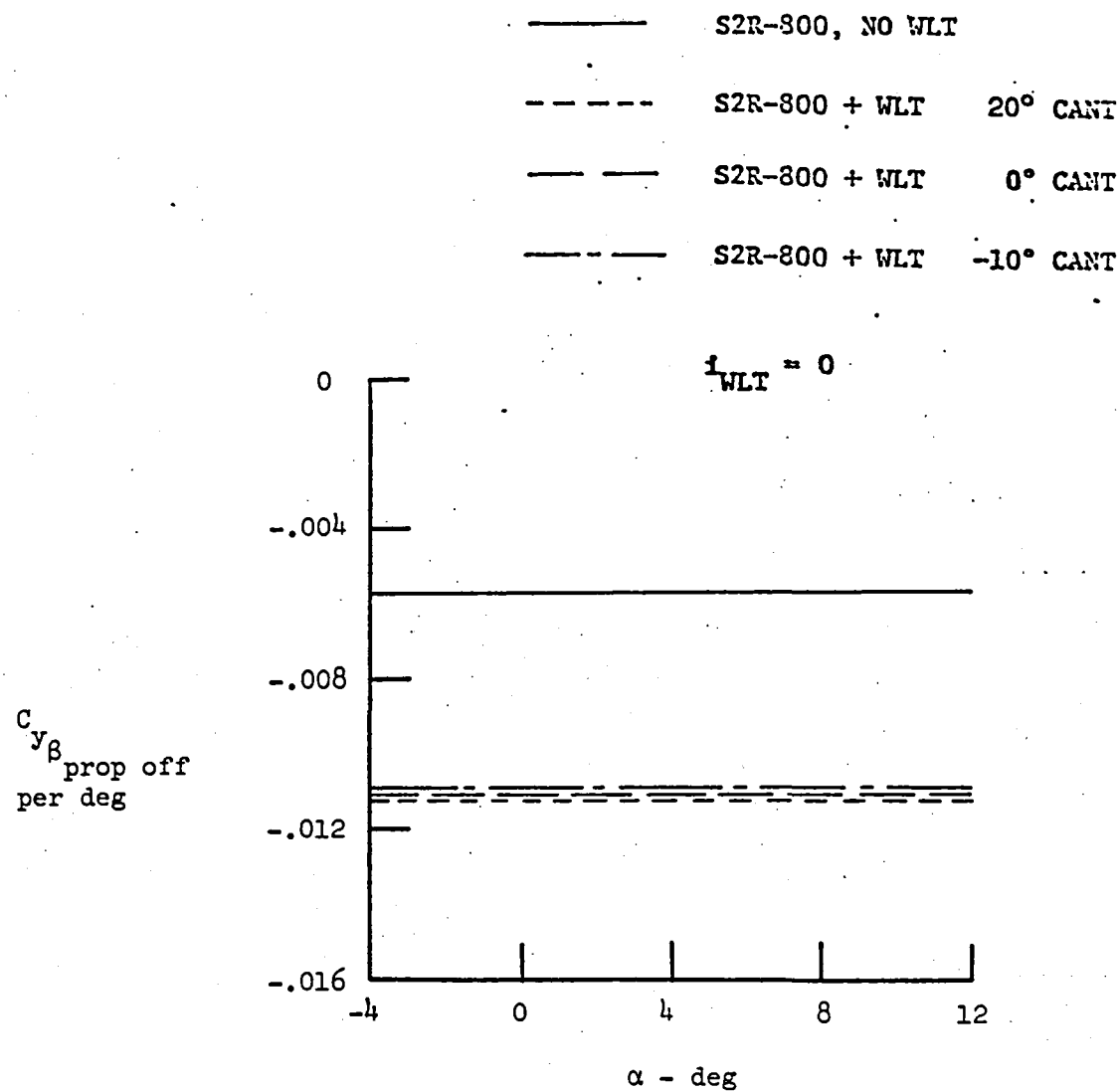


Figure 3.2.4: Effect of winglet cant angle on airplane $C_{y\beta}$ based on DATCOM methods.

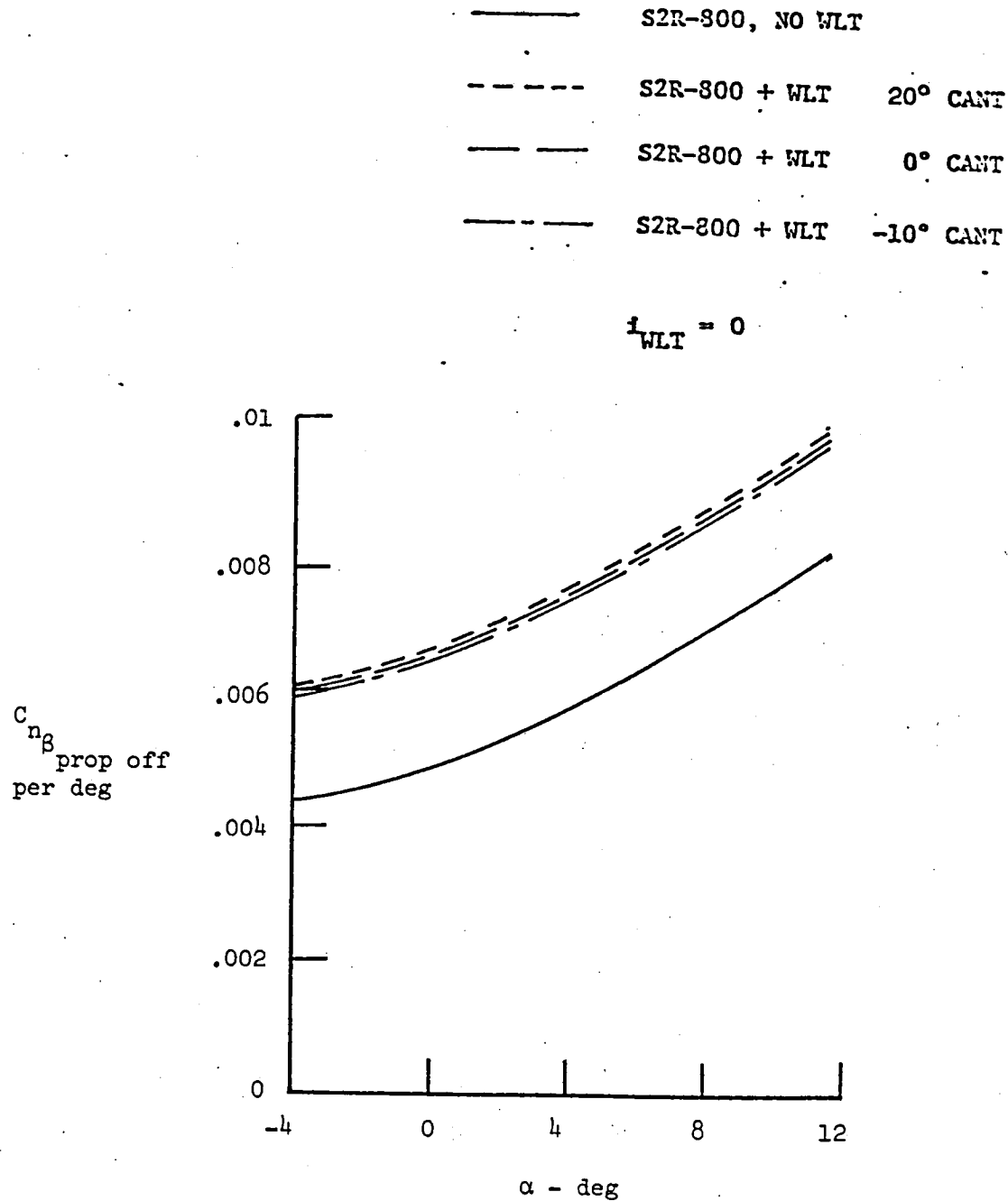


Figure 3.2.5: Effect of winglet cant angle on airplane $C_{n\beta}$ based on DATCOM methods.

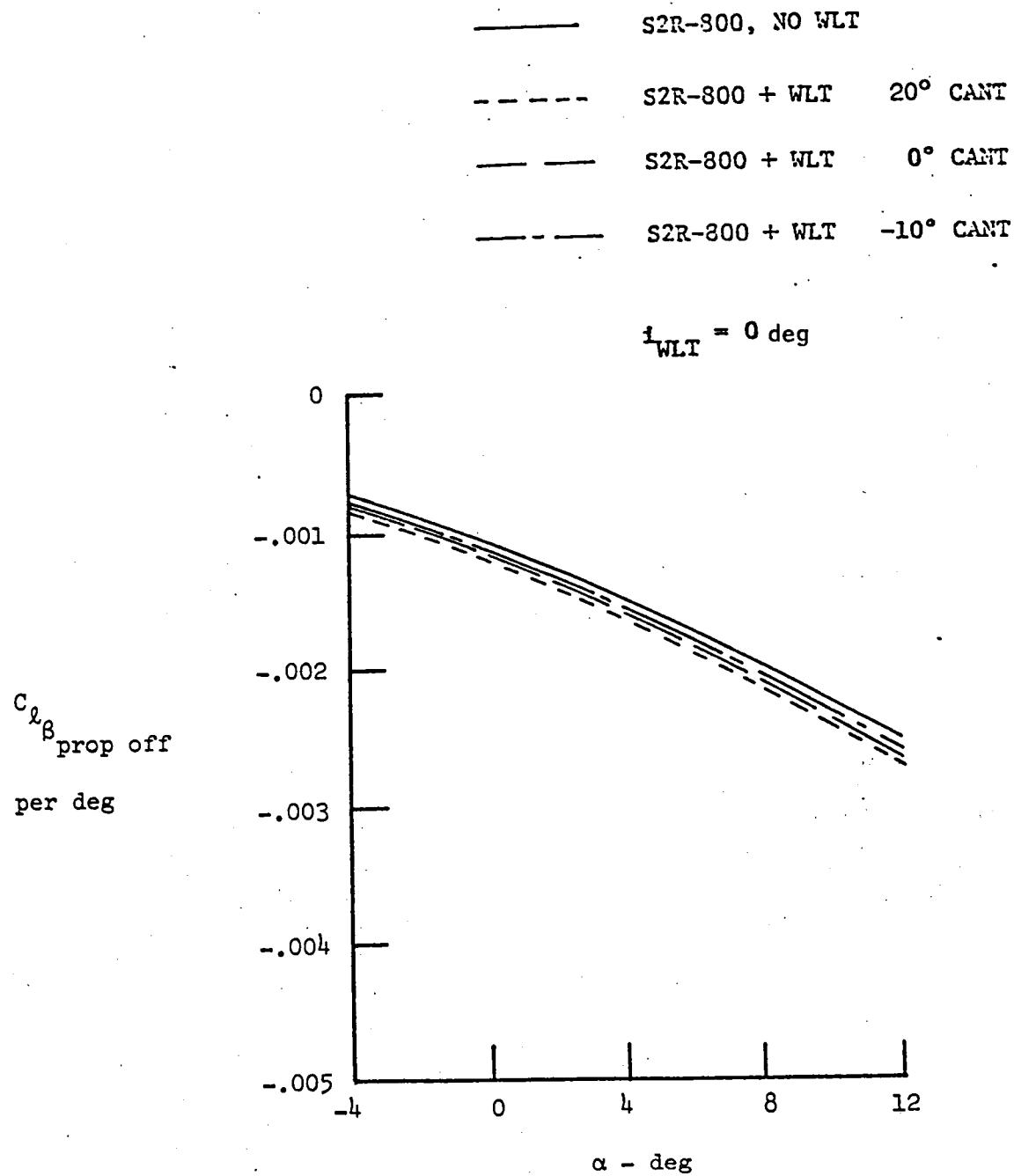


Figure 3.2.6: Effect of winglet cant angle on airplane $C_{\ell\beta}$ based on DATCOM methods.

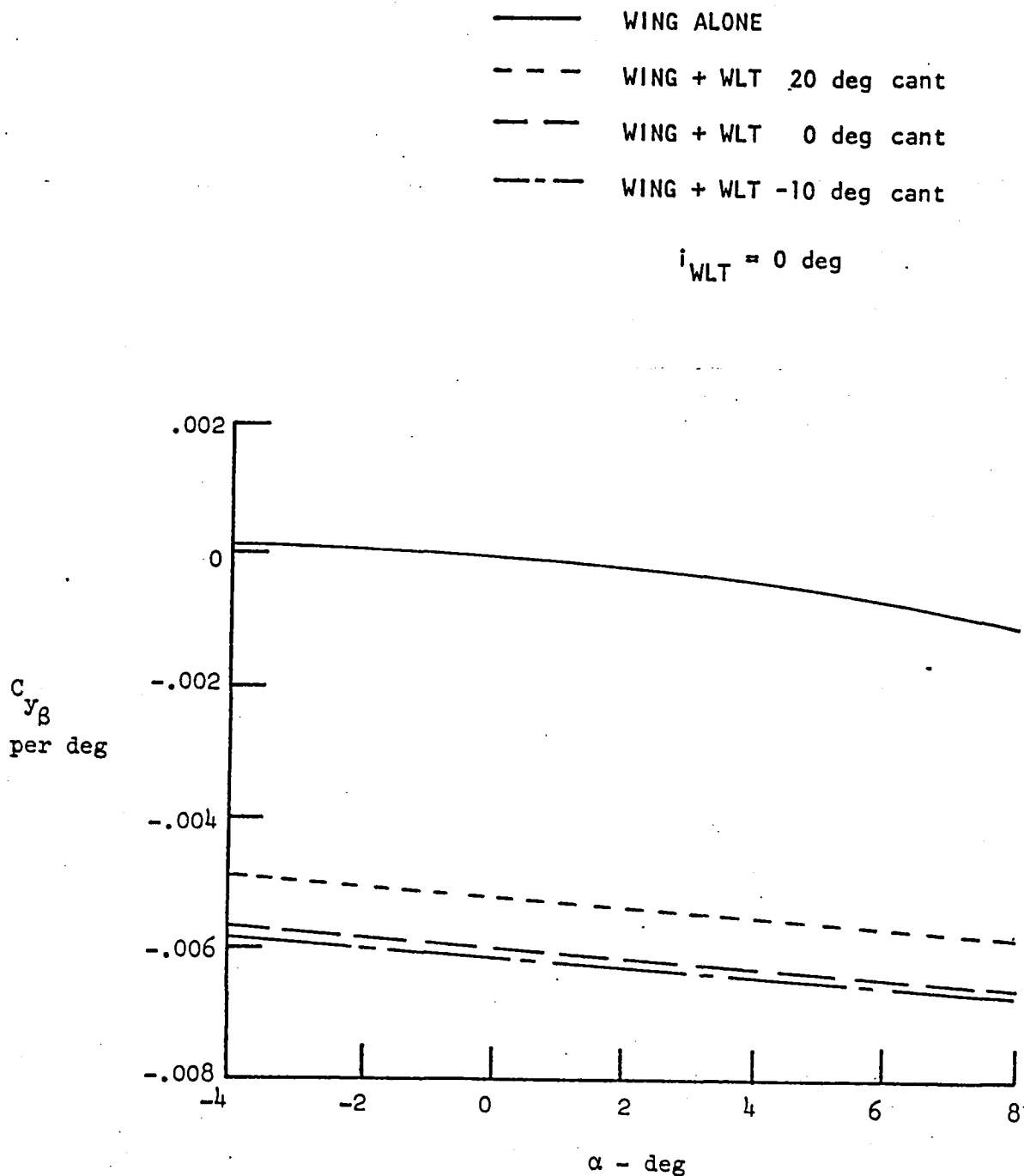


Figure 3.2.7: Effect of winglet cant angle on $C_{y\beta}$ based on QVLM computation for the S2R-800.

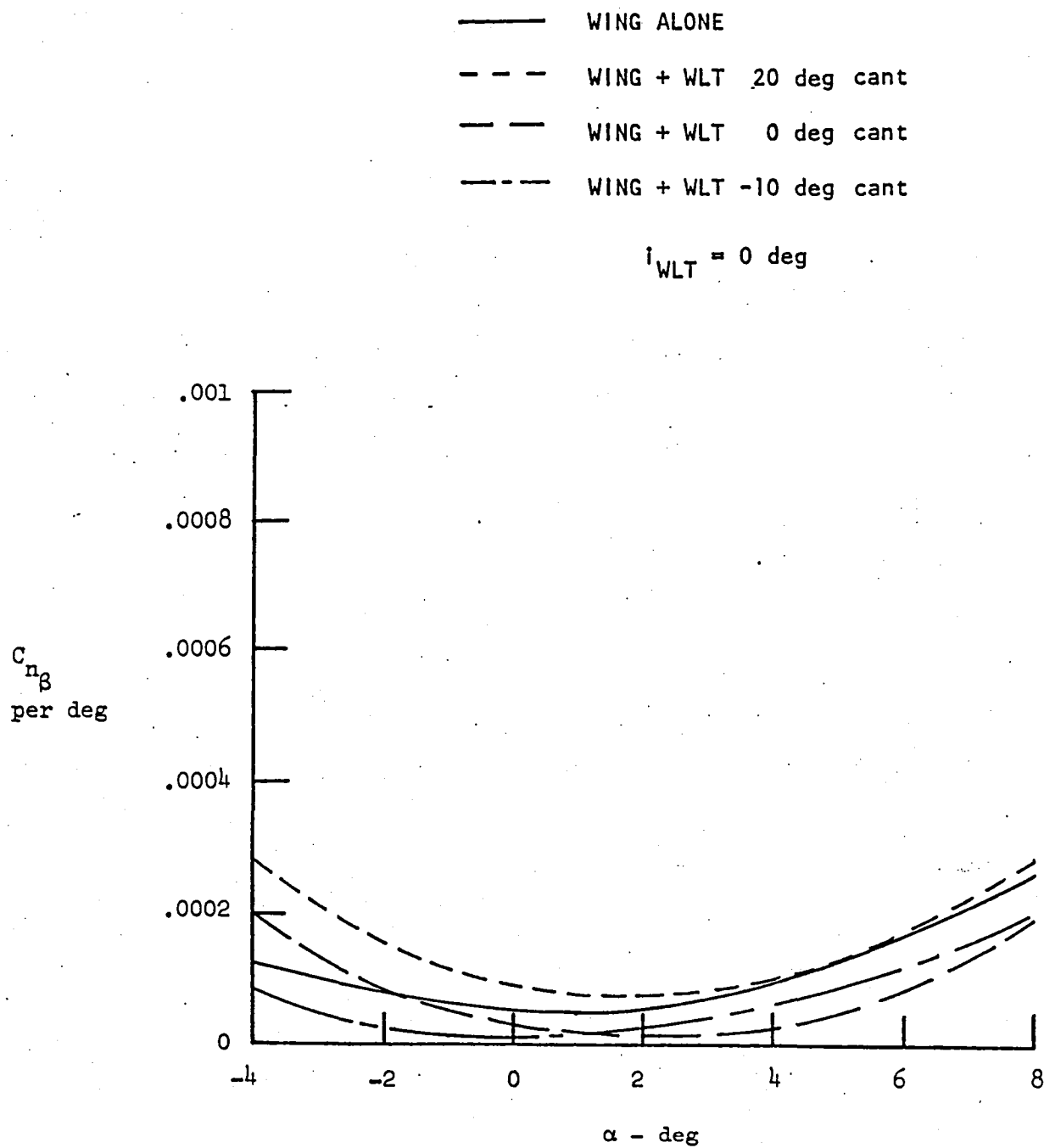


Figure 3.2.8: Effect of winglet cant angle on $C_{n\beta}$ based on QVLM computation for the S2R-800.

——— WING ALONE
 - - - - WING + WLT 20 deg cant
 - - - - WING + WLT 0 deg cant
 - - - - WING + WLT -10 deg cant

$$\alpha_{WLT} = 0 \text{ deg}$$

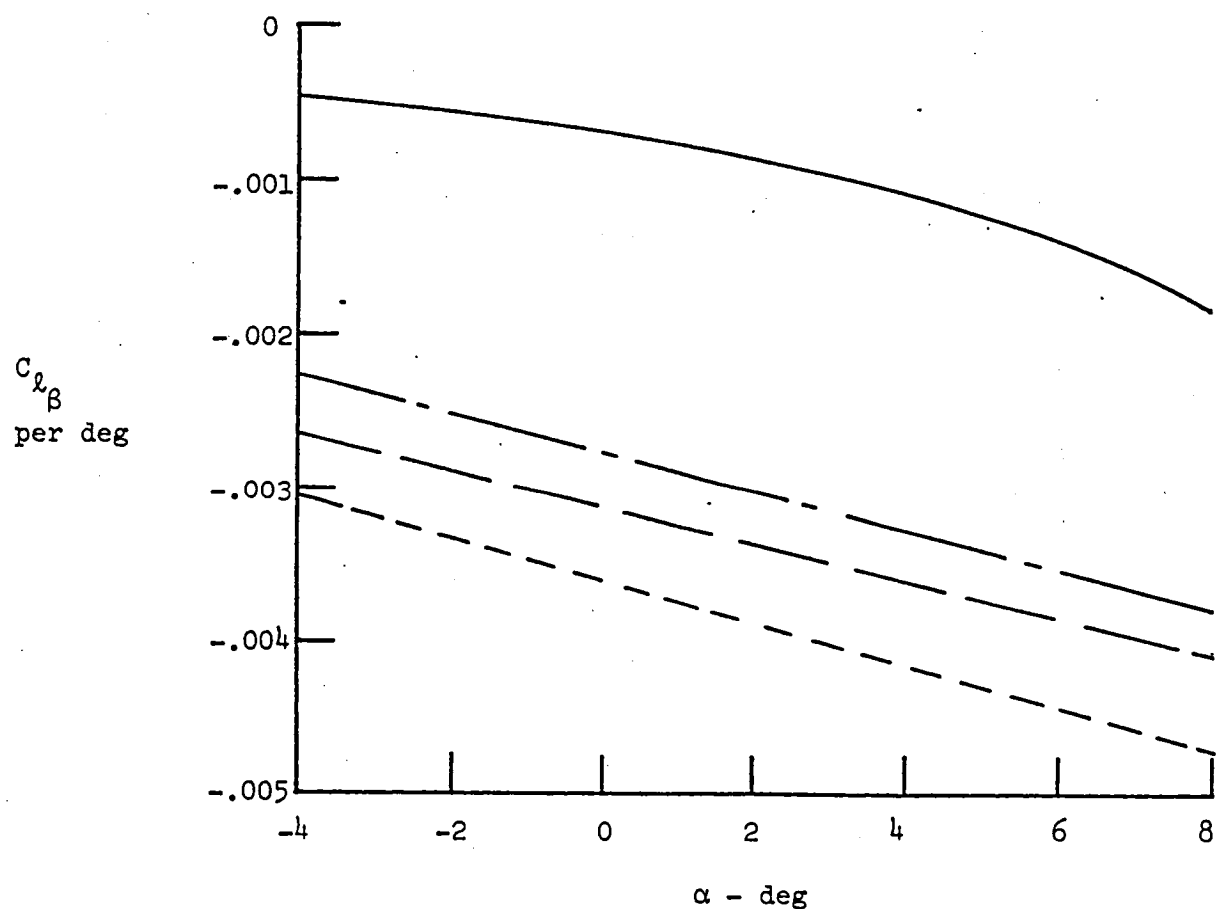


Figure 3.2.9: Effect of winglet cant angle on $C_{l\beta}$
 based on QVLM computation for the
 S2R-800.

CHAPTER 4

PREDICTION OF PROPELLER-OFF, HORIZONTAL TAIL-OFF LIFT CHARACTERISTICS USING AN ANALYTICAL METHOD

In this chapter the propeller-off, horizontal tail-off lift behavior of the Ayres Thrush will be discussed. This chapter presents the methods used in calculating the lift characteristics of the Thrush and illustrates the contribution of each relevant component to these characteristics. Table 2.1 lists the pertinent parameters and their magnitudes used in the analysis. All calculations were made in English units. Extensive use of Reference 1 was made to predict the lift behavior of the Thrush.

4.1 Zero Lift Angle of Attack, α_0

The zero lift angle of attack at low speeds of the complete airplane, minus the horizontal tail, is considered to be relatively independent of fuselage effects and is primarily determined by the wing airfoil properties. Therefore, the airplane zero lift angle will be found by considering only the wing including the effect of wing twist.

4.1.1 Wing Contribution, $(\alpha_0)_{\theta=0} + (\alpha_0)_\theta$

For untwisted constant section wings the zero lift angle of attack is given by Equation 4.1.1.1 from Reference 1.

$$(\alpha)_{\theta=0} = \alpha_i - \frac{C_{\ell_i}}{C_{\ell_a}} \quad \text{deg} \quad (4.1.1.1)$$

where:

α_i is the angle of attack for the wing section design lift coefficient, obtained from Table 2.1

C_{L_i} is the wing section design lift coefficient, from Table 2.1

C_{L_α} is the wing section lift curve slope, from Table 2.1

To account for wing twist, Equation 4.1.1.2 from Reference 1 is used.

$$(\alpha_o)_\theta = \left(\frac{\Delta\alpha_o}{\theta} \right) \theta \quad \text{deg.} \quad (4.1.1.2)$$

where:

$\frac{\Delta\alpha_o}{\theta}$ is the change in wing zero-lift angle of attack due to a unit change in linear wing twist, obtained from Figure 4.1.1.1
 θ is the twist of the wing tip with respect to the root section, in degrees (negative for washout), from Table 2.1.

Table 4.1.1.1 summarizes the wing contribution to the airplane zero lift angle of attack.

4.1.2 α_o of the Ayres Thrush

The zero lift angle of attack of the complete airplane, prop-off, horizontal tail-off, is considered to be identical to the wing-alone α_o . Therefore, for the Ayres Thrush:

$$\alpha_o = -3.69 \quad \text{deg}$$

4.2 Lift-Curve Slope, C_{L_α}

For a conventional horizontal tail-off configuration, the lift-curve slope in the linear angle-of-attack range can be found by considering the following components:

- (1) Wing, including interference effects
- (2) Fuselage, including nose lift and fuselage-wing interference.

4.2.1 Wing Contribution to $C_{L\alpha}$

The wing-alone lift-curve slope, based on exposed planform dimensions, for a straight tapered wing in the low subsonic region can be calculated using the standard Polhamus equation.

$$(C_{L\alpha})_w(e) = \frac{2\pi A_e / 57.3}{2 + \sqrt{\frac{A_e^2}{K^2} (1 + \tan^2 \Lambda_w c/2)} + 4} \text{ per deg} \quad (4.2.1.1)$$

where:

A_e is the aspect ratio of the wing based on its exposed planform, obtained from Table 2.1.

$$K = \frac{C_{L\alpha}}{2\pi}$$

$\Lambda_c/2$ is the wing sweep angle at the half-chord location, from Table 2.1.

Equation 4.2.1.2 from Reference 1 accounts for wing-fuselage interference on the wing contribution to $C_{L\alpha}$.

$$(C_{L\alpha})_w(f) = K_w(f) (C_{L\alpha})_w(e) \frac{S_e}{S_w} \text{ per deg} \quad (4.2.1.2)$$

where:

$K_w(f)$ is the ratio of the wing lift in the presence of the fuselage to the wing-alone lift, obtained from Figure 4.2.1.1.

S_e is the exposed wing area, obtained from Table 2.1.

The summary calculation for the wing contribution to $C_{L\alpha}$ is shown in Table 4.2.1.1.

For the Ayres Thrush:

$$(C_{L\alpha})_w(f) = 0.0732 \text{ per deg}$$

4.2.2 Fuselage Contribution to C_{L_α}

The fuselage contribution to C_{L_α} is accounted for in Equation 4.2.2.1 taken from Reference 1.

$$(C_{L_\alpha})_{f(w)} = [K_f(w) + K_N] (C_{L_\alpha})_{w(e)} \frac{S_e}{S_w} \text{ per deg} \quad (4.2.2.1)$$

where:

$K_f(w)$ is the ratio of the fuselage lift in the presence of the wing to the wing alone lift, obtained from Figure 4.2.1.1.

$$K_N = \frac{2}{57.3(C_{L_\alpha})_{w(f)}} (\frac{\pi r^2}{S_e}) \text{ and is the fuselage nose lift based on slender body theory where:}$$

r is the radius of the equivalent circular fuselage, obtained from Figure 2.1.1.

The summary calculation for the fuselage contribution to C_{L_α} is shown in Table 4.2.2.1

For the Ayres Thrush:

$$(C_{L_\alpha})_{f(w)} = 0.0130 \text{ per deg.}$$

4.2.3 C_{L_α} of the Complete Airplane, Horizontal Tail Off

The horizontal tail-off, power-off lift-curve slope of the airplane is given as:

$$C_{L_\alpha} = (C_{L_\alpha})_{w(f)} + (C_{L_\alpha})_{f(w)} \text{ per deg} \quad (4.2.3.1)$$

Table 4.2.3.1 summarizes the contribution of each component.

For the Ayres Thrush:

$$C_{L_\alpha} = 0.0862 \text{ per deg.}$$

4.3 Lift-Curve in the Non-Linear Region

To obtain a description of the non-linear portion of the lift-curve, propeller and horizontal tail off, it will be necessary to consider the following components:

- (1) the wing and wing-fuselage $C_{L_{max}}$
- (2) the wing and wing-fuselage angle of attack at $C_{L_{max}}$
- (3) the upper linearity of the wing lift-curve slope.

4.3.1 $C_{L_{max}}$ of the Wing, Wing-Fuselage

The maximum lift coefficient of a wing with twist may be estimated from the assumption that $C_{L_{max}}$ is reached when the local section lift coefficient, C_{λ} , at any position along the span is equal to the local $C_{\lambda_{max}}$ for the corresponding section. The method used is taken from Reference 2.

The first step in finding $C_{L_{max}}$ of the wing is to calculate the variation of the local section lift-coefficient with span location, at a total C_L of 1. This is done with Equation 4.3.1.1, which only applies to unswept, untapered, linearly twisted wings.

$$C_{\lambda} = C_{\lambda_a} + C_{\lambda_b} \quad (4.3.1.1)$$

where:

C_{λ_a} is the wing section lift coefficient due to wing angle of attack, given by Equation 4.3.1.2

C_{λ_b} is the wing section lift coefficient due to wing twist, given by Equation 4.3.1.3.

$$C_{L_a} = C_1 + (C_2 + C_3) \frac{4}{\pi} \sqrt{1 - \frac{\eta^2}{4}} \quad (4.3.1.2)$$

$$C_{L_b} = C_{L_a} \theta C_{L_a} C_4 (\eta + \frac{\Delta\alpha_0}{\theta}) \quad (4.3.1.3)$$

where:

C_1, C_2, C_3, C_4 are coefficients for additional and basic lift distributions, obtained from Figure 4.3.1.1

$$\eta = \frac{y}{b/2} \text{ and is the wing spanwise station}$$

θ is the wing twist measured from the wing root in degrees, negative for washout, from Table 2.1

$\frac{\Delta\alpha_0}{\theta}$ is the ratio of the change in wing zero lift angle of attack with wing twist, obtained from Figure 4.1.1.1.

Table 4.3.1.1 summarizes the calculation of the wing lift distribution. From this table the minimum value of the ratio of $(C_{L_{max}} - C_{L_b})$ to C_{L_a} @ $C_L = 1$ is considered to be the maximum lift coefficient of the wing; $C_{L_{max}}$ is the wing section maximum lift coefficient. Table 4.3.1.1 also summarizes the calculation of $C_{L_{max}}$ for the wing.

For the Ayres Thrush:

$$(C_{L_{max}})_w = 1.412$$

To account for the presence of the fuselage, Reference I gives the following equation:

$$\frac{(C_{L_{max}})_{wf}}{(C_{L_{max}})_w} = \frac{(C_{L_{max}})_{wf}}{(C_{L_{max}})_w} \quad (4.3.1.4)$$

where:

$\frac{(C_{L_{max}})_{wf}}{(C_{L_{max}})_w}$ is the ratio of the wing and fuselage $C_{L_{max}}$ to the wing-

alone $C_{L_{max}}$, obtained from Figure 4.3.1.2.

Table 4.3.1.2 summarizes the calculation for $C_{L_{max}}$ of the wing-fuselage.

For the Ayres Thrush:

$$(C_{L_{max}})_{wf} = 1.412.$$

4.3.2 The Wing and Wing-Fuselage Angle of Attack at $C_{L_{max}}$

For high-aspect-ratio, constant-section wings, the angle of attack at the wing $C_{L_{max}}$ is computed using Equation 4.2.3.1 from Reference 1.

$$(\alpha_{C_{L_{max}}})_w = \frac{(C_{L_{max}})_w}{(C_{L_{\alpha}})_w(e)} + \alpha_0 + \Delta\alpha_{C_{L_{max}}} \quad (4.3.2.1)$$

where:

$(C_{L_{max}})_w$ is obtained from Section 4.3.1 and is the wing maximum lift coefficient

$(C_{L_{\alpha}})_w(e)$ is obtained from Section 4.2.1 and is the exposed wing lift-curve slope

α_0 is obtained from Section 4.1.1 and is the wing zero lift angle of attack

$\Delta\alpha_{C_{L_{max}}}$ is the angle of attack increment for subsonic maximum lift, obtained from Figure 4.3.2.1.

To account for the fuselage, Reference 1 gives the following equation:

$$(\alpha_{C_{L_{max}}})_{wf} = \frac{(\alpha_{C_{L_{max}}})_{wf}}{(\alpha_{C_{L_{max}}})_w} \quad (4.3.2.2)$$

where:

$\frac{(\alpha_{C_L}^{\max})_{wf}}{(\alpha_{C_L}^{\max})_w}$ is the ratio of wing-fuselage angle of attack at C_L^{\max}

to the wing-alone angle of attack at C_L^{\max} , obtained from Figure 4.3.2.2.

A summary calculation for the angle of attack at C_L^{\max} is shown in Table 4.3.2.1.

For the Ayres Thrush:

$$(\alpha_{C_L}^{\max})_{wf} = 17.2 \text{ deg.}$$

4.3.3 Upper Limit of Linearity of the Lift Curve

The angle at which the lift-curve slope is no longer linear, for the tail-off Thrush configuration, is considered to be approximately equal to the corresponding angle for the wing-alone configuration. From Reference 1:

$$\alpha^+ = \alpha_1^+ + \frac{\Delta\alpha_o}{\theta} \cdot \theta \text{ deg} \quad (4.3.3.1)$$

where:

α_1^+ is the section angle of attack, in degrees, at which the lift-curve slope is no longer linear, from Table 2.1.

A summary calculation is shown in Table 4.3.3.1.

For the Ayres Thrush:

$$\alpha^+ = 8.1 \text{ degrees}$$

4.4 Summary

In this chapter an analytical method for predicting the lift behavior of the Ayres Thrush was presented. Table 4.4.1 below lists the

pertinent lift characteristics for the Ayres Thrush, horizontal tail and propeller off. Figure 4.4.1 compares these predictions to actual full-scale wind tunnel data.

Table 4.4.1: Lift Characteristics of the Ayres Thrush,
Tail and Propeller Off

<u>Symbol</u>	<u>Description</u>	<u>Reference</u>	<u>Magnitude</u>
α_0	Zero lift angle of attack, deg.	Section 4.1.1	-3.69
$C_{L\alpha}$	Linear lift-curve slope, per deg.	Section 4.2.1	0.0862
$C_{L_{max}}$	Maximum lift coefficient	Section 4.3.1	1.412
$\alpha_{C_{L_{max}}}$	Angle of attack at the maximum lift coefficient, deg.	Section 4.3.2	17.2
α^+	Angle of attack for lift-curve slope is no longer linear, deg.	Section 4.3.3	8.1

Table 4.1.1.1: Wing Contribution to α_o

<u>Symbol</u>	<u>Description</u>	<u>Reference</u>	<u>Magnitude</u>
α_i	Angle of attack at wing section design lift coefficient, deg.	Table 2.1	0.4933
c_{ℓ_i}	Wing section design lift coefficient	Table 2.1	0.5067
c_{ℓ_α}	Wing section angle of attack, per deg.	Table 2.1	0.105
$(\alpha_o)_{\theta=0}$	Zero lift angle of attack for untwisted wing, deg.	Equation 4.1.1.1	-4.33
$\frac{\Delta \alpha_o}{\theta}$	Change in zero lift angle of attack due to wing twist	Figure 4.1.1.1	-0.427
θ	Wing twist, negative for washout, deg.	Table 2.1	-1.5
$(\alpha_o)_\theta$	Zero lift angle of attack for twisted wing, deg.	Equation 4.1.1.2	0.6405

Summary: $(\alpha_o)_{\theta=0} + (\alpha_o)_\theta = -3.69$ deg.

Table 4.2.1.1: Wing Contribution to C_{L_α}

<u>Symbol</u>	<u>Description</u>	<u>Reference</u>	<u>Magnitude</u>
A_e	Exposed wing aspect ratio.	Table 2.1	5.253
K	$C_L / 2\pi$		0.9576
$\Lambda_w c/2$	Wing sweep at half chord, deg.	Table 2.1	0
$(C_{L_\alpha})_w(e)$	Exposed wing lift-curve slope, per deg.	Equation 4.2.1.1	0.0735
$K_w(f)$	Wing-fuselage interference factor	Figure 4.2.1.1	1.1
S_e	Exposed wing area, m^2 (ft^2)	Table 2.1	27.45 (295.5)
S_w	Total wing area, m^2 (ft^2)	Table 2.1	30.34 (326.6)

Summary: $(C_{L_\alpha})_w(f) = 0.0732$ per deg.

Table 4.2.2.1: Fuselage Contribution to C_{L_α}

<u>Symbol</u>	<u>Description</u>	<u>Reference</u>	<u>Magnitude</u>
$K_f(w)$	Fuselage-wing interference factor	Figure 4.2.1.1	0.16
K_N	Nose lift factor	Section 4.2.2	0.0359
$(C_{L_\alpha})_{w(e)}$	Wing lift-curve slope based on the exposed wing geometry, per deg.	Section 4.2.1	0.0735
S_e	Exposed wing area, m^2 (ft^2)	Table 2.1	27.45 (295.5)
S_w	Total wing area, m^2 (ft^2)	Table 2.1	30.34 (326.6)

Summary: $(C_{L_\alpha})_{f(w)} = 0.0130$ per deg.

Table 4.2.3.1: Linear C_{L_α} of the Ayres Thrush

$(C_{L_\alpha})_w(f)$	$(C_{L_\alpha})_f(w)$	$(C_{L_\alpha})_{\text{prop off}}$ horiz. tail off
<u>Table 4.2.1.1</u>	<u>Table 4.2.2.1</u>	<u>Equation 4.2.3.1</u>
.0732	0.0130	.0862

Table 4.3.1.1: Maximum Wing Lift Coefficient

n	C_{l_a} <u>Eq. 4.3.1.2</u>	C_{l_b} <u>Eq. 4.3.1.3</u>	$\frac{C_{l_{\max}} - C_{l_b}}{C_{l_a}}$
0	1.160	.0322	1.412
0.1	1.156	.0246	1.424
0.2	1.543	.0170	1.447
0.3	1.120	.00941	1.482
0.35	1.106	.00572	1.505
0.4	1.088	.00211	1.533
0.45	1.168	-.00138	1.565
0.5	1.045	-.00472	1.603
0.6	0.988	-.0108	1.701
0.7	0.914	-.0159	1.844
0.8	0.816	-.0195	2.070
0.9	0.675	-.0205	2.505
1.0	0.300	-.0110	5.603

Table 4.3.1.2: Summary Calculation for Wing-Fuselage $C_{L_{\max}}$

<u>Symbol</u>	<u>Description</u>	<u>Reference</u>	<u>Magnitude</u>
$\frac{(C_{L_{\max}})_{wf}}{(C_{L_{\max}})_w}$	Ratio of the wing and fuselage $C_{L_{\max}}$ to the wing-alone $C_{L_{\max}}$	Figure 4.3.1.2	1.0
Summary: $(C_{L_{\max}})_{wf} = 1.412$			

Table 4.3.2.1: Summary Calculation for $\alpha_{C_{L_{\max}}}$

<u>Symbol</u>	<u>Description</u>	<u>Reference</u>	<u>Magnitude</u>
$(C_{L_{\max}})_w$	Wing maximum lift coefficient	Section 4.3.1	1.412
$(C_{L_{\alpha_w}})_w(e)$	Exposed wing lift-curve slope, per deg	Section 4.2.1	.0735
α_{o_w}	Wing zero lift angle of attack, deg.	Section 4.1.1	-3.69
$\Delta\alpha_{C_{L_{\max}}}$	Increment in angle of attack for wing maximum lift, deg.	Figure 4.3.2.1	1.2
$\frac{(\alpha_{C_{L_{\max}}})_{wf}}{(\alpha_{C_{L_{\max}}})_w}$	Ratio of wing-fuselage angle of attack at $C_{L_{\max}}$ to the wing-alone angle of attack at $C_{L_{\max}}$	Figure 4.3.2.2	1.03

Summary: $(\alpha_{C_{L_{\max}}})_{wf} = 17.2 \text{ deg.}$

Table 4.3.3.1: Summary for α^+ Calculations

<u>Symbol</u>	<u>Description</u>	<u>Reference</u>	<u>Magnitude</u>
α_1^+	Section angle of attack at which the lift-curve slope is no longer linear, deg.	Table 2.1	7.5
$\frac{\Delta\alpha}{\theta}$	Incremental zero lift angle due to wing twist	Figure 4.1.1.1	-0.43
θ	Wing-tip twist with respect to the wing root, neg for washout, deg.	Table 2.1	-1.5

Summary: $\alpha^+ = 8.1$ deg.

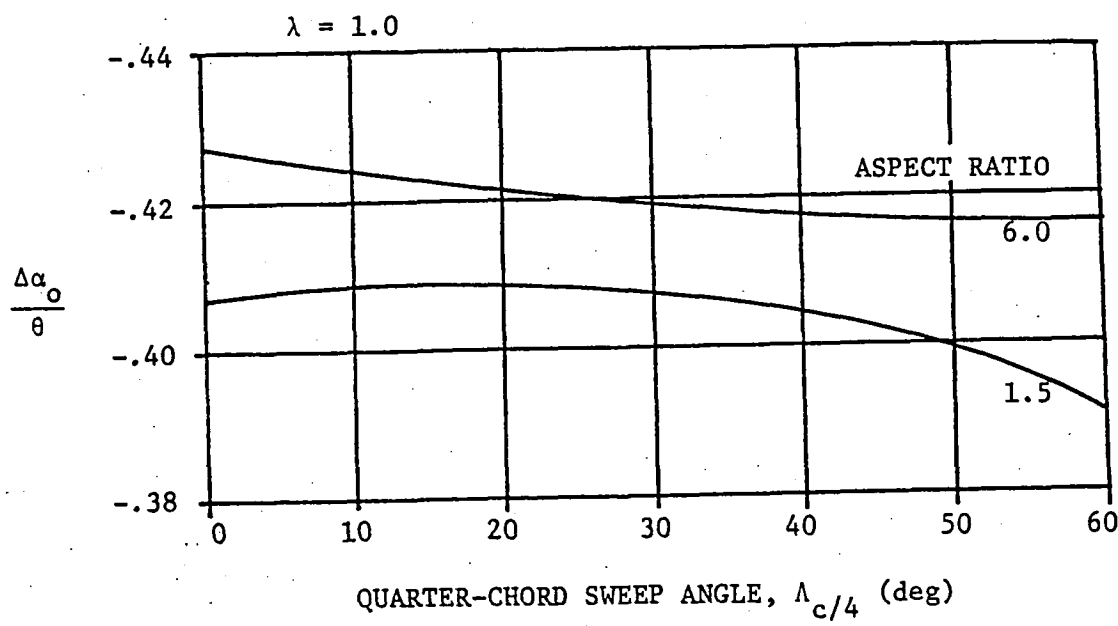


Figure 4.1.1.1: Change in Wing Zero Lift Angle of Attack
Due to Wing Twist (Reference 1)

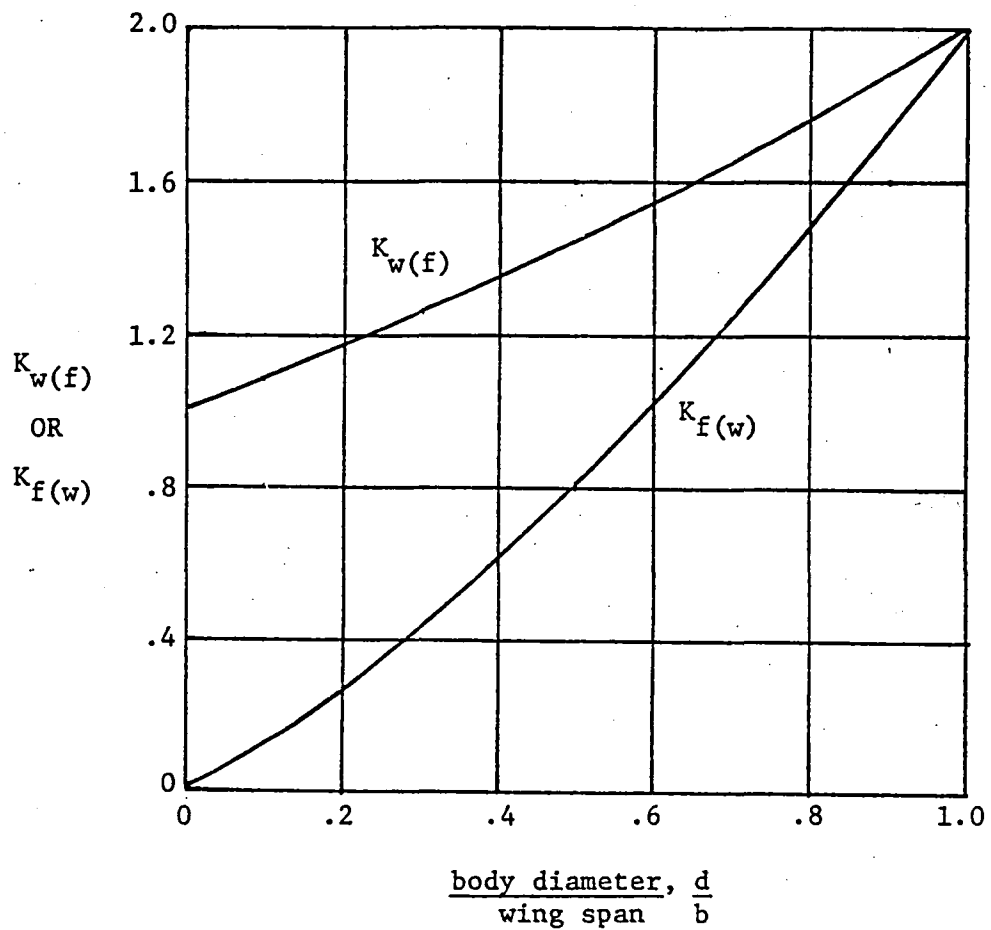


Figure 4.2.1.1: Lift Ratios $K_w(f)$ and $K_f(w)$
(Reference 1)

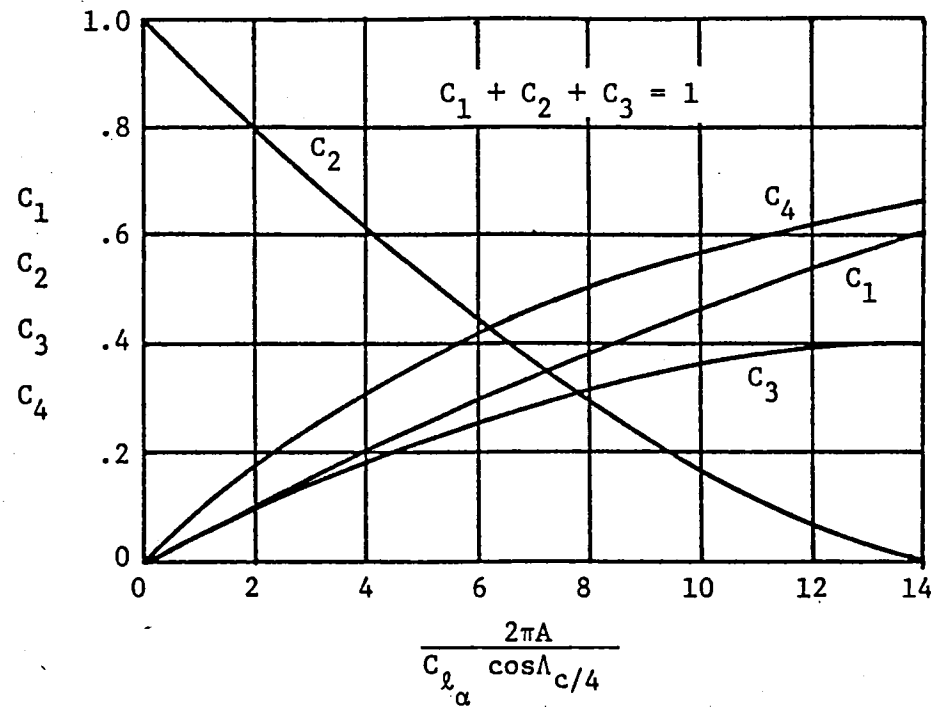


Figure 4.3.1.1: Coefficients for Additional and Basic Lift Distribution (Reference 2)

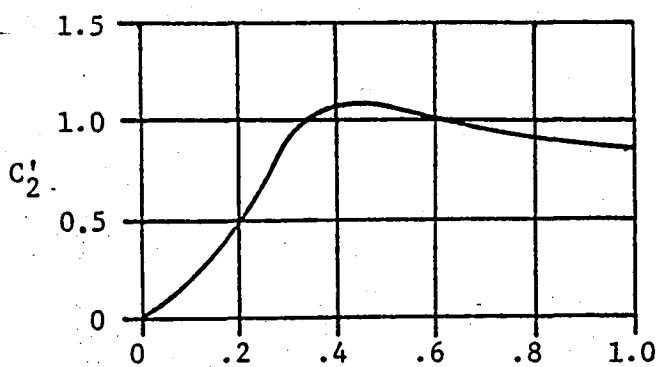


Figure 4.3.1.2(a): Taper Ratio Correction Factor
 $C_{L_{max}}$ (Reference 1)

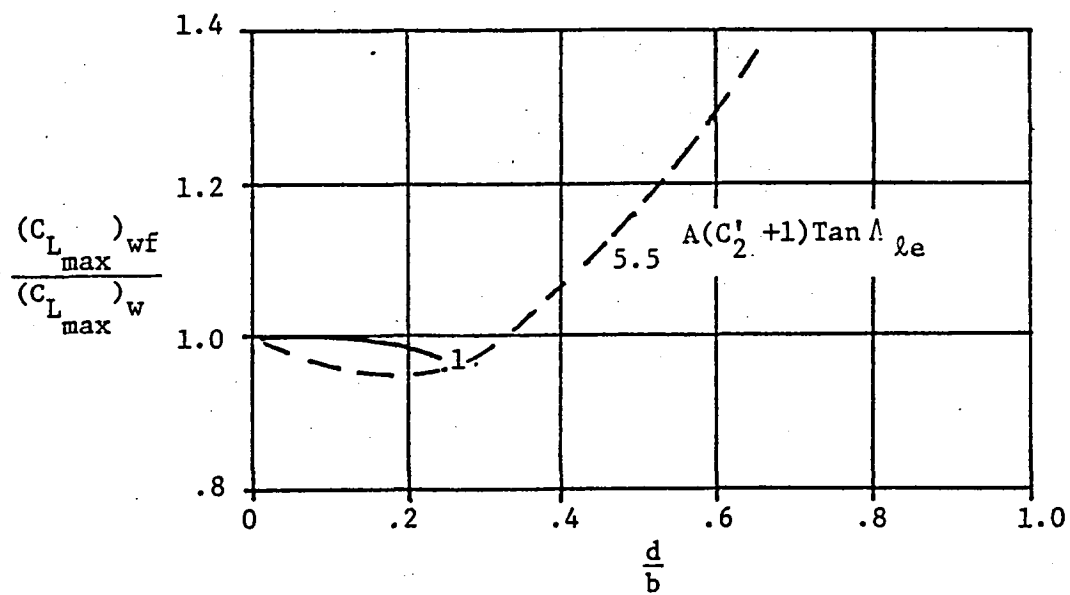


Figure 4.3.1.2(b): Wing-Fuselage Maximum Lift (Reference 1)

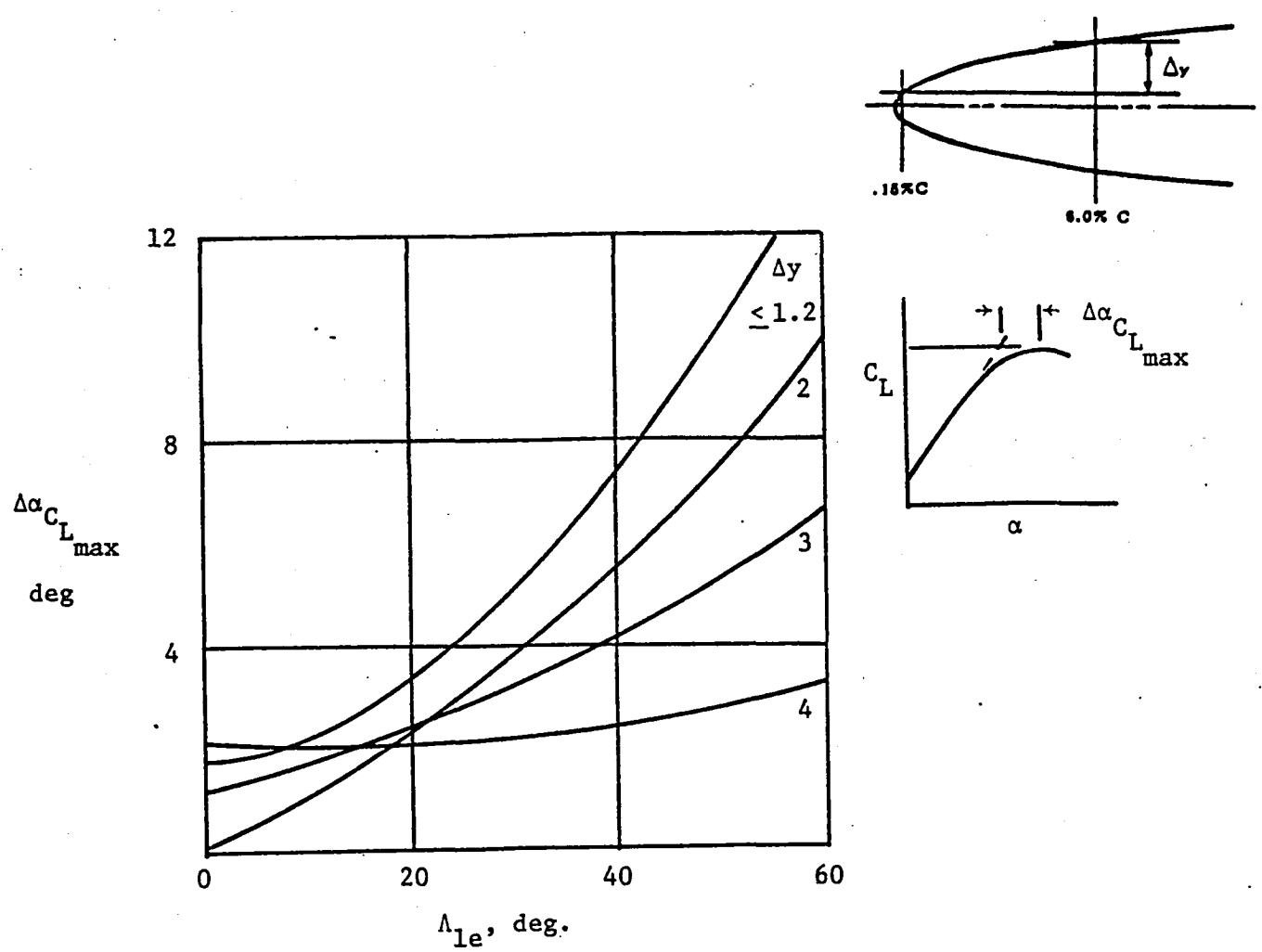


Figure 4.3.2.1: Angle of Attack Increment for Subsonic Maximum Lift (Reference 1)

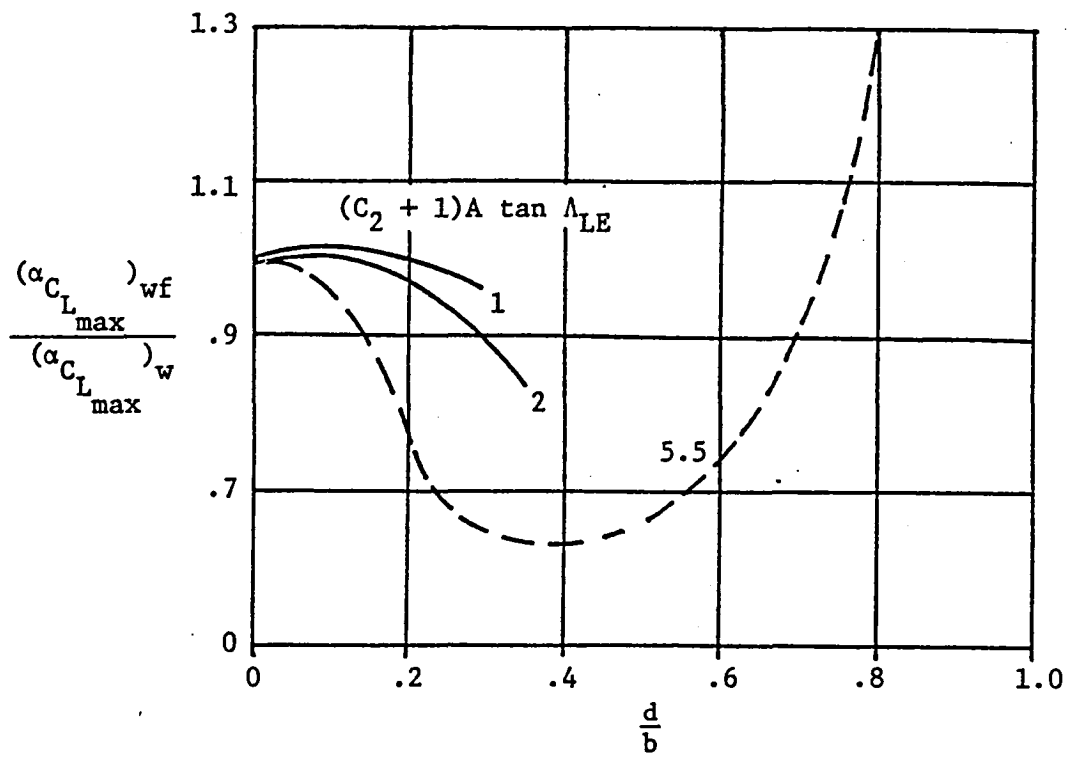


Figure 4.3.2.2: Angle of Attack for Maximum Lift.
(Reference 1)

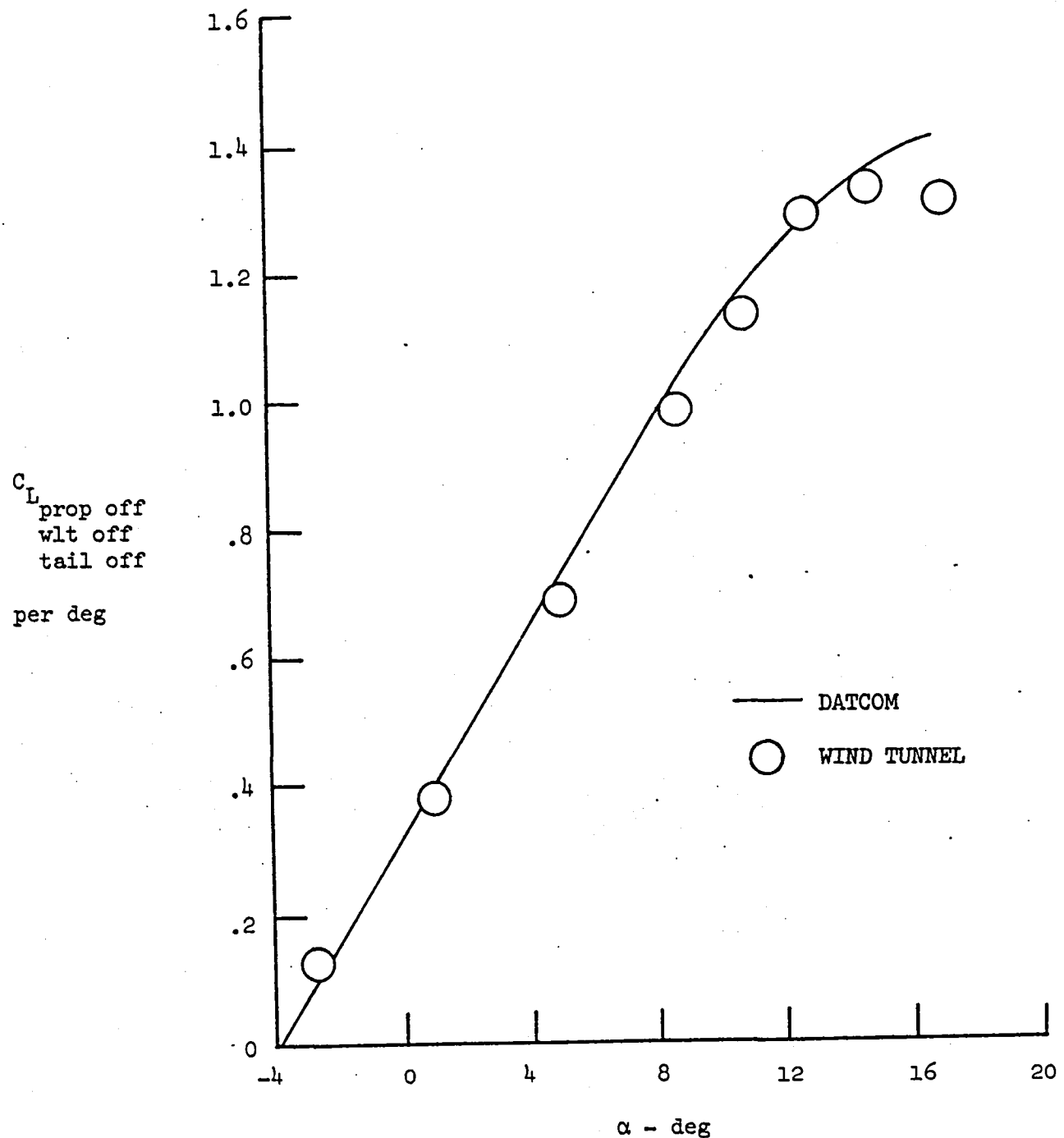


Figure 4.4.1: S2R-800 lift curve based on DATCOM methods.

CHAPTER 5

PREDICTION OF PROPELLER-OFF LATERAL-DIRECTIONAL STATIC STABILITY USING AN AYALYTICAL METHOD

In this chapter an analytical method for predicting the propeller-off, lateral-directional behavior of the Ayres Thrush will be discussed. The derivatives that are considered here are the side force due to sideslip derivative, $C_{y\beta}$; dihedral effect, $C_{\lambda\beta}$; and directional stability, $C_{n\beta}$. The methods used are primarily from Reference 1.

5.1 Side Force Derivative, $C_{y\beta}$

The side force due to sideslip, $C_{y\beta}$, of the complete airplane is found by considering the contributions of the following components:

- (1) Wing
- (2) Fuselage
- (3) Vertical tail
- (4) Winglets

Unless the horizontal tail has large twist or dihedral, it can be safely ignored in the calculations. These contributions to $C_{y\beta}$ can be represented by:

$$(C_{y\beta})_{WLT OFF} = (C_{y\beta})_{WING} + (C_{y\beta})_f + (C_{y\beta})_{V(wfh)} \quad (5.1.1)$$

$$(C_{y\beta})_{WLT ON} = (C_{y\beta})_{WLT OFF} + (C_{y\beta})_{WLT} \quad (5.1.2)$$

5.1.1 Wing Contribution

The wing contribution to $C_{y\beta}$ is primarily due to wing dihedral.

This can be computed by Equation 5.1.1.1 from Reference 1.

$$(C_{y\beta})_w = -0.0001(\Gamma_w) \text{ per deg} \quad (5.1.1.1)$$

where :

Γ_w is the wing dihedral angle in degrees.

For the Ayres Thrush the wing dihedral angle is 3.5 degrees.

Therefore,

$$(C_{y\beta})_w = -.00035 \text{ per deg}$$

5.1.2 Fuselage Contribution to $C_{y\beta}$

The fuselage side-force due to sideslip contribution can be considered as the sum of the side forces on the body and the wing-body interference. The fuselage alone is the main contributor. The wing-fuselage interference is primarily a function of wing vertical position on the fuselage. The total fuselage contribution to $C_{y\beta}$ at subsonic Mach numbers is given by Equation 5.1.2.1 from Reference 1.

$$(C_{y\beta})_f = K_1 (C_{y\beta})_B \frac{\bar{V}}{S_w}^{2/3} \text{ per deg} \quad (5.1.2.1)$$

where :

K_1 is the wing-fuselage interference factor, obtained from

Figure 5.1.2.1

$(C_{y\beta})_B$ is the body alone side force due to sideslip. For an estimation of the body side force due to sideslip, slender-body theory can be used, which gives $(C_{y\beta})_B = -0.0195 \text{ per deg.}$

\bar{V} is the fuselage volume, obtained from Figure 2.1.1

S_w is the wing area, from Table 2.1

Table 5.1.2.1 is a summary calculation for the fuselage contribution to $C_{y\beta}$.

5.1.3 Vertical Tail Contribution to $C_{y\beta}$

The vertical tail contribution to $C_{y\beta}$ is affected by the location of the horizontal tail, the fuselage crossflow on the vertical tail, and the wing-fuselage-induced sidewash.

Reference 1 accounts for horizontal tail and crossflow effects by computing an effective aspect ratio. The vertical tail effective aspect ratio is:

$$A_{v_{eff}} = A_v \left(\frac{A_v(f)}{A_v} \right) \left\{ 1 + K_h \left[\frac{A_v(fh)}{A_v(f)} - 1 \right] \right\} \quad (5.1.3.1)$$

where:

$\frac{A_v(f)}{A_v}$ is the ratio of the aspect ratio of the vertical tail in the presence of the fuselage to that of the isolated tail, obtained from Figure 5.1.3.1

A_v is the geometric aspect ratio of the vertical tail, from Table 2.1

$\frac{A_v(fh)}{A_v(f)}$ is the ratio of the vertical tail aspect ratio in the presence of the horizontal tail and fuselage to that of the panel in the presence of the fuselage alone, obtained from Figure 5.1.3.1

K_h is a factor accounting for the relative size of the horizontal and vertical tails, obtained from Figure 5.1.3.1.

Table 5.1.3.1 shows the summary calculations made to obtain the effective aspect ratio of the vertical tail.

The effective aspect ratio found is used to calculate the lift-curve slope of the vertical tail. The standard Polhamus equation is used for this calculation.

$$(C_{L_\alpha})_v(fh) = \frac{2\pi A_v^2}{2 + \sqrt{\frac{A_v^2}{K_v^2} (1 + \tan^2(\Lambda_{c/2})_v) + 4}} \text{ per rad} \quad (5.1.3.1)$$

where:

$$K_v = \frac{(C_{L_\alpha})_v}{2\pi}$$

$(\Lambda_{c/2})_v$ is the mid-chord sweep angle of the vertical tail, obtained from Table 2.1

Table 5.1.3.1 summarizes the calculation for computing $(C_{L_\alpha})_v$.

The complete vertical tail contribution to C_{y_β} is given in Equation 5.1.3.2 from Reference 1. This equation adjusts the vertical tail lift-curve slope to account for wake and sidewash effects.

$$(C_{y_\beta})_v(wfh) = -K'_1 (C_{L_\alpha})_v(fh) \left(1 + \frac{\partial \sigma}{\partial \beta}\right) \frac{\bar{q}_v S_v}{\bar{q}_\infty S_w} \text{ per rad} \quad (5.1.3.2)$$

where:

K'_1 is a factor which accounts for the relative size of the fuselage near the vertical tail to the size of the tail, from

Figure 5.1.3.1.

$$\left(1 + \frac{\partial \sigma}{\partial \beta}\right) \frac{\bar{q}_v}{\bar{q}_\infty} = .725 + 3.06 \frac{S_v/S_w}{1 + \cos(\Lambda_{c/4})_v} + \frac{0.4 Z_w}{(w_f)_w} + 0.009 A_w \quad (5.1.3.3)$$

where:

$(\Lambda_{c/4})_v$ is the quarter-chord sweep of the vertical tail, obtained from Table 2.1

Z_w is the vertical distance from the centerline of the equivalent fuselage to the quarter-chord point of the root chord of the exposed wing panel, obtained from Figure 2.1.1

$(w_f)_w$ is the width of the equivalent circular fuselage at the wing, obtained from Figure 2.1.1.

Table 5.1.3.1 shows the summary calculations used to find the vertical tail contribution to C_{y_β} .

5.1.4 Winglet Contribution to C_{y_β}

Strictly speaking, at the present time there exist no analytical methods for calculating winglet effect on C_{y_β} . However, in this section this contribution will be approximated by treating the winglets as vertical tails at the wing tips.

Twin vertical tails are treated in Reference 1. This method includes the effect of sidewash. Depending on winglet geometry, an effective aspect ratio is calculated from Figure 5.1.4.1:

$$(C_{y_\beta})_{WLT} = \frac{-(C_{y_\beta})_{v(wfh)}}{(C_{y_\beta})_{v_{eff}}} (C_{y_\beta})_{v_{eff}} \frac{2 S_{WLT}}{57.3 S_w} \text{ per deg} \quad (5.1.4.1)$$

where:

$\frac{(C_{y_\beta})_{v(wfh)}}{(C_{y_\beta})_{v_{eff}}}$ is a mutual interference factor, obtained from Figure

5.1.4.1

$(C_{y_\beta})_{v_{eff}}$ is the lift-curve slope of one vertical-tail panel, per rad, obtained from Figure 5.1.4.1.

To account for winglet cant angle effect on the side-force derivative, the following expression is used:

$$(C_{y\beta})_{WLT} = -.0001 (\Gamma_{WLT}) \frac{2S_{WLT}}{S_w}, \text{ per deg} \quad (5.1.4.2)$$

where:

Γ_{WLT} is the winglet cant angle (see Figure 2.2).

Summary calculations are shown in Table 5.1.4.1.

5.1.5 $C_{y\beta}$ of the Complete Airplane, Winglets On and Winglets Off

The side-force due to sideslip derivative, $C_{y\beta}$, of the Ayres Thrush, winglets and power off, is:

$$(C_{y\beta})_{WLT \text{ OFF}} = -.0056 \text{ per deg.}$$

Table 5.1.5.1 summarizes the calculations and lists the effect of winglet cant angle on $C_{y\beta}$ of the airplane.

5.2 Yawing Moment Derivative, C_{n_β}

The weathercock stability, C_{n_β} , is found by considering the contributions of the following airplane components:

- (1) Wing
- (2) Fuselage, including wing-fuselage interference
- (3) Tails
- (4) Winglets

These contributions to C_{n_β} can be represented by:

$$(C_{n_\beta})_{\substack{\text{PROP OFF} \\ \text{WLT OFF}}} = (C_{n_\beta})_w + (C_{n_\beta})_{f(w)} + (C_{n_\beta})_{v(wfh)} \quad \text{per deg} \quad (5.2.1)$$

$$(C_{n_\beta})_{\substack{\text{PROP OFF} \\ \text{WLT ON}}} = (C_{n_\beta})_{\substack{\text{PROP OFF} \\ \text{WLT OFF}}} + (C_{n_\beta})_{\text{WLT}} \quad \text{per deg} \quad (5.2.2)$$

5.2.1 Wing Contribution to C_{n_β}

The wing contribution to weathercock stability is primarily due to the asymmetrically induced drag distribution caused by an asymmetrical lift distribution.

For low subsonic speeds, Reference 1 gives the yawing moment derivative as:

$$(C_{n_\beta})_w = \frac{C_L^2}{57.3} \left\{ \frac{1}{4\pi A_w} - \frac{\tan \Lambda_c/4}{\pi A_w (A_w + 4 \cos \Lambda_c/4)} \left[\cos \Lambda_c/4 - \frac{A_w}{2} + \frac{-A_w^2}{8 \cos \Lambda_c/4} + \frac{6 \bar{x} \sin \Lambda_c/4}{c_w A_w} \right] \right\} \quad \text{per deg} \quad (5.2.1.1)$$

where, as obtained from Table 2.1:

A_w is the wing aspect ratio

$\Lambda_{c/4}$ is the sweep of the wing quarter-chord line

\bar{c}_w is the wing mean aerodynamic chord

\bar{x} is the location of the wing aerodynamic center behind the center of gravity on the mean aerodynamic chord.

Since the wing on the S2R-800 is unswept, Equation 5.2.1.1 reduces to:

$$(C_{n\beta})_w = \frac{C_{Lw}^2}{229.2 \pi A_w} \text{ per deg} \quad (5.2.1.2)$$

where:

C_{Lw} is the wing lift coefficient from Figure 5.2.1.1.

The contribution of the wing to $C_{n\beta}$ of the subject airplane is calculated in Table 5.2.1.1 to be:

$$(C_{n\beta})_w = .000239 C_{Lw}^2 \text{ per deg}$$

5.2.2 Fuselage Contribution to $C_{n\beta}$

The net contribution of the fuselage and wing-fuselage interference to $C_{n\beta}$, based on wing area and wing span and referenced to a selected center-of-gravity position, may be obtained from the following equation:

$$(C_{n\beta})_{f(w)} = -K_N \frac{(S_f)_s}{S_w} \frac{l_f}{b_w} \quad (5.2.2.1)$$

where:

$(S_f)_s$ is the fuselage side area, from Figure 2.1.1

S_w is the wing area, from Table 2.1

l_f is the fuselage length, from Figure 2.1.1

K_N is an empirical correlating factor for fuselage plus wing-fuselage interference, obtained from Figure 5.2.2.1.

The contribution of the fuselage of the subject airplane to C_{n_β} is calculated in Table 5.2.2.1.

5.2.3 Vertical Tail Contribution to C_{n_β}

The contribution of the vertical tail to the weathercock stability in the presence of the wing, fuselage, and horizontal tail is obtained from:

$$(C_{n_\beta})_{v(wfh)} = -(C_{y_\beta})_{v(wfh)} \left\{ \frac{l_v \cos \alpha - z_v \sin \alpha}{b_w} \right\} \text{ per deg} \quad (5.2.3.1)$$

where:

$(C_{y_\beta})_{v(wfh)}$ is the contribution of the vertical tail to the side force due to sideslip, obtained from Section 5.1.3

l_v , z_v are the distances from the center of gravity to the quarter chord of the vertical tail mean aerodynamic chord, parallel and perpendicular, respectively, to the x-body axis with z_v positive below the center of gravity, obtained from Figure 2.1.4.

The contribution of the vertical tail to the weathercock stability of the subject airplane is calculated in Table 5.2.3.1.

5.2.4 Winglet Contribution to C_{n_β}

Winglet contribution to C_{n_β} is obtained in a similar manner to the vertical tail calculations.

$$(C_{n_\beta})_{WLT} = -(C_{y_\beta})_{WLT} \left\{ \frac{l_{WLT} \cos \alpha - z_{WLT} \sin \alpha}{b_w} \right\} \text{ per deg} \quad (5.2.4.1)$$

where :

$(C_{y\beta})_{WLT}$ is the side force due to sideslip of the winglets,
from Section 5.1.4

l_{WLT} , Z_{WLT} are the distances from the center of gravity to the
quarter chord of the winglet mean aerodynamic chord, parallel and
perpendicular, respectively, to the x-body axis with Z_{WLT} positive
below the center of gravity, obtained from Figure 2.2.

This approximate method does not take into account winglet-wing
interference or changes in wing span loading that winglets produce.
Both of these effects can be significant.

The contribution of the winglets to $C_{n\beta}$ of the subject airplane
is calculated in Table 5.2.4.1.

5.2.5 Weathercock Stability of the Complete Airplane, Winglets on and Winglets Off

The weathercock stability, $C_{n\beta}$, of the subject airplane, winglets
and power off, is given by Equation 5.2.1. Table 5.2.5.1 summarizes
the calculations and lists the effects of winglet cant angle on $C_{n\beta}$.

5.3 Rolling Moment Derivative, $C_{\lambda\beta}$

The airplane rolling moment due to sideslip, $C_{\lambda\beta}$, is composed of the following contributions:

- (1) Wing
- (2) The effect of the fuselage on the wing contribution
- (3) Vertical tail
- (4) Winglets

These contributions to $C_{\lambda\beta}$ can be represented as :

$$(C_{\lambda\beta})_{\substack{\text{PROP OFF} \\ \text{WLT OFF}}} = (C_{\lambda\beta})_w + (C_{\lambda\beta})_{f(w)} + (C_{\lambda\beta})_{v(wfh)} \text{ per deg} \quad (5.3.1)$$

$$(C_{\lambda\beta})_{\substack{\text{PROP OFF} \\ \text{WLT ON}}} = (C_{\lambda\beta})_{\substack{\text{PROP OFF} \\ \text{WLT OFF}}} + (C_{\lambda\beta})_{\text{WLT}} \text{ per deg} \quad (5.3.2)$$

5.3.1 Wing Contribution to $C_{\lambda\beta}$

At low angles of attack and subsonic speeds, the dihedral effect contribution by the wing is primarily a function of wing aspect ratio, taper ratio, and dihedral angle.

$$C_{\lambda\beta} = C_{L_w} \frac{C_{\lambda\beta}}{C_L}_A + \Gamma_w \frac{C_{\lambda\beta}}{\Gamma_w} \text{ per deg} \quad (5.3.1.1)$$

where:

C_{L_w} is the wing lift coefficient, from Figure 5.2.1.1

$\frac{C_{\lambda\beta}}{C_L}_A$ is the effect of uniform geometric dihedral on $C_{\lambda\beta}$, obtained from Figure 5.3.1.1

$\frac{C_{\lambda\beta}}{\Gamma_w}$ is the aspect ratio contribution to $C_{\lambda\beta}$, obtained from

Figure 5.3.1.2

Γ_w is the wing geometric dihedral, from Table 2.1.

The contribution of the wing to $C_{\ell\beta}$ of the subject airplane is calculated in Table 5.3.1.1.

5.3.2 Effect of Fuselage on Wing Contribution to $C_{\ell\beta}$

While the contribution of the fuselage alone to $C_{\ell\beta}$ is negligible, the fuselage does influence the flow over the wing which can alter the wing contribution significantly. Equation 5.3.2.1 from Reference 1 accounts for this wing-fuselage interference.

$$(C_{\ell\beta})_{f(w)} = \frac{1.2\sqrt{A_w}}{57.3} \frac{z_w}{b_w} \left(\frac{h+w}{b_w} \right) - .0005\sqrt{A_w} \left(\frac{(d_f)_w}{b_w} \right)^2 \Gamma_w \text{ per deg} \quad (5.3.2.1)$$

where:

$(d_f)_w$ is the diameter of the equivalent circular fuselage at the wing, obtained from Figure 2.1.1

z_w is the vertical position of wing below centerline of equivalent circular fuselage, from Figure 2.1.1

h is the height of the fuselage at the wing location, obtained from Figure 2.1.1

w is the width of the fuselage at the wing location, obtained from Figure 2.1.1.

The wing-fuselage interference effects on $C_{\ell\beta}$ of the subject airplane are calculated in Table 5.3.2.1.

5.3.3 Vertical Tail Contribution to $C_{\ell\beta}$

The vertical tail contributes to the airplane $C_{\ell\beta}$ by virtue of the rolling moment produced by the vertical tail side force due to

sideslip. Equation 5.3.3.1 from Reference 1 is used to determine the vertical tail contribution.

$$(C_{\ell_\beta})_{v(wfh)} = -(C_{y_\beta})_{v(wfh)} \left\{ \frac{z_v \cos \alpha + l_v \sin \alpha}{b_w} \right\} \text{per deg} \quad (5.3.3.1)$$

where:

$(C_{y_\beta})_{v(wfh)}$ is the vertical tail side force due to sideslip in the presence of the wing, fuselage, and horizontal tail, from Table 5.1.3.1

z_v is the perpendicular distance from the x-body axis to the quarter chord of the vertical tail mean aerodynamic chord, from

Figure 2.1.4

l_v is the distance along the x-body axis from the center of gravity to the quarter chord of the vertical tail mean aerodynamic chord, from Figure 2.1.4.

The contribution of the vertical tail to the C_{ℓ_β} of the subject airplane is calculated in Table 5.3.3.1.

5.3.4 Winglet Contribution to C_{ℓ_β}

The contribution of the winglets to C_{ℓ_β} is calculated in a similar manner as the vertical tail contribution. Since the method presented in this section does not account for span loading variations induced by the winglets, it can be assumed that the method will tend to be inaccurate. Also, separation and interference effects are neglected, which can lead to large errors. However, since no analytical methods exist for predicting winglet contribution to C_{ℓ_β} , Equation 5.3.4.1 will be used to approximate it.

$$(C_{\ell_\beta})_{WLT} = -(C_{y_\beta})_{WLT} \left\{ \frac{z_{WLT} \cos \alpha + l_{WLT} \sin \alpha}{b_w} \right\} \text{ per deg} \quad (5.3.4.1)$$

where:

$(C_{y_\beta})_{WLT}$ is the winglet side force due to sideslip, obtained from Table 5.1.5.1

z_{WLT} is the perpendicular distance from the x-body axis to the quarter chord of the winglet mean aerodynamic chord, from Figure 2.2

l_{WLT} is the distance along the x-body axis from the center of gravity to the quarter chord of the winglet mean aerodynamic chord, from Figure 2.2.

The contribution of the vertical tail to the C_{ℓ_β} of the subject airplane is calculated in Table 5.3.4.1.

5.3.5 C_{ℓ_β} of the Complete Airplane, Winglets On and Winglets Off

The dihedral effect, C_{ℓ_β} , of the complete airplane, winglets and power off, is given by Equation 5.3.1. Table 5.3.5.1 summarizes the calculations and lists the effects of winglet cant angle on C_{ℓ_β} of the subject airplane.

Table 5.1.2.1: Fuselage Contribution to $C_{y\beta}$

<u>Symbol</u>	<u>Description</u>	<u>Reference</u>	<u>Magnitude</u>
z_w	Distance from body centerline to 1/4 point of exposed wing root chord, m (ft)	Figure 2.1.1	.43 (1.4)
h	Maximum body height at wing-body intersection, m (ft)	Figure 5.2.2.1	1.62 (5.32)
K_i	Wing fuselage interference factor	Figure 5.1.2.1	1.25
\bar{V}	Fuselage volume, m^3 (ft^3)	Table 2.1	7.72 (254.8)
s_w	Wing area, m^2 (ft^2)	Table 2.1	30.34 (326.6)
$(C_{y\beta})_B$	Body side force due to sideslip, per deg	Potential theory	-0.0195

Table 5.1.3.1: Vertical Tail Contribution to C_{y_β}
 (a) Effective Aspect Ratio

<u>Symbol</u>	<u>Description</u>	<u>Reference</u>	<u>Magnitude</u>
s_h	Horizontal tail area, m^2 (ft^2)	Table 2.1	5.25 (56.47)
s_v	Vertical tail area, m^2 (ft^2)	Table 2.1	2.12 (27.77)
b_v	Vertical tail span, m (ft)	Table 2.1	1.51 (4.96)
A_v	Vertical tail aspect ratio	Table 2.1	1.08
$(c_v)_h$	Vertical tail chord at horizontal tail, m (ft)	Figure 2.1.4	1.78 (5.84)
$x_{ach}(c_v)_{t_e}$	Distance from leading edge of vertical tail to a.c. of horizontal tail, in plane of horizontal tail, m (ft)	Figure 2.1.4	.3048 (1.0)
$z_{crh}(c_r)_v$	Distance from root chord of vertical tail to root chord of horizontal tail, m (ft)	Figure 2.14	-3048 (-1.0)
$(d_f)_v$	Depth of fuselage at quarter-root chord of vertical tail, m (ft)	Figure 2.1.1	.61 (2.0)
$\frac{A_v(f)}{A_v}$	Ratio of vertical tail aspect ratio in presence of fuselage to isolated vertical tail aspect ratio	Figure 5.1.3.1 (a)	1.53
$\frac{A_v(fh)}{A_v(f)}$	Ratio of vertical tail aspect ratio in presence of fuselage and horizontal tail to aspect ratio of tail in presence of fuselage alone	Figure 5.1.3.1 (b)	0.925
k_h	Relative tail size factor	Figure 5.1.3.1	1.18

Summary: $A_{v_{eff}} = 1.51$

Table 5.1.3.1: (Continued)

(b) Vertical Tail Lift Curve Slope

<u>Symbol</u>	<u>Description</u>	<u>Reference</u>	<u>Magnitude</u>
$A_{v_{\text{eff}}}$	Effective vertical tail aspect ratio	Table 2.1	1.51
$(\Lambda_{c/2})_v$	Vertical tail half-chord sweepback, deg	Table 2.1	-3.4
$(C_L)_v$	Vertical tail section lift curve slope, per rad	Table 2.1	5.655
k_v	$\frac{(C_L)_v}{2\pi}$		0.9

Summary: $(C_L)_v(fh) = 2.145 \text{ per rad} = 0.0374 \text{ per deg}$

Table 5.1.3.1: (Concluded)

(c) Vertical Tail Contribution to $C_{y\beta}$

<u>Symbol</u>	<u>Description</u>	<u>Reference</u>	<u>Magnitude</u>
S_w	Wing reference-area, m^2 (ft^2)	Table 2.1	30.34 (326.6)
$(\Lambda_c/4)_v$	Vertical tail quarter-chord sweep angle, deg	Table 2.1	14
Z_w	Distance from equivalent fuselage centerline, m (ft)	Figure 2.1.1	0.43 (1.4)
$(w_f)_w$	Width of equivalent fuselage at wing, m (ft)	Figure 2.1.1	1.26 (4.15)
A_w	Wing aspect ratio	Table 2.1	5.81
$(1 + \frac{\partial \sigma}{\partial \beta}) \frac{\bar{q}_v}{\bar{q}_\infty}$	Wing wake and fuselage sidewash factor	Equation 5.1.3.3	1.02
K'_1	Relative body size to tail size parameter	Figure 5.1.3.4	0.850

Summary: $(C_{y\beta})_{v(wfh)} = -.00225$ per deg

Table 5.1.4.1: Winglet Contribution to $C_{y\beta}$
 (a) Zero Cant Angle

<u>Symbol</u>	<u>Description</u>	<u>Reference</u>	<u>Magnitude</u>
b'_v	Tail span above wing plane, m (ft)	Table 2.1	1.52 (4.98)
b_v	Total tail span, m (ft)	Table 2.1	1.52 (4.98)
b_w	Wing span, m (ft)	Table 2.1	13.27 (43.55)
$(d_f)_{WLT}$	Fuselage diameter at winglet quarter-root chord, m (ft)	Figure 2.1.1	1.62 (5.32)
l_f	Length of fuselage, m (ft)	Figure 2.1.1	8.5 (27.88)
S_{WLT}	Winglet area, m^2 (ft^2)	Table 2.1	1.8 (19.34)
A_v	Tail (winglet) aspect ratio	Table 2.1.	1.28
$A_{v_{eff}}$	Twin tails (winglets) effective aspect ratio	Figure 5.1.4.1	1.51
$(C_{y\beta})_{v_{eff}}$	Lift curve slope of one vertical tail panel (winglet), per rad	Figure 5.1.4.1	2.6
$\frac{(C_{y\beta})_{v(wfh)}}{(C_{y\beta})_{v_{eff}}}$	Mutual interference factor	Figure 5.1.4.1	1.0

Summary: $(C_{y\beta})_{WLT, CANT=0} = -0.00537$ per deg

Table 5.1.4.1: (Continued)

(b) $(C_{y\beta})_{WLT}$ Due to Cant Angle

<u>Cant Angle, deg</u>	$(C_{y\beta})_{WLT}$, per deg (Equation 5.1.4.2) CANT
+20	-.000237
0	0
-10	.000118

Table 5.1.4.1: (Concluded)

(c) Summary

<u>Cant Angle, deg</u>	$(C_{y\beta})_{WLT} =$ $\frac{(C_{y\beta})_{WLT}}{\Gamma_{WLT=0}} + \frac{(C_{y\beta})_{WLT}}{\Gamma_{WLT}}$, per deg
+20	-0.00561
0	-.00537
-10	-.00525

Table 5.1.5.1: $C_{y\beta}$ of the Complete Airplane

<u>Symbol</u>	<u>Description</u>	<u>Reference</u>	<u>Magnitude</u>
$(C_{y\beta})_{w_T}$	Wing contribution, per deg	Section 5.1.1	-.00035
$(C_{y\beta})_f$	Fuselage contribution, per deg	Table 5.1.2.1	-.003
$(C_{y\beta})_{v(wfh)}$	Contribution of vertical tail in presence of wing, body and horizontal tail, per deg	Table 5.1.3.1	-.00225
$(C_{y\beta})_{WLT\ 20^\circ}$	Contribution of winglets with 20-degree cant, per deg	Table 5.1.4.1	-.00561
$(C_{y\beta})_{WLT\ 0^\circ}$	Contribution of winglets with no cant, per deg	Table 5.1.4.1	-.00537
$(C_{y\beta})_{WLT\ -10^\circ}$	Contribution of winglets with -10° cant, per deg	Table 5.1.4.1	-.00525

Summary: Winglets off $C_{y\beta} = -.0056$ per deg

Winglets on

20° cant $C_{y\beta} = -.0112$

0° $C_{y\beta} = -.0110$

-10° $C_{y\beta} = -.0108$

Table 5.2.1.1: Wing Contribution to $C_{n\beta}$

<u>Symbol</u>	<u>Description</u>	<u>Reference</u>	<u>Magnitude</u>
A_w	Wing aspect ratio	Table 2.1	5.81
$\Lambda_c/4$	Sweep of wing quarter-chord line, deg	Table 2.1	0
\bar{c}	Wing mean aerodynamic chord, m (ft)	Table 2.1	2.29 (7.5)
C_{Lw}	Wing lift coefficient	Figure 5.2.1.1	$f(\alpha)$

Summary: $(C_{n\beta})_w = 0.000239 C_{Lw}^2$ per deg

①

②

③

Figure 5.2.1.1

<u>α, deg</u>	<u>C_{Lw}</u>	<u>$(C_{n\beta})_w = 0.000239(2)^2$</u>
-4	-0.025	.00000598
0	0.27	.000174
4	0.56	.0000750
8	0.86	.000177
12	1.15	.000316

Table 5.2.2.1: Fuselage Contribution to $C_{n\beta}$

<u>Symbol</u>	<u>Description</u>	<u>Reference</u>	<u>Magnitude</u>
$(S_f)_s$	Fuselage side area, m^2 (ft^2)	Figure 2.1.1	8.36 (90)
S_w	Wing area, m^2 (ft^2)	Table 2.1	30.34 (326.6)
l_f	Length of fuselage, m (ft)	Figure 2.1.1	8.5 (27.88)
b_w	Wing span, m (ft)	Table 2.1	13.27 (43.55)
Z_w	Vertical position of wing below center-line of equivalent fuselage, m (ft)	Figure 2.1.1	0.43 (1.41)
$(w_f)_w$	Width of equivalent fuselage at the wing, m (ft)	Figure 2.1.1	1.26 (4.15)
x_m, h, h_1, h_2	Geometric fuselage parameters, m (ft)	Figure 5.2.2.1	as listed
K_N	Empirical factor for fuselage $C_{n\beta}$ in presence of wing	Figure 5.2.2.1	.0024

Summary : $(C_{n\beta})_{f(w)} = -0.000423$ per deg

Table 5.2.3.1: Vertical Tail Contribution to $C_{n\beta}$

<u>Symbol</u>	<u>Description</u>	<u>Reference</u>	<u>Magnitude</u>
$(C_{y\beta})_{v(wfh)}$	Contribution of vertical tail to side force due to sideslip, per deg	Table 5.1.3.1	-0.00225
l_v	Distance along x-body axis from center of gravity to quarter chord of vertical tail mean aerodynamic chord, m (ft)	Figure 2.1.4	5.09 (16.7)
z_v	Perpendicular distance from x-body axis to quarter chord of vertical tail mean aerodynamic chord, m (ft)	Figure 2.1.4	-1.07 (-3.5)
b_w	Wing span, m (ft)	Table 2.1.2	13.27 (43.55)

Summary: $(C_{n\beta})_{v(wfh)} = 0.000863 \cos \alpha + 0.000181 \sin \alpha$ per deg

<u>①</u> α , deg	<u>②</u> $\cos ①$	<u>③</u> $\sin ①$	$(C_{n\beta})_{v(wfh)} = 0.000863 ② + 0.000181 ③$
-4	0.9976	-0.06976	.000848
0	1	0	.000863
4	0.9976	0.06976	.000874
8	0.9903	0.1392	.000880
12	0.9781	0.2079	.000882

Table 5.2.4.1: Winglet Contribution to $C_{n\beta}$

<u>Symbol</u>	<u>Description</u>	<u>Reference</u>	<u>Magnitude</u>
$(C_y)_WLT$	Contribution of winglets to side force due to sideslip, per deg	Table 5.1.4.1	As listed
ℓ_{WLT}	Distance along x-body axis from center of gravity to quarter chord of winglet mean aerodynamic chord, m (ft)	Figure 2.2	.44 (1.44)
z_{WLT}	Perpendicular distance from x-body axis to quarter chord of winglet mean aerodynamic chord, m (ft)	Figure 2.2	-.43 (-1.4)
b_w	Wing span, m (ft)	Table 2.1.2	13.27 (43.55)

Summary: $(C_{n\beta})_{WLT} = -(C_y)_{WLT} [.0331 \cos \alpha + .032 \sin \alpha]$ per deg

5.25

<u>① α, deg</u>	<u>② $\cos ①$</u>	<u>③ $\sin ①$</u>	<u>④ $(C_{n\beta})_{WLT}$ 20°</u>	<u>⑤ $(C_{n\beta})_{WLT}$ 0°</u>	<u>⑥ $(C_{n\beta})_{WLT}$ -10°</u>
-4	0.9976	-0.06976	-.000172	.000166	.000162
0	1	0	0.000185	.000178	.000174
4	0.9976	0.06976	0.000197	.000190	.000185
8	0.9903	0.1392	0.000208	.000200	.000196
12	0.9781	0.2079	0.000218	.000210	.000205

Table 5.2.5.1: $C_{n\beta}$ of the Complete Airplane: Winglets On and Winglets Off

α , deg	$(C_{n\beta})_{\text{PROP OFF}}$ WLT OFF, per deg	$(C_{n\beta})_{\text{PROP OFF}}$ WLT ON 20° , per deg	$(C_{n\beta})_{\text{PROP OFF}}$ WLT ON 0° , per deg	$(C_{n\beta})_{\text{PROP OFF}}$ WLT -10° , per deg
-4	0.000419	0.000591	0.000585	0.000581
0	0.000457	0.000642	0.000635	0.000631
4	0.000526	0.000723	0.000716	0.000711
8	0.000634	0.000842	0.000834	0.000830
12	0.000775	0.000993	0.000985	0.000980

Table 5.3.1.1: Wing Contribution to C_{L_B}

<u>Symbol</u>	<u>Description</u>	<u>Reference</u>	<u>Magnitude</u>
C_{L_w}	Wing lift coefficient	Figure 5.2.2.1	$f(\alpha)$
A_w	Wing aspect ratio	Table 2.1	5.81
λ_w	Wing taper ratio	Table 2.1	1.0
$\Lambda_{c/2}$	Sweep of wing half-chord line, deg	Table 2.1	0
Γ_w	Wing geometric dihedral, deg	Table 2.1	3.5
$\frac{C_{L_B}}{C_{L_w}}$	Low-speed variation of C_{L_B} as a function of C_{L_w} , per deg	Figure 5.3.1.1	-0.0018
$\frac{C_{L_B}}{\Gamma_w}$	Effect of geometric dihedral on C_{L_B} , per $(\text{deg})^2$	Figure 5.3.1.2	-0.00021

Summary: $(C_{L_B})_w = -0.000735 - .0018 C_{L_w}$ per deg

① ② ③

<u>α, deg</u>	<u>C_{L_w}</u>	<u>$(C_{L_B})_w = -0.000735 +$</u> <u>-0.0018 ②</u>
-4	-0.025	-0.00069
0	0.27	-0.00122
4	0.56	-0.00174
8	0.86	-0.00229
12	1.15	-0.00280

Table 5.3.2.1: Effect of Fuselage on Wing Contribution to $C_{\lambda \beta}$

<u>Symbol</u>	<u>Description</u>	<u>Reference</u>	<u>Magnitude</u>
A_w	Wing aspect ratio	Table 2.1	5.81
b_w	Wing span, m (ft)	Table 2.1	13.27 (43.55)
z_w	Vertical position of wing below centerline of equivalent circular fuselage, m (ft)	Figure 2.1.1	0.43 (1.4)
$(d_f)_w = h_w$	Diameter of equivalent circular fuselage at wing, m (ft)	Figure 2.1.1	1.26 (4.15)
Γ_w	Wing geometric dihedral, deg	Table 2.1	3.5

Summary: $(C_{\lambda \beta})_{f(w)} = 0.000271$ per deg

Table 5.3.3.1: Vertical Tail Contribution to $C_{\ell \beta}$

<u>Symbol</u>	<u>Description</u>	<u>Reference</u>	<u>Magnitude</u>
$(C_{y \beta})_{v(wfh)}$	Vertical side force due to sideslip in presence of wing, fuselage, and horizontal tail, per deg	Table 5.1.3.1	-0.00225
z_v	Distance from x-body axis to quarter chord of vertical mean aerodynamic chord, m (ft)	Figure 2.1.4	-1.07 (-3.5)
l_v	Distance along x-body axis from center of gravity to quarter chord of vertical-tail mean aerodynamic chord, m (ft)	Figure 2.1.4	5.09 (16.7)
b_w	Wing span, m (ft)	Table 2.1	13.27 (43.55)

Summary: $(C_{\ell \beta})_{v(wfh)} = -0.000181 \cos \alpha + .000863 \sin \alpha$, per deg

<u>①</u> α , deg	<u>②</u> $\cos ①$	<u>③</u> $\sin ①$	$(C_{\ell \beta})_{v(wfh)} = -0.000181 ② + .000863 ③$
-4	0.9976	-0.06926	-0.000241
0	1	0	-0.000181
4	0.9976	0.06976	-0.000120
8	0.9903	0.1392	-0.000059
12	0.9781	0.2079	0.000002

Table 5.3.4.1: Winglet Contribution to $C_{\ell \beta}$

<u>Symbol</u>	<u>Description</u>	<u>Reference</u>	<u>Magnitude</u>
$(C_y)_\beta^{\text{WLT}}$	Contribution of winglets to side force due to sideslip, per deg	Table 5.1.4.1	As listed
ℓ_{WLT}	Distance along x-body axis from center of gravity to quarter chord of winglet mean aerodynamic chord, m (ft)	Figure 2.2	.44 (1.44)
z_{WLT}	Perpendicular distance from x-body axis to quarter chord of winglet mean aerodynamic chord, m (ft)	Figure 2.2	-.43 (-1.4)
b_w	Wing span, m (ft)	Table 2.1	13.27 (43.55)

Summary: $(C_{\ell \beta})_{\text{WLT}} = -(C_y)_\beta^{\text{WLT}} [-0.0321 \cos \alpha + 0.0331 \sin \alpha]$ per deg

①	②	③	④	⑤	⑥
$\alpha, \text{ deg}$	$\cos ①$	$\sin ①$	$(C_{\ell \beta})_{\text{WLT}} 20^\circ$	$(C_{\ell \beta})_{\text{WLT}} 0^\circ$	$(C_{\ell \beta})_{\text{WLT}} -10^\circ$
-4	0.9976	-0.06976	-0.000192	-0.000184	-0.000180
0	1	0	-0.000180	-0.000172	-0.000168
4	0.9976	0.06976	-0.000167	-0.000159	-0.000155
8	0.9903	0.1392	-0.000154	-0.000146	-0.000142
12	0.9781	0.2079	-0.000137	-0.000131	-0.000128

Table 5.3.5.1: $C_{l\beta}$ of the Complete Airplane: Winglets On and Winglets Off

α , deg	$C_{l\beta}$ PROP OFF WLT OFF, per deg	$C_{l\beta}$ PROP OFF WLT 20°, per deg	$C_{l\beta}$ PROP OFF WLT 0°, per deg	$C_{l\beta}$ PROP OFF WLT -10°, per deg
-4	-0.00066	-0.000852	-0.000844	-0.000841
0	-0.00113	-0.00131	-0.00130	-0.00129
4	-0.00160	-0.00178	-0.00176	-0.00176
8	-0.00208	-0.00223	-0.00222	-0.00222
12	-0.00253	-0.00267	-0.00266	-0.00265

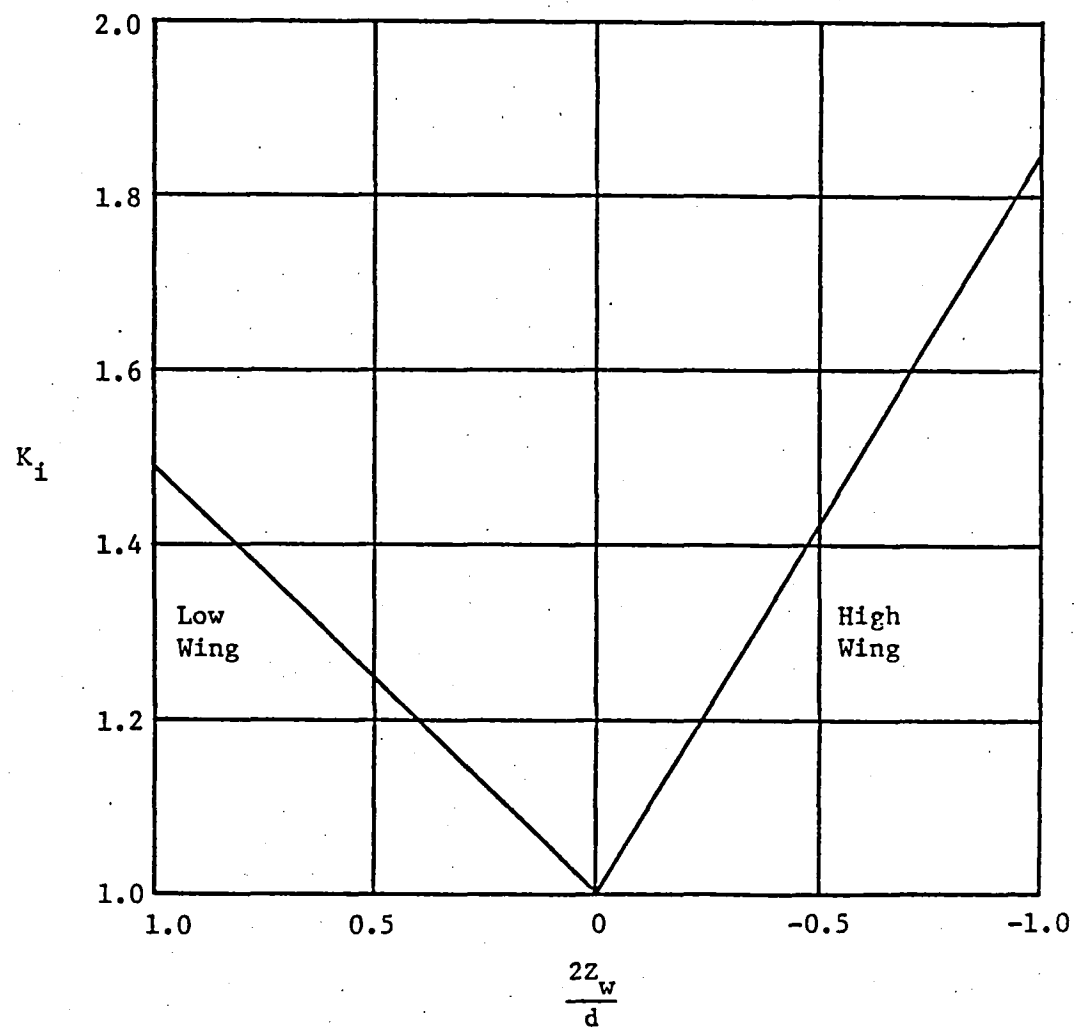


Figure 5.1.2.1: Wing-body interference factor for sideslip derivative $C_{y\beta}$ (Reference 1)

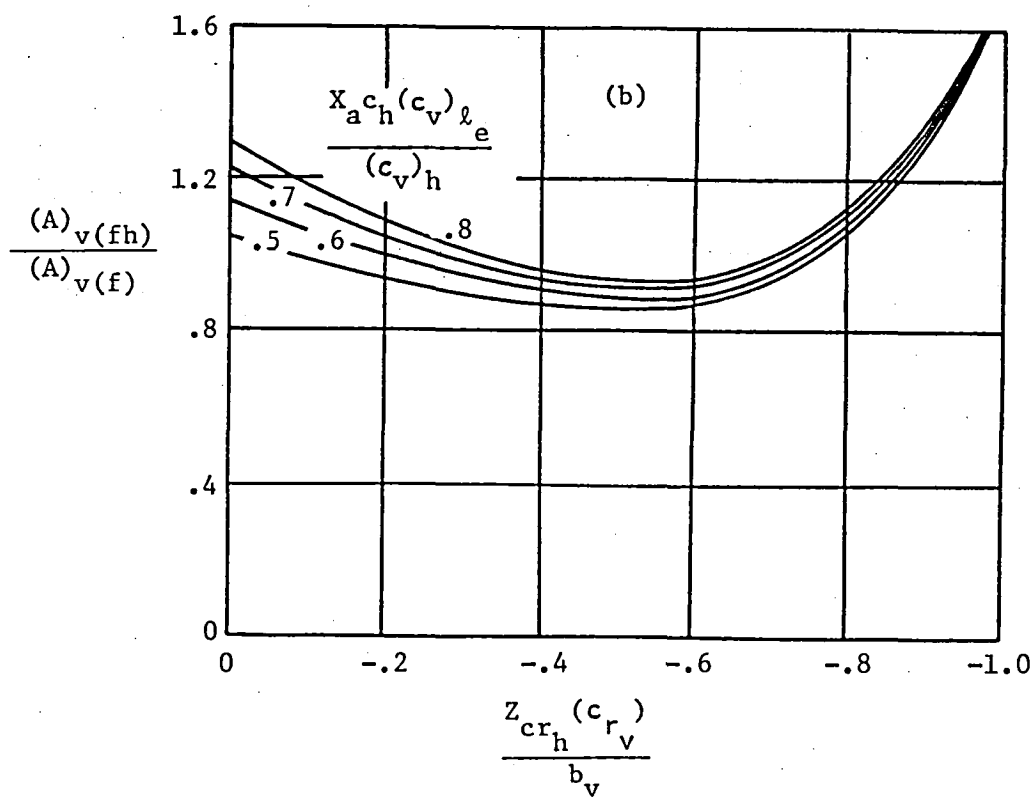
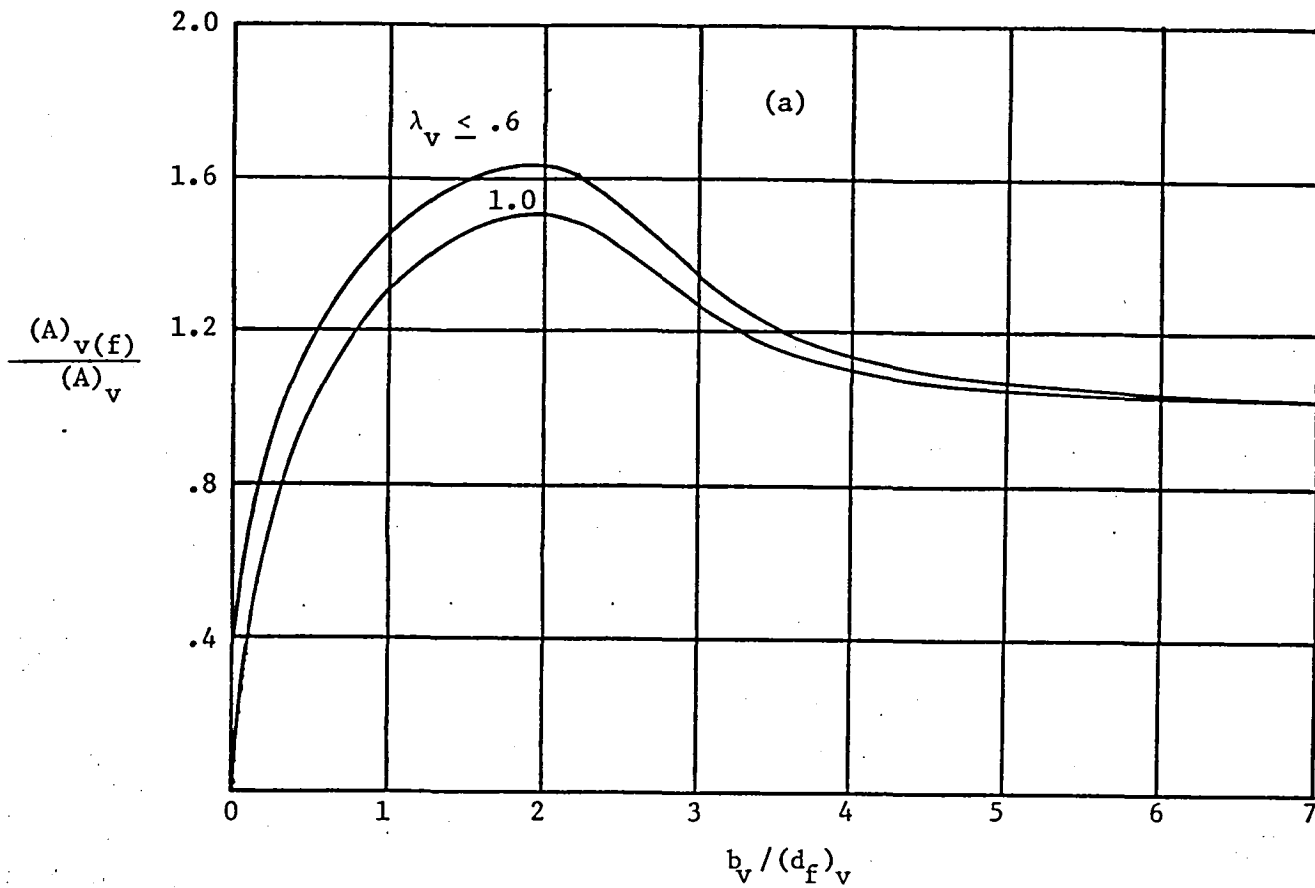


Figure 5.1.3.1: Charts for estimating $(c_y)_v(wfh)$ for single vertical tails (Reference 1)

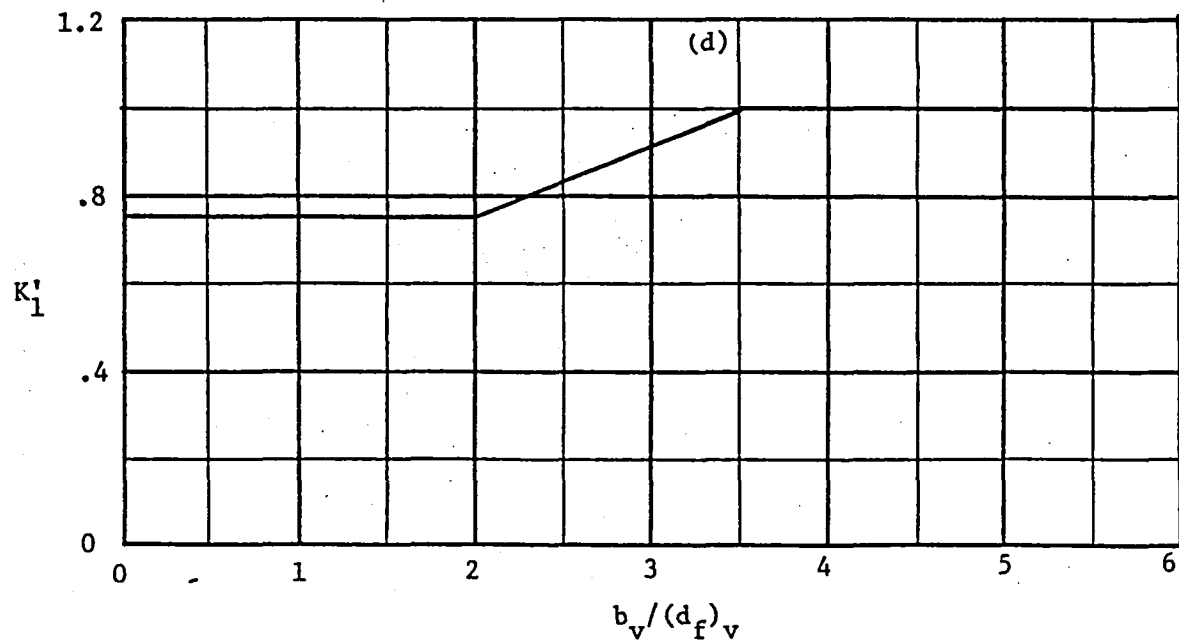
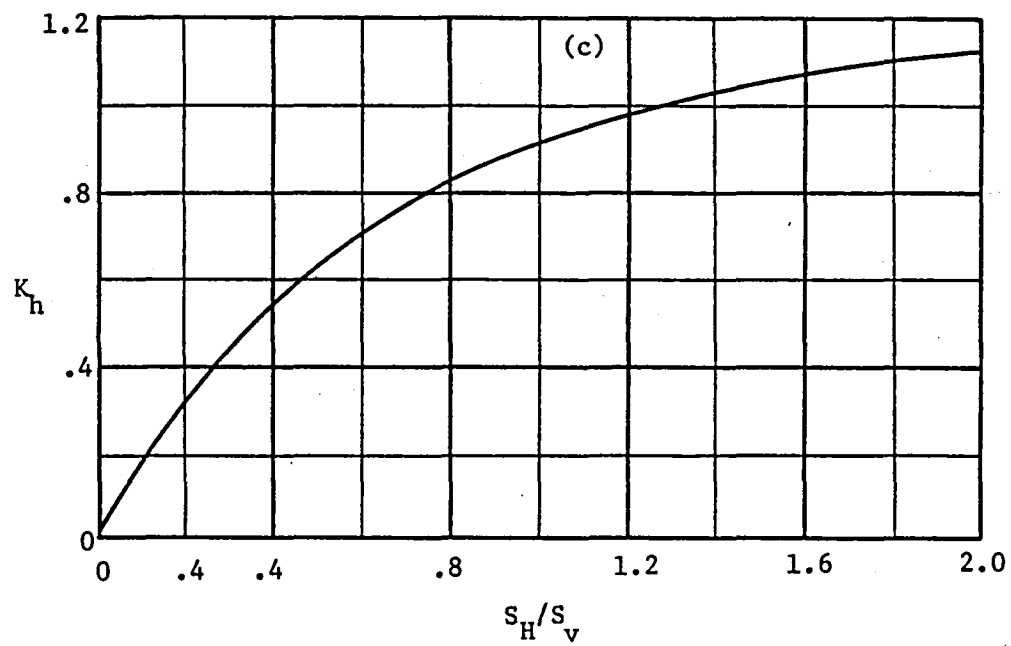


Figure 5.1.3.1 (concluded): Charts for estimating $(C_{y_\beta})_{v(wfh)}$
for single vertical tails (Reference 1)

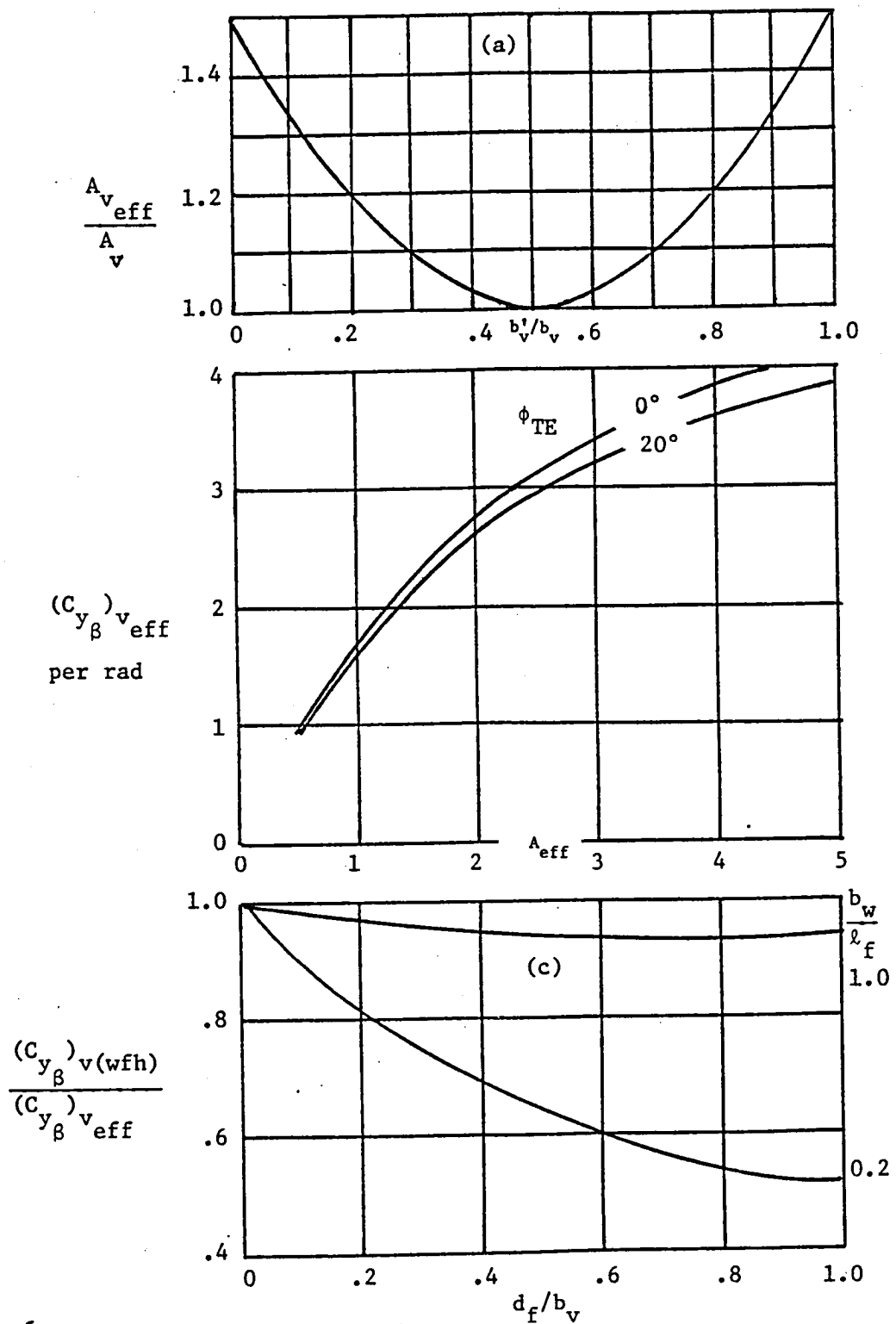


Figure 5.1.4.1: Charts for estimating winglet contribution to C_{y_β} (Reference 1)

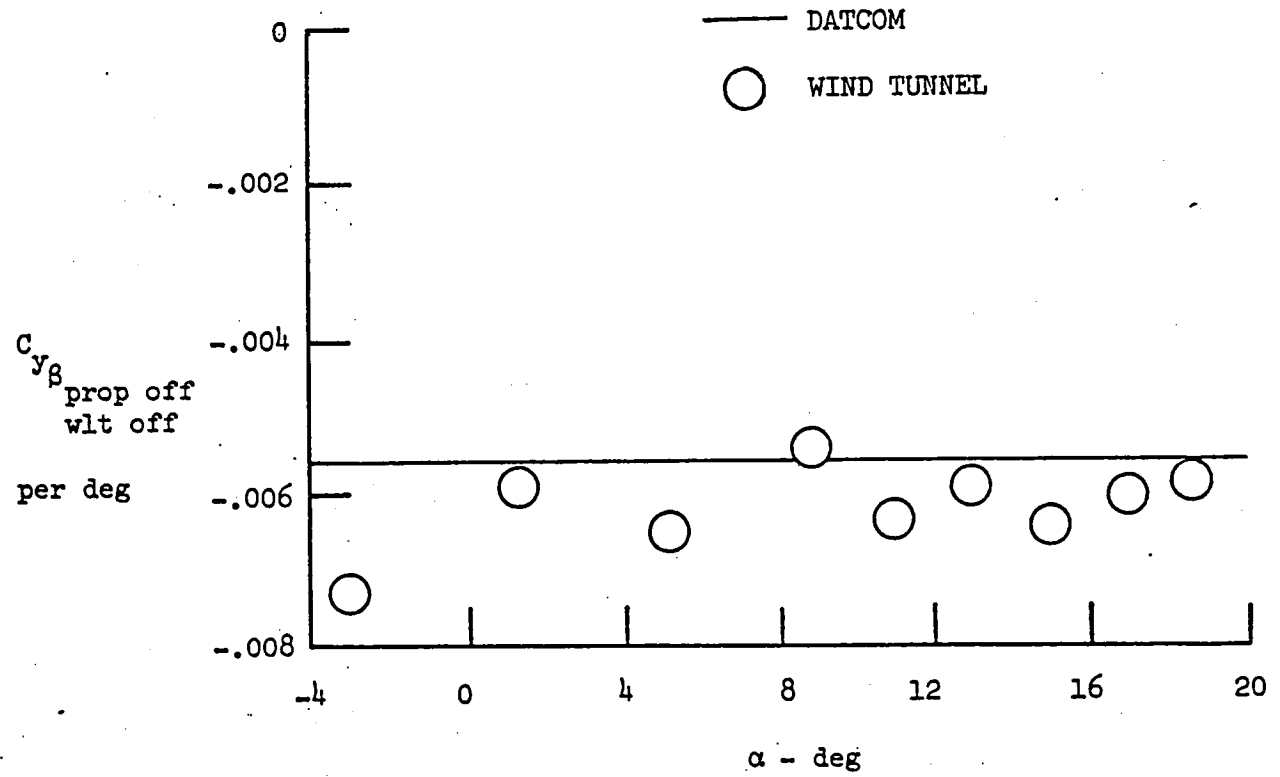


Figure 5.1.5.1: Comparison of predicted $C_{y\beta}$, winglets off,
 to full-scale wind tunnel data for the
 Ayres Thrush S2R-800.

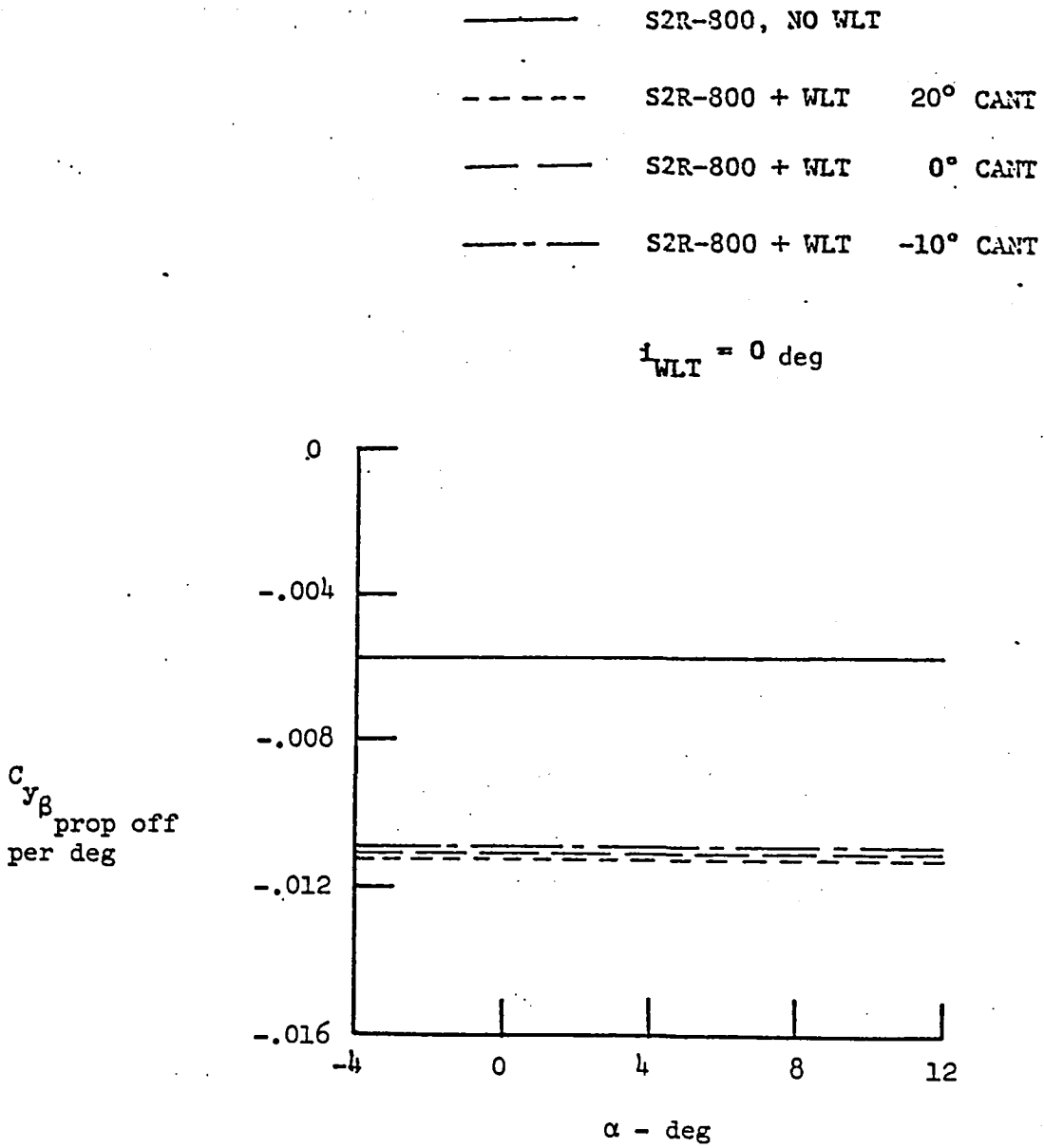


Figure 5.1.5.2: Effect of winglet cant angle on airplane $C_{y\beta}$ based on DATCOM methods.

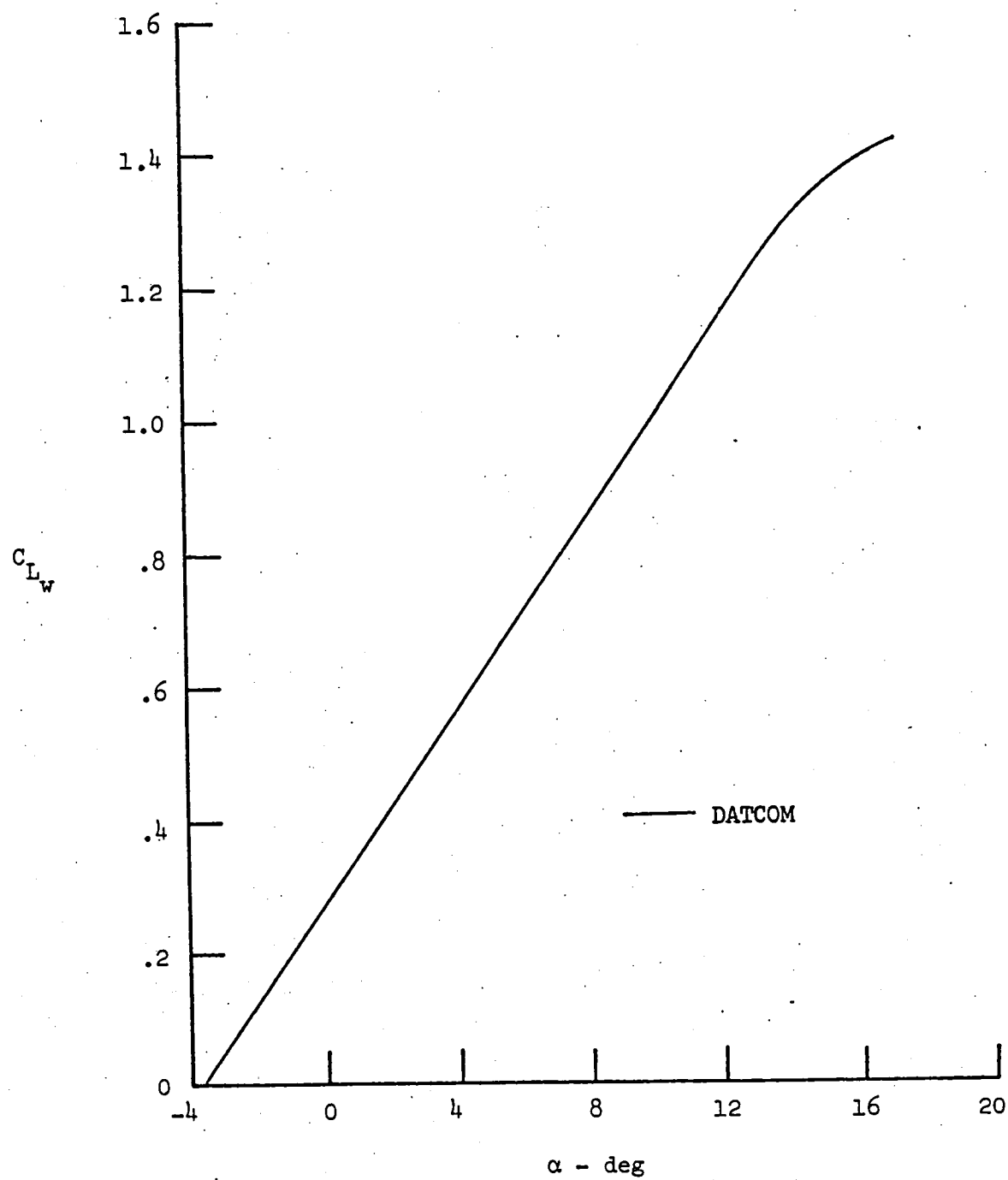


Figure 5.2.1.1: Wing alone lift curve for the S2R-800 (Reference 1).

For subject airplane -

$$x_m = 2.21 \text{ m} \quad h = 1.62 \text{ m}$$

$$l_f = 8.5 \text{ m} \quad h_1 = 1.46 \text{ m}$$

$$w_{\max} = 1.26 \text{ m} \quad h_2 = 0.79 \text{ m}$$

$$(S_f)_s = 13.88 \text{ m}^2 \quad N_{Re} = 20 \times 10^6$$

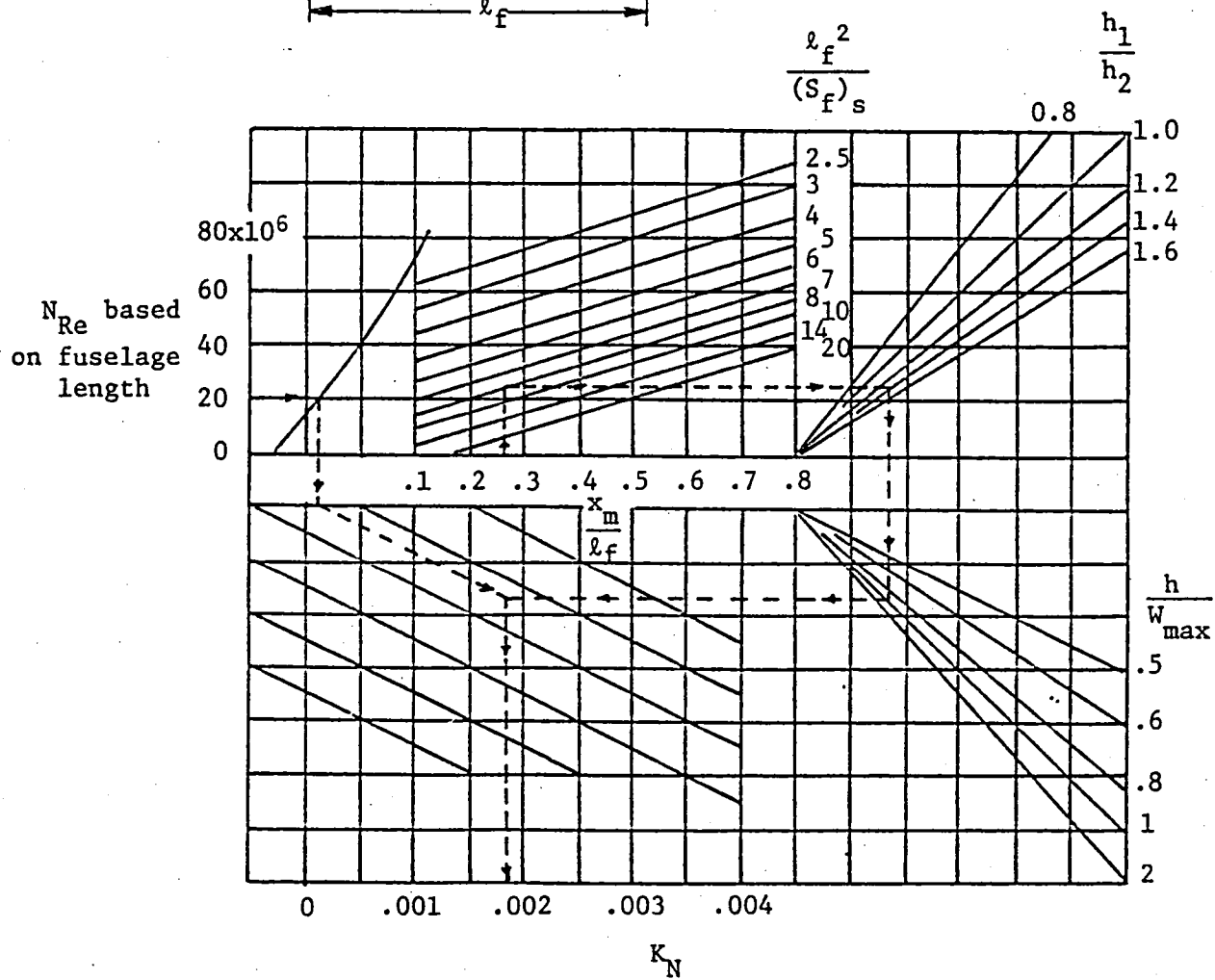
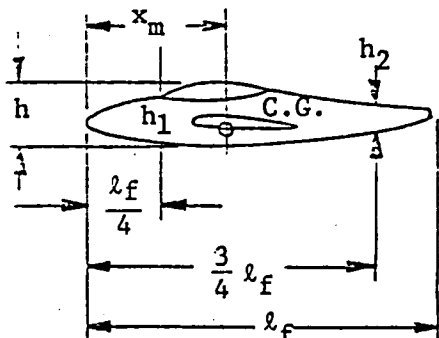


Figure 5.2.2.1: Empirical factor K_N related to the derivative C_{n_B} for the fuselage plus wing-fuselage interference (Reference 1).

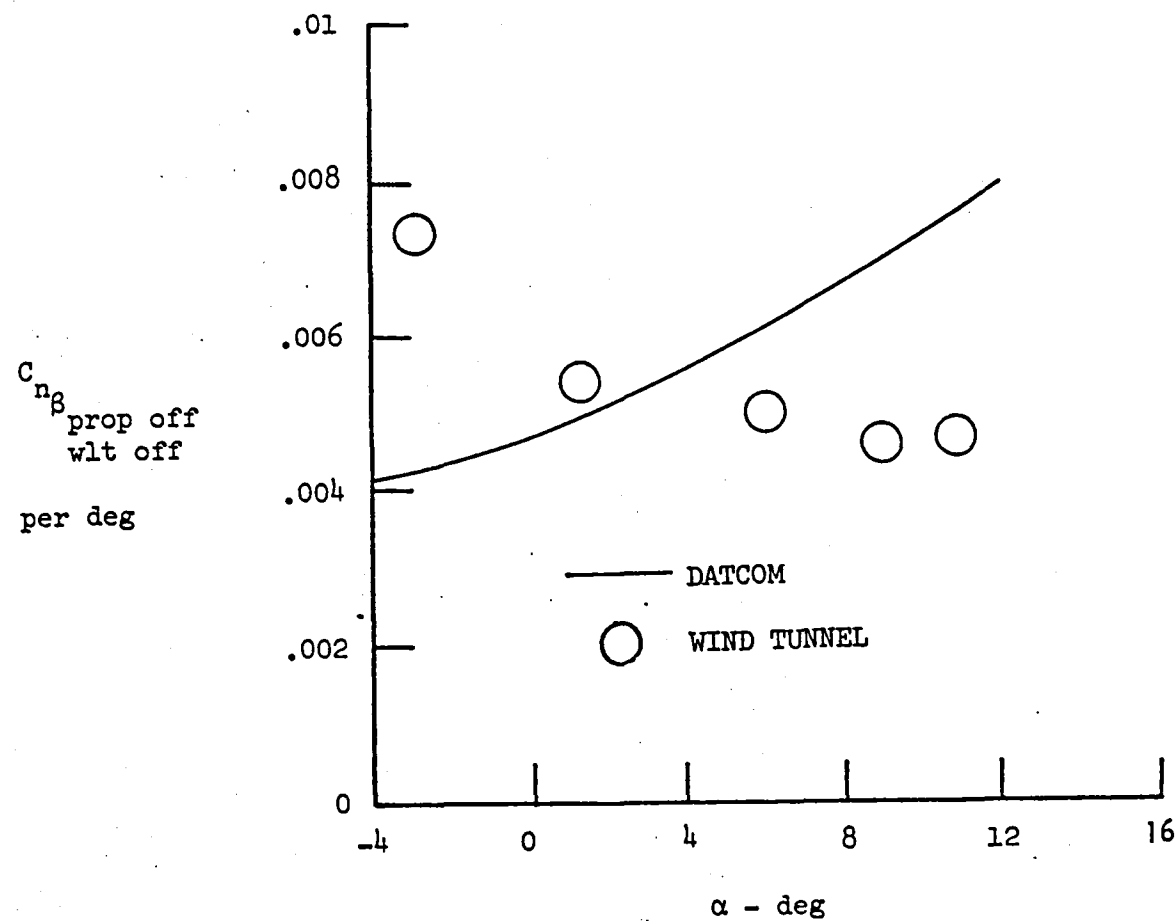


Figure 5.2.5.1: Comparison of predicted $C_{n\beta}$,
 winglets off, to full scale wind
 tunnel data for the Ayres Thrush
 S2R-800.

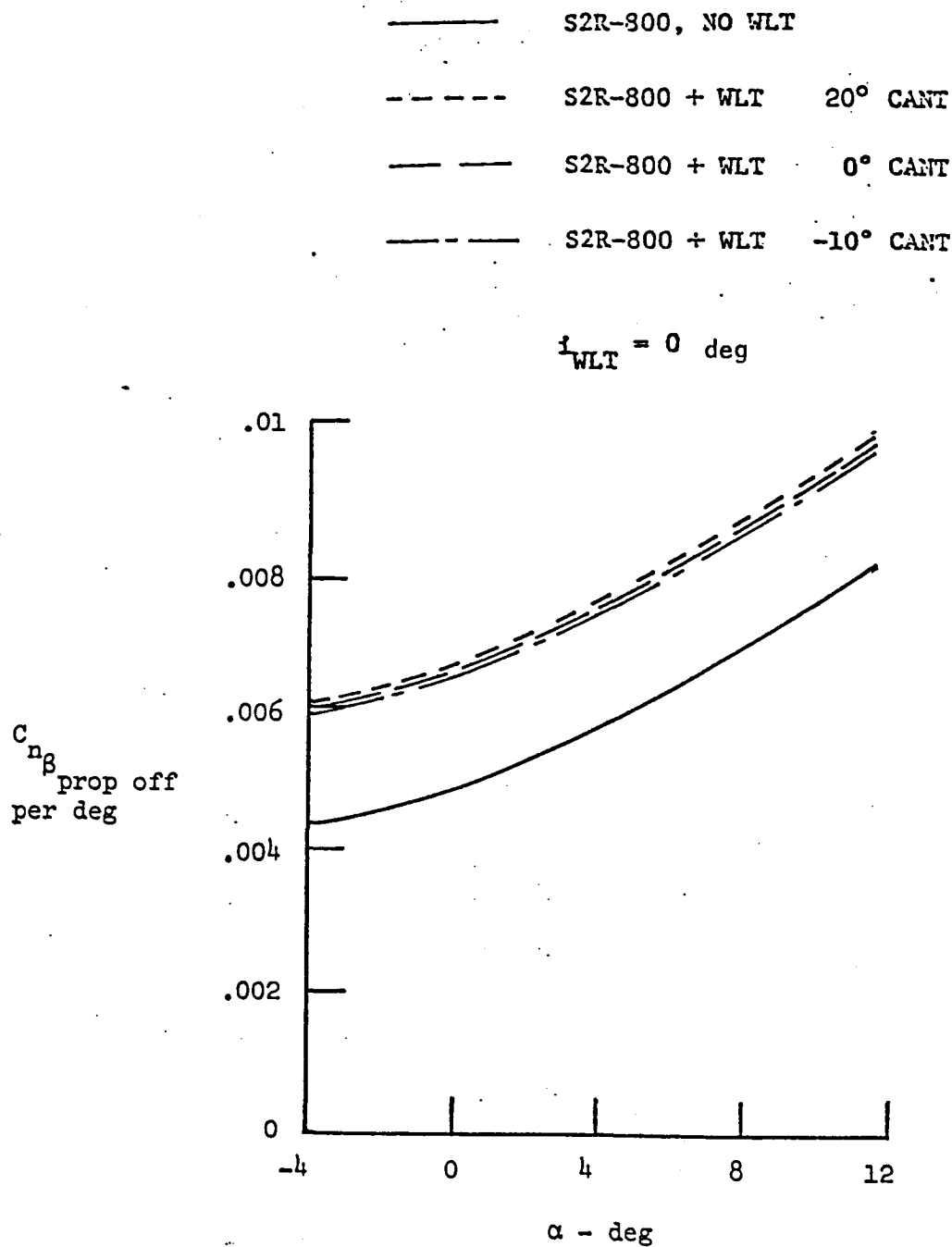


Figure 5.2.5.2: Effect of winglet cant angle on airplane $C_{n\beta}$ based on DATCOM methods.

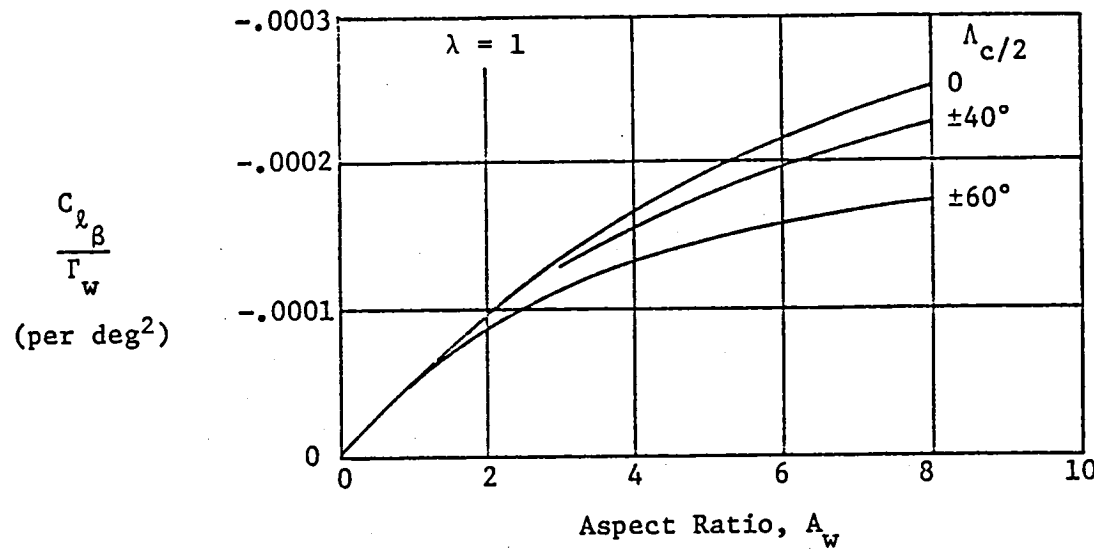


Figure 5.3.1.1: Effect of wing dihedral on wing $C_{l\beta}$ (Reference 1)

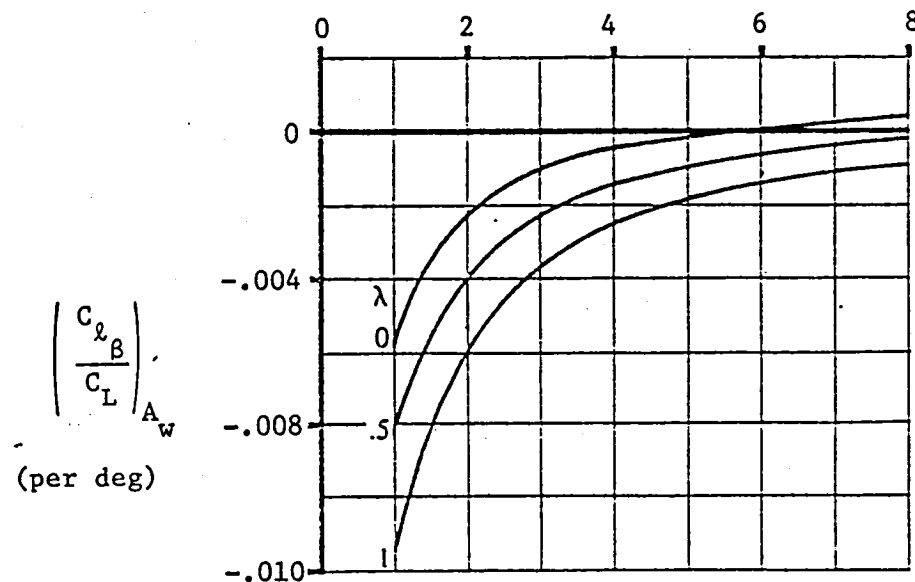


Figure 5.3.1.2: Aspect ratio contribution to $C_{l\beta}$ (Reference 1)

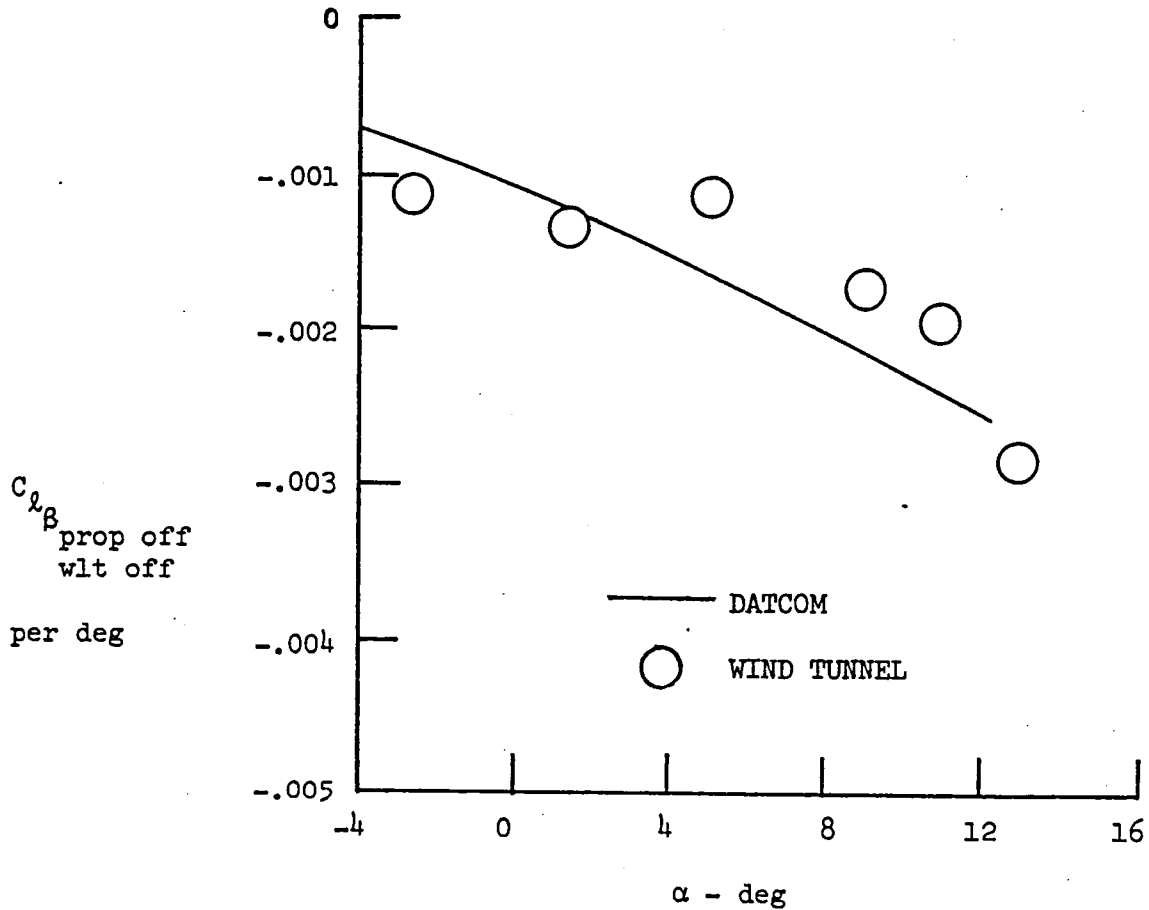


Figure 5.3.5.1: Comparison of predicted $C_{l\beta}$,
 winglets off, to full scale wing
 tunnel data for the Ayres Thrush
 S2R-800.

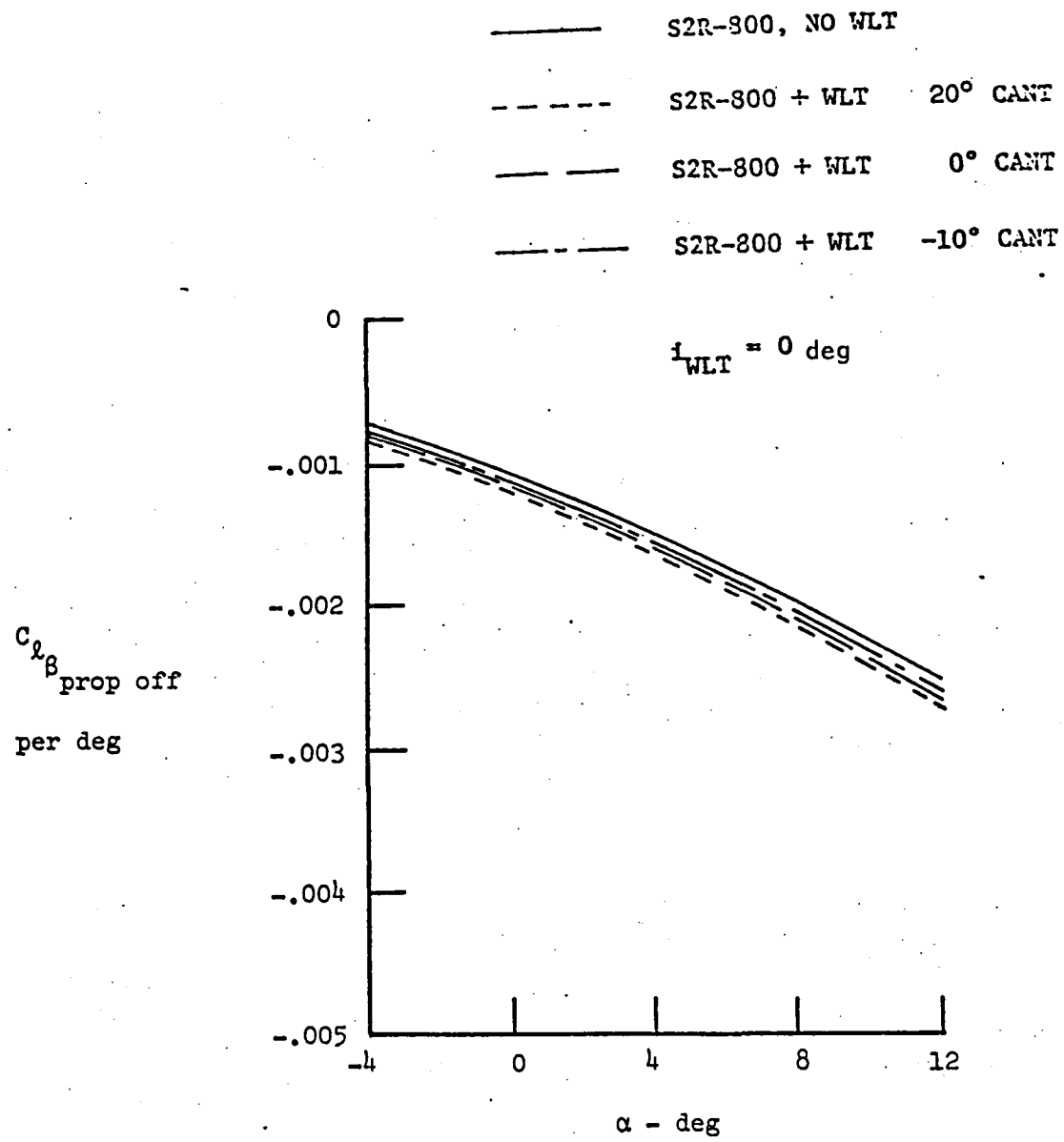


Figure 5.3.5.2 : Effect of winglet cant angle on airplane $C_l \beta$ based on DATCOM methods.

CHAPTER 6

PREDICTION OF LIFT AND STABILITY CHARACTERISTICS USING A COMPUTER METHOD

In this chapter the Quasi-Vortex Lattice Method (QVLM), developed by Lan (Reference 3) is used to predict the power-off lift curve slope and zero lift angle for the S2R-800. $C_{y\beta}$, $C_{n\beta}$ and $C_{l\beta}$ are also calculated.

6.1 Description of QVLM

In QVLM the lifting surface is divided into a number of small lifting elements. The continuous vortex distribution representing the wing in a uniform flow is replaced with a discrete one. Wing edge square-root singularities and the Cauchy singularity in the downwash integral are theoretically accounted for. A mathematical description of QVLM is included in Reference 3.

6.1.1 Program Capabilities

The QVLM program used to predict stability derivatives for the Ayres Thrush has these following noteworthy features:

- 1) It is applicable to nonplanar wing configurations, such as wing-winglet combinations.
- 2) It cannot account for the fuselage effect on the stability derivatives.
- 3) If the airplane tails do not have camber, their effect on stability derivatives cannot be computed.
- 4) Arbitrary wing camber shapes defined at three spanwise stations or less are used in the program through cubic

spine interpolation.

- 5) The vortex-lift effect is calculated through the use of Polhamus' suction analogy.

6.2 QVLM-Predicted C_{L_α} and α_0

For computing C_{L_α} , QVLM assumes attached potential flow and sets the wing angle of attack to 1 radian. The program outputs C_L where $C_{L_\alpha} = C_L$. Since attached potential flow is assumed, separation effects and stall behavior cannot be predicted. For the Ayres Thrush $C_{L_\alpha} = 0.0715$ per deg as predicted by QVLM (Reference 3).

For computing α_0 , several C_L 's were computed at different angles of attack. The zero lift angle could then be found by interpolation. For the Ayres Thrush:

$$(\alpha_0)_{QVLM} = -3.7 \text{ deg.}$$

These results are compared to full-scale wind-tunnel data in Figure 6.2.1.

6.3 QVLM-Predicted C_y , C_n , and C_ℓ

The QVLM calculations were done for winglets on and winglets off. The winglet cant angles were $+20^\circ$, 0° , and -10° . Since the version of QVLM used for these calculations could not account for fuselage effects, it was not possible to compare these results with the available S2R-800 wind-tunnel data. The results are plotted in Figures 6.3.1 to 6.3.3. It is noted that Reference 4 (Figure 39) contains small scale model wind tunnel data on the effect of winglet cant on C_ℓ .

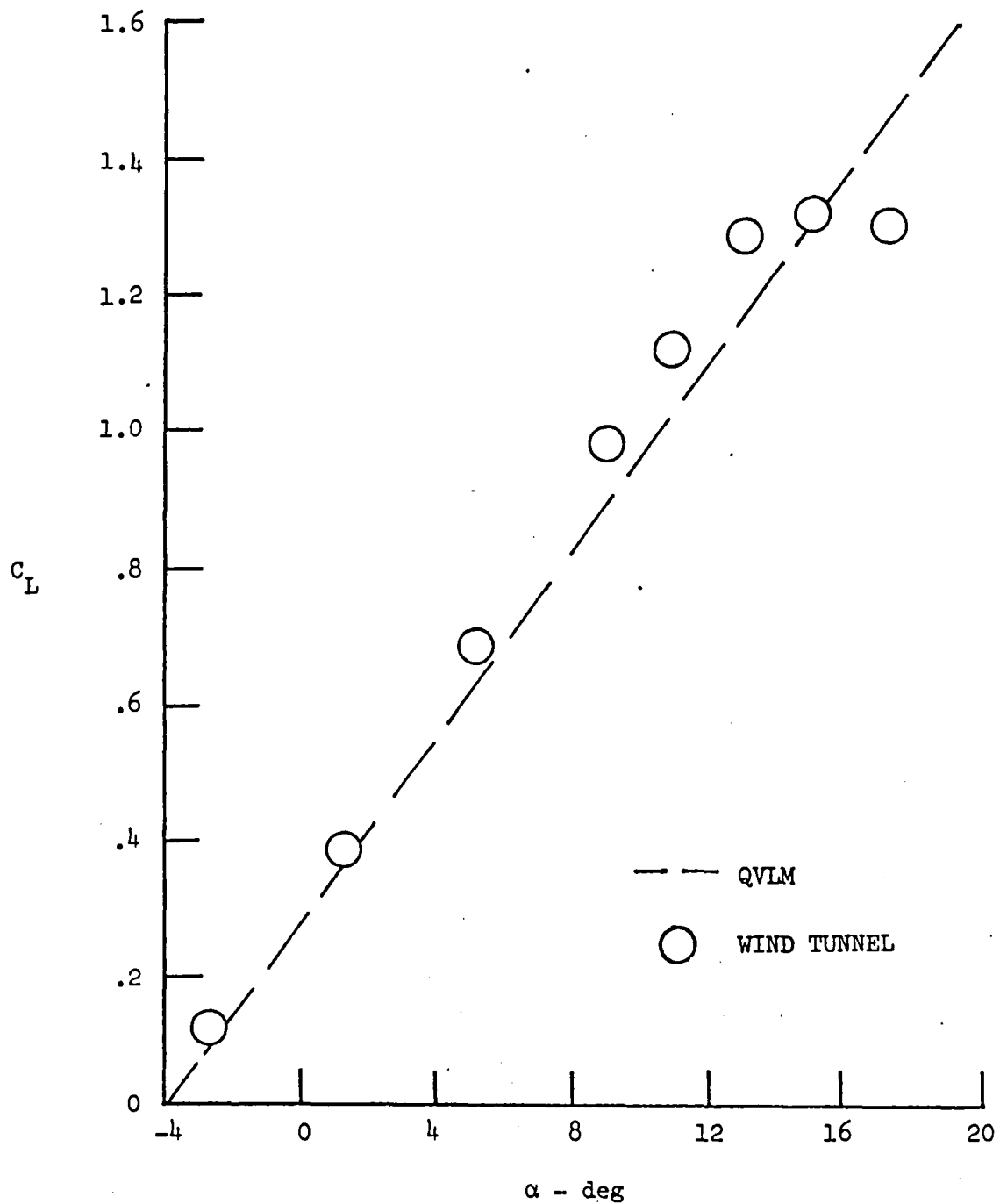


Figure 6.2.1: Lift curve of the S2R-800 based on QVLM computation.

——— WING ALONE
 - - - WING + WLT 20 deg cant
 - - - WING + WLT 0 deg. cant
 - - - WING + WLT -10 deg cant
 $i_{WLT} = 0 \text{ deg}$

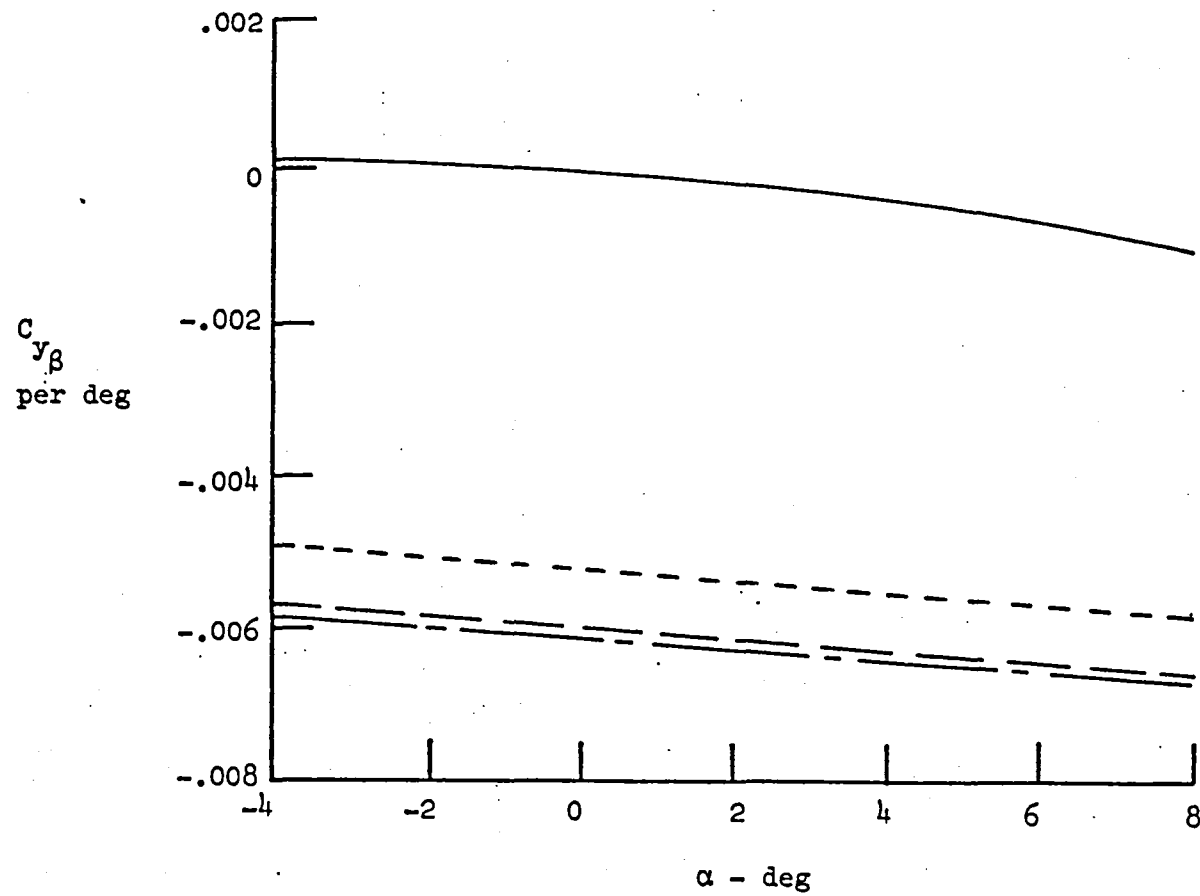


Figure 6.3.1: Effect of winglet cant angle on $C_{y\beta}$ based on QVLM computation for the S2R-800.

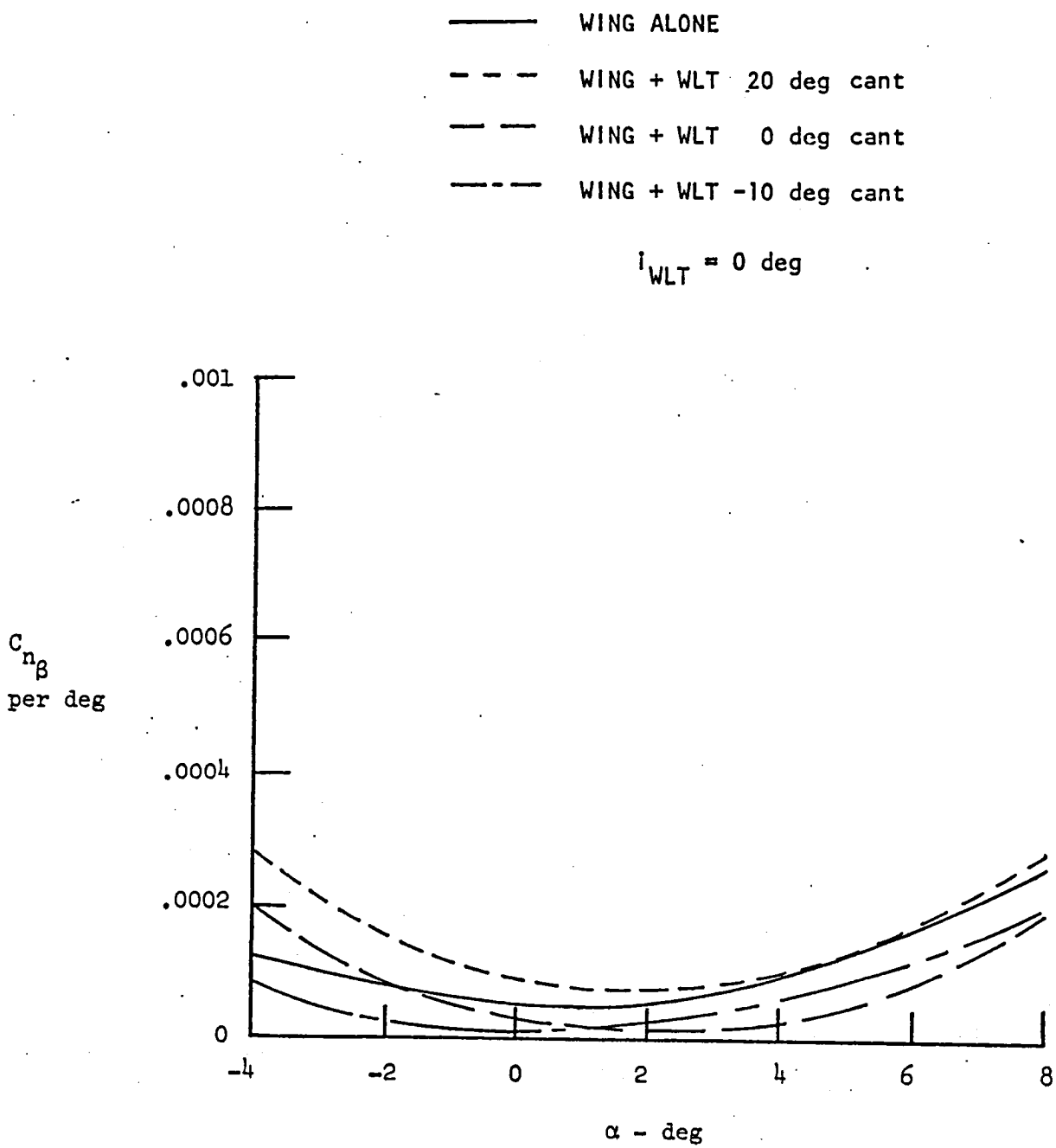


Figure 6.3.2: Effect of winglet cant angle on C_{n_B} based on QVLM computation for the S2R-800.

——— WING ALONE
 - - - - WING + WLT 20 deg cant
 - - - - WING + WLT 0 deg cant
 - - - - WING + WLT -10 deg cant

$$i_{WLT} = 0 \text{ deg}$$

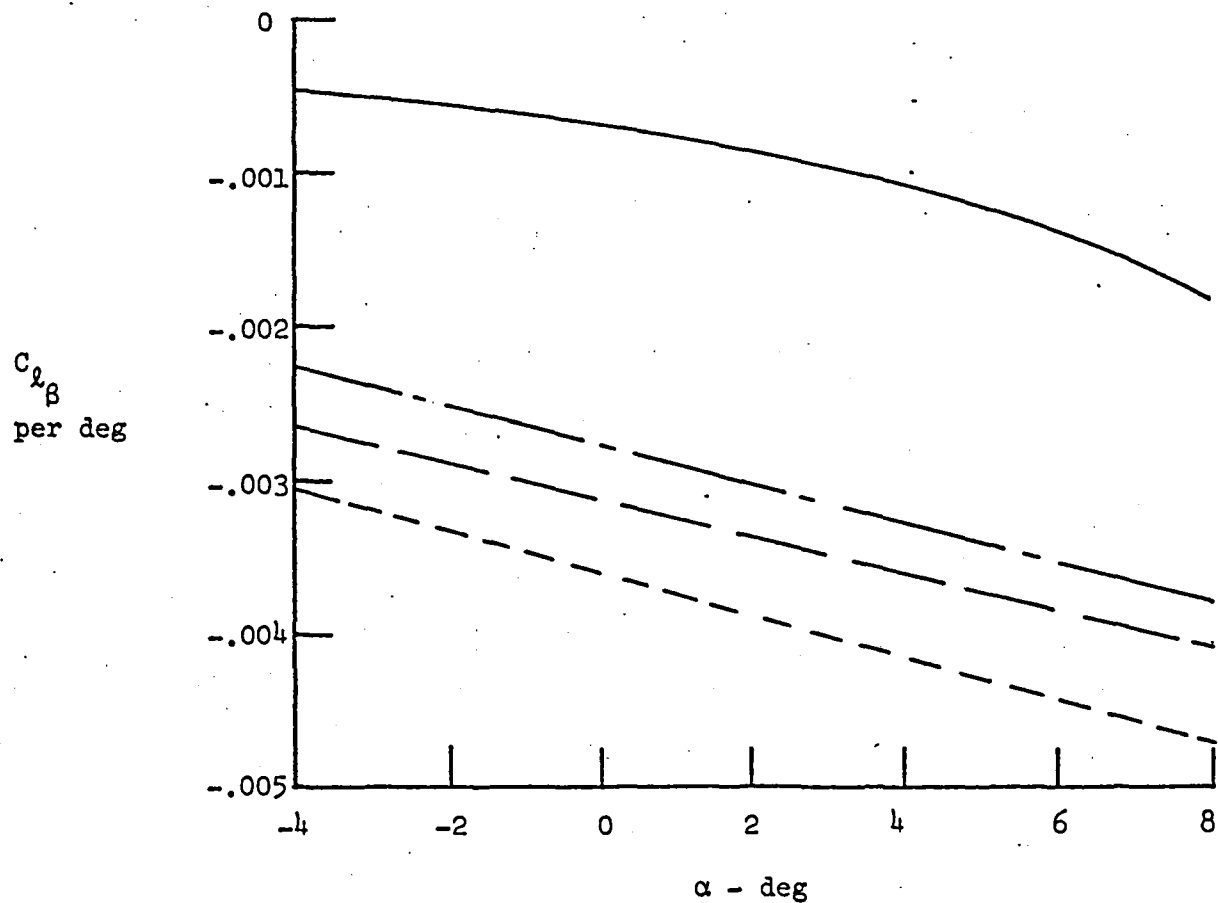


Figure 6.3.3: Effect of winglet cant angle on $C_{l\beta}$ based on QVLM computation for the S2R-800.

CHAPTER 7

CONCLUSIONS AND RECOMMENDATIONS

In this report an analytical method (Reference 1) and a computer method (Reference 3) were presented and used to calculate selected lift characteristics and sideslip derivatives of the Ayres Thrush S2R-800. Where possible, these results were compared to full-scale wind-tunnel data and to each other. Based on these comparisons, the following conclusions and recommendations are made:

1. The analytical method of Reference 1 and computer method of Reference 3 both give C_{ℓ_α} and α_0 values which correlated well with the wind-tunnel data. The analytical method gives a good "ball-park" estimation of the nonlinear lift behavior, while the computer method of Reference 3 does not apply to the nonlinear region.
2. The analytical predictions of Reference 1 for the sideslip derivatives C_{y_β} , C_{n_β} and C_{ℓ_β} show good agreement with wind-tunnel data. The predicted C_{y_β} is within 10 percent of the average tunnel C_{y_β} value. While the trends with angle of attack are opposite, the nominal predicted C_{n_β} agrees with the average tunnel C_{n_β} . Separation and interference effects caused by the fuselage need to be incorporated in the analytical method. The predicted C_{ℓ_β} compares well with wind-tunnel results.
3. The predictions by the method of Reference 3 indicate that winglet cant angle has a significant influence on the sideslip derivatives. From Figures 6.3.1-6.3.3 it is evident that the inwardly canted winglets have the least effect on the lateral-directional stability of the Ayres Thrush. Therefore, it appears that the use of inwardly ..

canted winglets may offer a means of minimizing chemical spray wake interaction effects without degrading handling qualities (see Reference 4).

4. Computer results show that the analytical method of reference 1 is deficient in predicting winglet effect on the sideslip derivatives. It is recommended that a more accurate analytical method for calculating winglet effect on the sideslip derivatives, incorporating the following procedure, be developed.

- a) To account for wing span loading increase due to winglets (endplate effect), calculate a modified wing aspect ratio based on winglet area.
- b) Calculate winglet C_{α} based on airfoil section properties and adjusted for finite span.
- c) Based on wind-tunnel data, calculate and plot wing-winglet interference factors.
- d) Using the values calculated above, follow the procedure developed in this report, making modifications where common sense dictates.

REFERENCES

1. Finck, R. D.; and Hoak, D. E., "USAF Stability and Control DATCOM," Air Force Dynamics Laboratory, Wright Patterson Air Force Base, Ohio, October 1960 (Revised 1975).
2. Torenbeek, E., Synthesis of Subsonic Airplane Design, Delft University Press, Delft, Netherlands, 1976.
3. Lan, C. E., "A Quasi Vortex Lattice Method in Thin Wing Theory," Journal of Aircraft, Vol. 11, No.9, September 1974, pp. 518-527.
4. Johnson, J. L., Jr.; McLemore, H. C.; White, R.; and Jordan, F.L., Jr., "Full Scale Wind-Tunnel Investigation of an Ayres S2R-800 Thrush Agricultural Airplane," SAE Paper 790618, 1979.

1. Report No. NASA CR-165710	2. Government Accession No.	3. Recipient's Catalog No.	
4. Title and Subtitle Comparison of Selected Lift and Sideslip Characteristics of the Ayres Thrush S2R-800, Winglets Off and Winglets On, To Full-Scale Wind-Tunnel Data		5. Report Date April 1981	6. Performing Organization Code
7. Author(s) J. Roskam and M. Williams		8. Performing Organization Report No. KU-FRL-399-3	
9. Performing Organization Name and Address The University of Kansas Center for Research, Inc. 2291 Irving Hill Drive - Campus West Lawrence, KS 66045		10. Work Unit No.	
12. Sponsoring Agency Name and Address National Aeronautics and Space Administration Washington, DC 20546		13. Type of Report and Period Covered Contractor Report	
		14. Sponsoring Agency Code 530-01-13-01	
15. Supplementary Notes Langley Technical Monitor: Dr. Bruce J. Holmes Use of commercial products or names of manufacturers in this report does not constitute official endorsement of such products or manufacturers, either expressed or implied, by the National Aeronautics and Space Administration.			
16. Abstract This report represents comparisons of analytically-predicted and wind tunnel-measured lift and sideslip characteristics of the Ayres Thrush S2R-800, winglets off and winglets on. Specifically, the derivatives calculated and compared to full-scale wind-tunnel data (where available) are: C_L , C_L _{max} , C_y , C_n , and C_{α} . All calculations were done in the stability axes system. The winglets used were constructed of modified GA(w)-2 airfoils.			
17. Key Words (Suggested by Author(s)) Agricultural Aircraft Aerial Applications General Aviation Winglets Stability derivatives		18. Distribution Statement Unclassified - Unlimited Subject Category 02	
19. Security Classif. (of this report) Unclassified	20. Security Classif. (of this page) Unclassified	21. No. of Pages 116	22. Price* A06

